Effects of Plate Subduction on the Earth's Deep Water Cycles

Dissertation zur Erlangung des Doktorgrades
der Mathematisch-Naturwissenschaftlichen Fakultät
der Christian-Albrechts-Universität zu Kiel

vorgelegt von
Lars Helmuth Rüpke
aus Hamburg

Kiel
2004

Referent: Prof. Jason Phipps Morgan
Koreferent: Prof. Matthias Hort
Tag der mündlichen Prüfung: 22. April 2004
Zum Druck genehmigt: Kiel, den 5. Mai 2004

Prof. Wulf Depmeier (Dekan)

Hiermit erkläre ich, dass die vorliegende Abhandlung, abgesehen der Beratung durch meine akademischen Lehrer, nach Inhalt und Form meine eigene Arbeit darstellt. Ferner habe ich weder diese noch eine ähnliche Arbeit an einer anderen Abteilung oder Hochschule im Rahmen eines Prüfungsverfahrens vorgelegt.

Lars Helmuth Rüpke

Zusammenfassung

Die fundamentale Unsicherheit im globalen geochemischen Wasserzyklus der Erde ist die Menge an Wasser, die an Subduktionszonen zurück in den tieferen Erdmantel transportiert wird. An konvergenten Plattengrenzen werden große Mengen an Wasser in den oberen Erdmantel eingebracht. Dieses Wasser ist in subduzierten Sedimenten, hydratisierter Ozeankruste und serpentinisiertem Mantel chemisch gebunden. Während der Subduktion setzten metamorphe Mineralumwandlungen den größten Teil dieses Wasser in Tiefen <200km wieder frei. Der resultierende Fluidfluss von der abtauchenden Platte führt im Mantelkeil zu einer Schmelzpunkterniedrigung und so zu Aufschmelzung und schließlich zu Vulkanismus. Es ist jedoch möglich, dass ein bislang nur wenig bekannter, kleinerer Teil des subduzierten Wassers während der Subduktion chemisch gebunden bleibt. In diesem Fall, würde Oberflächenwasser zurück in den tieferen Erdmantel transportiert, so dass Subduktionszonen ein potentielles Bindeglied zwischen dem Wasserzyklus der Ozeane und dem des Erdmantels darstellen. Ein genaueres Verständnis des Wasserhaushalts von Subduktionszonen ist somit wichtig, um Subduktionszonen-Vulkanismus und die chemische Entwicklung des Erdmantels besser zu verstehen.

In dieser Arbeit wird ein numerisches Subduktionszonenmodell benutzt, um sowohl Wasserfreisetzung als auch Wasserrückführung in den Erdmantel quantitativ zu untersuchen. Mit dem im Rahmen dieser Doktorarbeit entwickelten Modell wird die Wasserfreisetzung in subduzierten Sedimenten, hydratisierter Ozeankruste und serpentinisiertem lithosphärischen Mantel berechnet. Die numerischen Experimente zeigen, dass Wasserfreisetzung in der abtauchenden Platte sehr wahrscheinlich ein kontinuierlicher Prozess ist. Die lithologische Schicht in der die Fluide freigesetzt werden ändert sich jedoch mit der Tiefe. In geringen Tiefen entwässert subduziertes Sediment, dann folgt die hydratisierte Kruste und schließlich der serpentinisierte Mantel. Diese Tiefenabhängigkeit der Fluidquelle kann einen Einfluss auf die Mobilisierung von Spurenelementen haben. Eine Modellstudie der Zentral-Amerikanischen Subduktionszone zeigt, dass sich Änderungen in der Fluidquelle unter der vulkanischen Front im Chemismus der eruptierten Laven widerspiegeln

können. Die Modellrechnungen zeigen, dass Magmabildung unter der vulkanischen Front Nicaraguas wahrscheinlich aus intensiver Wasserfreisetzung in serpentinisiertem Mantel resultiert. Der hohe Fluidfluss von der abtauchenden Platte in den Mantelkeil führt zu einer effizienten Spurenelement-Mobilisierung von der abtauchenden Platte in den Mantelkeil, was in einer Anreicherung dieser Elemente in den eruptierten Laven deutlich wird. Die Hauptfluidquelle unter Costa Rica ist die subduzierte Ozeankruste, welche weniger Wasser freisetzt. Der reduzierte Fluidfluss führt dazu, dass Spurenelement-Mobilisierung weniger effizient ist. Die Folge ist, dass die eruptierten Schmelzen in Costa Rica keine deutliche Anreicherung in Spurenelementen zeigen, die von der abtauchenden Platte stammen.

Weiterhin zeigen die Ergebnisse der Modellversuche zur Plattenentwässerung, dass serpentinisierter Mantel nicht nur eine wichtige Fluidquelle während der Subduktion ist, sondern auch die chemisch stabilste lithologische Schicht ist, um Wasser in den tieferen Mantel zu subduzieren. Um diese potentielle Subduktion von Wasser in den tieferen Erdmantel genauer zu untersuchen, wird das numerische Modell zur Wasserfreisetzung an konvergenten Plattengrenzen, mit einem parameterisierten Mantelkonvektionsmodell verknüpft. Dieses kombinierte Modell erlaubt die Bestimmung der zeitlichen Entwicklung von Wasserentgasung an Mittelatlantischen Rücken und Hotspots und Wasserrückführung in den Mantel an Subduktionszonen seit Entstehung der Erde. Die numerischen Experimente zeigen, dass der Erdmantel fast vollständig entgast ist ($\sim$93%) und heute nur noch $\sim \frac{1}{3}$ seines urpsrünglichen Wassers besitzt. Dies impliziert, dass der größte Teil des derzeitigen "Mantel-Wassers" recyceltes Oberflächenwasser ist. Um diese Ergebnisse zu testen, werden theoretische Wasserkonzentrationen für OIB und MORB berechnet und mit gemessenen Werten verglichen. Dieser Vergleich zeigt, dass die theoretischen und gemessenen Werte sehr gut übereinstimmen. Dies bedeutet, dass ein Mantelevolutionsszenario wahrscheinlich erscheint, in dem der gesamte Mantel als eine Einheit konvektiert und in dem Subduktion ein wichtige Rolle spielt, um Wasser und chemisch angereichertes Material zurück in den Mantel zu führen.

Abstract

The substantial uncertainty in the Earth's geochemical water cycle is the amount of water that is recycled into the deeper mantle at subduction zones. At a convergent margin, significant amounts of chemically bound water are subducted. This water is released during subduction by metamorphic reactions from the slab's sediment, crustal, and mantle portions. The released fluids flux the mantle wedge where they are thought to trigger arc melting. However, a yet largely unconstrained smaller fraction of the subducted water may 'survive' sub-arc water release to be recycled into the deeper mantle. Plate subduction may therefore act as a water 'filter' between the Earth's surface and deep water cycles. Water cycling beneath an arc is therefore closely related to recycling and melting processes at convergent margins.

This thesis uses numerical models to quantitatively explore the subduction zone water cycle. Central to these studies is a newly developed chemo-thermo-mechanical subduction zone model that solves for fluid release during subduction. The modeling results show that fluids are most likely continuously released from the slab. However, the 'host' lithology of these fluids changes with depth from sediments, to hydrated oceanic crust, to serpentinized mantle. This change in slab fluid source with depth may have strong chemical implications for trace element recycling at a subduction zone. To explore the interrelation between fluid release and trace element recycling the model is adapted to the Central American subduction zone. This case study shows that changes in fluid source may be reflected in variations in arc lava chemistry. The modeled pattern of fluid release beneath Nicaragua show that serpentinized mantle is the dominant fluid source at sub-arc depths. The resultant vigorous fluid flux from the slab into the sub-arc mantle leads to efficient leaching of trace elements from the slab. This efficient slab-mantle transport is reflected in the produced arc lavas enrichment in slab derived elements. Fluid release beneath Costa Rica appears to be dominated by crustal dehydration and is less intense. The reduced fluid flux results in less efficient trace element mobilization, so that the Costa Rican melts do not show a clear enrichment in slab derived elements.

Furthermore, in a series of model runs the efficiency of slab dehydration during subduction is explored. It is found that subducted sediments and oceanic crust efficiently dewater during subduction and that deep water recycling at subduction zones may easily be dominated by residual serpentinites.

To further explore potential deep water recycling, this thesis next combines the 2D chemo-thermo-mechanical subduction zone mode with a parameterized convection model of the mantle's evolution. This 'joint' model solves for the global geologic water cycle, i.e. the outgassing of water at ridges and hotspots and the recycling of water at subduction zones through time. It is found that for a wide parameter range the Earth's mantle will have highly outgassed (up to 93%) and presently contains only $\sim \frac{1}{3}$ of its initial water. This implies that most of the water currently stored in the Earth's mantle is recycled surface water. The Earth's deep and surface water cycle therefore appear to be still in close contact. To test this mantle evolution scenario theoretical water concentrations in the different chemical mantle components are determined. It is found that these water concentrations are in striking agreement with measured water concentrations in OIB and MORB. We therefore suggest a plum-pudding whole mantle convection evolution scenario in which plate subduction plays an important role in partially filtering the water content of the recycled sediments and crust that form the sources of the more enriched mantle plums. In this scenario the most primitive mantle components (FOZO) are 'wetter' than the recycling associated mantle components (HIMU&EM) and the even drier mantle source that melts to make MORB.

Contents

List of Figures

List of Tables

Chapter 1

Introduction

Plate subduction belongs to the great geodynamic processes that shape the Earth's surface and interior. When plates collide at a convergent margin, oceanic lithosphere may be recycled back into the mantle. Since the Earth is neither shrinking nor expanding plate recycling at subduction zones has to be balanced by the creation of new seafloor at mid-ocean ridges. The competing processes of plate subduction and plate formation are important ingredients of plate tectonics and have managed to go into a quasi-steady-state of mantle recycling.

Plate tectonics, however, is a unique feature of our planet that is presently not observed on other planets (e.g. Sleep 2000). On Earth, plate tectonics goes hand-in-hand with mantle convection - the Earth's preferred way of losing its heat. Other planets show other styles of tectonics and tend to lose their heat differently: Venus seems to experience complete resurfacing events while Mars loses its heat mostly by plume activity. But what makes the Earth different from its neighboring planets? Key for understanding the mechanisms of plate tectonics is the question of how to make subduction zones (Regenauer-Lieb and Kohl 2003). While plate formation at mid-ocean ridges results from convective upwelling and melting, subduction initiation requires the failure of an entire lithospheric plate. Rupturing an entire plate is, however, mechanically difficult and requires significant weakening of the plate in order to make failure and subduction possible. It has recently been argued

that the presence of water on the Earth is what makes the Earth different from other planets and plate tectonics possible. Regenauer-Lieb et al. (2001) showed that in the presence of water the strength of a tectonic plate may be sufficiently reduced for subduction to initiate. Water may therefore play a key role in global mantle dynamics.

But where does the water on Earth come from? The young Earth probably contained both dissolved water in its mantle and accreted exospheric water. However, it is likely that all exospheric water was lost from the young Earth during the strong moon forming impact, so that only mantle water remained. Subsequent strong volcanic activity on the young Earth led to outgassing of water into the exosphere and ultimately to the formation of the oceans. However, this 'standard' theory that the oceans have been exhaled from the mantle during upwelling and melting at mid-ocean ridges and hotspots may have to be slightly modified to include the potential re-injection of water into the mantle at subduction zones.

At a subduction zone, an incoming oceanic plate subducts along a weak fault beneath an overriding plate. The downgoing plate is commonly thought to have undergone a variety of high- and low-temperature alteration processes during its lifetime that led to its partial hydration. During subduction, this water is released by metamorphic reactions into the mantle wedge to trigger arc melting. The produced melts start to rise buoyantly in diapiric structures towards the characterized chain of arc volcanoes that is usually located $\sim$100km above the downgoing plate. However, not all water brought into a subduction zone is released from the slab. A small water fraction may 'survive' sub-arc water release to be transported into the deeper mantle. This re-injection of water at subduction zones is the substantial uncertainty in the Earth's global geochemical water cycle. Water recycling at subduction zones implies that the Earth 'surface' and 'deep' water cycle are still in close contact through the competing processes of water outgassing at mid-ocean ridges and hotspots and water recycling at convergent margins. Understanding the subduction zone water cycle is therefore essential for understanding melting and recycling processes at subduction zones themselves as well as the geochemical evolution of the Earth's mantle. This study contributes to a better understanding of these geodynamic processes by ex-

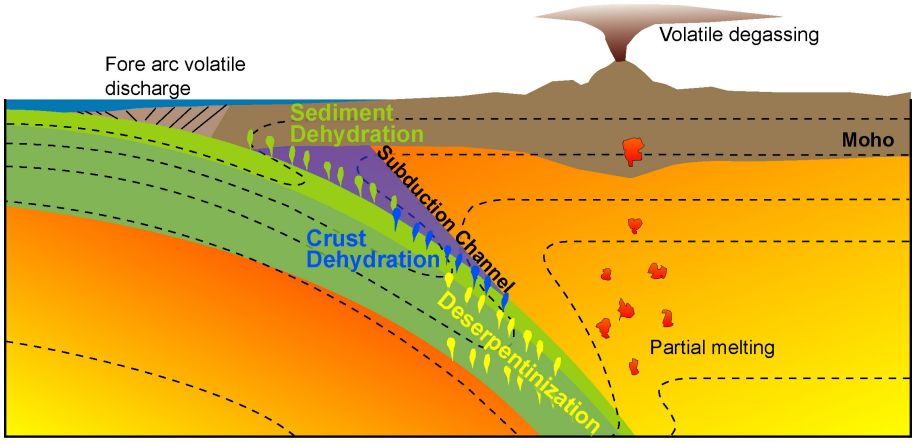

Figure 1.1: *Schematic drawing of fluid release beneath an arc. Colored 'drops' mark metamorphic fluid release from the slab and contour lines schematically show the depression of geotherms at a subduction zone. Depending on the depth of slab dehydration, the released fluids may (1) be discharged at cold vent sites in the fore arc region, (2) rise buoyantly along the 'subduction channel', or (3) trigger melting in the mantle wedge.*

ploring both the 'global' geochemical water cycle of the mantle and the 'local' subduction zone water cycle.

1.1 Water cycling at a subduction zone

Water cycling beneath an arc is determined by the amount of water that is subducted, subsequent fluid release from the slab, and the amount of water that is re-injeted into the deeper mantle. The amount of water that is subducted depends on the degree of alteration that the subducting plate has undergone during its lifetime. Chemical hydration of an oceanic plate starts at a mid-ocean ridge where hydrothermal circulation leads to water influx into the crust. As the plate ages, hydration slowly continues during alteration processes at the seafloor. Additionally, sediments containing pore water and chemically bound water are deposited onto the plate. Close to the trench, during plate bending, normal faulting may provide the pathways for sea water to reach and react with the cold lithospheric mantle to make serpentine thereby additionally hydrating the incoming

plate.

During subduction, water is continuously released from the slab (Fig. 1.1). The host lithology of the released fluids changes with depth from sediments to hydrated crust to serpentinized mantle. The consequences of slab fluid release depend upon the thermal regime into which these fluids are released and slab fluid release can be roughly divided into three stages (Fig. 1.1):

(1) Initial water release occurs at depths <20km from sediments. Here, under cold conditions, the released fluids will either migrate along the fault zone towards the trench or will rise along new faults, formed within the upper plate by hydrofracturing, towards the upper slope. In either case, these rising fluids are likely to be expelled back into the oceans at cold vent sites in the fore-arc region (Hensen et al. 2004). Shallow slab water release may, therefore, be important for understanding water cycling in the fore-arc and processes within the fault zone that is seismically most active at a subduction zone, the seismogenic zone.

(2) Intermediate depth water release (20-100) km occurs at p-T conditions too cold to trigger arc melting. These fluids, released from sediments and crust, may moreover rise buoyantly along the slab-wedge interface (subduction channel) to hydrate the cold upper mantle wedge. This 'subduction channel' is a potential transport path for deep fluids back towards the trench and for the reemergence of high pressure rocks (Gerya et al. 2002). Studying 'intermediate' depth slab dehydration is, therefore, important for understanding processes at the base of the overlying plate and for the history of higher pressure metamorphic rocks that are brought back to the surface.

(3) Deep sub-arc water release occurs at depths >100km and is thought to trigger arc melting. Fluids are released from sediments, crust, and serpentinized mantle into the hot sub-arc mantle where they reduce the ambient mantle's solidus temperature to flux-melt it. On their way from the slab into the mantle wedge these fluids interact with and scavenge elements from the slab thereby transporting slab derived elements into the arc melting region and eventually back to the surface during volcanic activity. The surface observational evidence for this slab to arc transport process is the typical chemical slab

signal in arc lavas. Arc lava chemistry deviates from the chemistry of normal MORB by the addition of mobile, incompatible elements that are commonly thought to derive from the slab (e.g. Elliot et al. 1997). Sub-arc water release is therefore essential for understanding the origin of arc volcanism.

1.2 Subduction and the chemical evolution of the Earth

The Earth mantle, as it is sampled by mid-ocean ridge basalts (MORB) and ocean island basalts (OIB), contains several isotopically distinct chemical mantle components (Hofmann 1997). The most enriched components are associated with the recycling of sediments and OIB (EM1 & EM2) and oceanic crust (HIMU). Although it is now commonly accepted that plate recycling at subduction zones plays an important role for the chemical evolution of the Earth's mantle, the detailed effects of deep plate subduction remain not fully understood. These uncertainties result from two major unknowns about subduction: (1) how often do slabs penetrate the 660km discontinuity to subduct into the deeper mantle and (2) what is the exact chemical composition (and water content) of deeply subducted slabs?

Recent, high-resolution mantle tomography studies show that some slabs do penetrate into the deeper mantle (Hilst et al. 1997) and that plumes may originate within the lower and upper mantle (Montelli et al. 2004), so that strictly layered mantle flow appears to be more and more unlikely. This implies that recycled slabs will ultimately be able to mix with the entire mantle mélange and that the existence of long-lived distinct chemical 'reservoirs' in the mantle appears less likely as previously assumed.

The chemical composition of deeply subducted slabs is more difficult to assess - it depends upon the plate's composition prior to subduction and the alteration processes that a plate undergoes during subduction. This alteration of a subducting slab depends upon the metamorphic reactions that take place during subduction and these reactions are con-

trolled by the thermal regime. Currently numerical models are the most promising tool to study the thermal and petrologic structure of subduction zones.

1.3 Numerical modeling of subduction zones

One way to study remote mantle and subduction zone processes is by numerical modeling. Over the past decades a variety of different modeling approaches have been proposed. These subduction zone models range from simple kinematic models to complex 2 and 3-D dynamic models.

The first family of models were the so-called 'kinematic' models (e.g. Peacock 1996; Davies and Stevenson 1992; Peacock and Wang 1999). In these purely fluid dynamic models the subducting slab is a prescribed kinematic boundary layer and the flow field is completely prescribed by the boundary conditions, so that mantle flow and eventually also the temperature field are in steady-state. Kinematic models have the advantage that they can easily be modified to match complex slab geometries and have mainly been used to map the thermal structure of specific subduction zones. This family of models is, however, now considered to be obsolete, since kinematic models do not provide any inside into the dynamics of subduction zones and do not allow the implementation of any feedback mechanisms between the thermal, chemical, and flow solution.

The so-called 'dynamic' models belong to a new class of fluid dynamic subduction zone models (e.g. Kincaid and Sacks 1997; van Hunen et al. 2000; Billen and Gurnis 2001; Funiciello et al. 2003; Ruepke et al. 2002). In these models the flow field is no longer in steady-state. Buoyancy forces enter the flow field calculation, i.e. the slab is generally no longer a prescribed boundary layer but a cold density 'anomaly' that affects the ambient mantle's flow field. To simplify the implementation of changing densities most subduction zone models apply the so-called Boussinesq approximation. In this approximation a density change affects only the body force (gravity) calculation but does not result in a volume change, so that the equations for incompressible viscous flow remain valid. The

thermal solution of these models is time dependent but may evolve towards a 'pseudo' steady-state when the coupled flow and thermal solution reach an 'equilibrium' state.

1.4 Outline and objectives of the thesis

The overall objective of this thesis is to explore water cycling beneath an arc with numerical models. To achieve this goal, a chemo-thermo-dynamical subduction zone model was developed that self-consistently solves for fluid release from a subducting slab. This model, explained in chapter 2, is used to explore various aspects of water beneath an arc. In chapter 3, I use this model to explore how changes in the incoming plate's hydration, thermal structure, and speed may affect sub-arc water release. Especially, the efficiency of water release is studied. Furthermore, the subduction model is coupled to a parameterized mantle convection model . This coupled model solves for the geochemical water cycle of the Earth's mantle, i.e. the outgassing of water at mid-ocean ridges and hotspots and the re-injection of water into the deeper mantle at subduction zones.

In chapter 4 the results of a case study for the Central American subduction zone are presented. In this study, example model runs are performed for the Nicaraguan and Costa Rican arc sections. A special emphasis of this case study is put on the question of how variations in the pattern of sub-arc fluid release may affect trace element recycling beneath the different arc secions.

Chapter 5 focusses on the global implications of deep water recycing at subduction zones. Using the coupled model presented chapter 3, predicted water concentrations in the different chemical mantle components are calculated and compared to measured data. Furthermore, a mantle evolution scenario is presented that provides a possible explanations for the variations in water concentrations currently observed among the different chemical mantle components.

The chapters 3-5 have been written as stand-alone scientific papers: chapter 3 and 5 have been submitted for publication and are currently in review; chapter 4 has already been

published. Furthermore, this thesis contains an appendix with one article that I have contributed to as a co-author. This paper shows some of my additional work during the time of this thesis work that is only loosely related to the main topics of this thesis. It addresses the potential causes of the Messinian Salinity Crisis (Duggen et al. 2003).

Chapter 2

A chemo-thermo-mechanical model

In this chapter the details of the model formulation are presented. I will describe all components of the chemo-thermo-mechanical model that are used in the subsequent chapters to explore water release and deep water recycling at subduction zones. The 2-D model solves for temperature, mantle flow, and water release using a combined finite-differences, finite-element, and tracer particle advection algorithm.

2.1 The temperature solver

In the model formulation, the time dependent thermal solution depends on diffusion and advection of heat as well as the generation or consumption of latent heat by metamorphic reactions. Additional heat sinks or sources are not implemented; also shear heating is not accounted for in the model formulation because its magnitude appears to be too unconstrained to be properly implemented. The temperature field can therefore be determined from the following equation:

$$\frac{\partial T}{\partial t} + \left(u\frac{\partial T}{\partial x} + w\frac{\partial T}{\partial z} \right) - \kappa \left(\frac{\partial^2 T}{\partial x^2} + \frac{\partial^2 T}{\partial z^2} \right) + \Psi = 0 \tag{2.1}$$

Here, u, w, x, and z are the horizontal and vertical velocity and distance components. T is the temperature, t time, and Ψ is a source term that accounts for endo- and exothermic

Symbol	Meaning	Value	Dimension
$\mathbf{A}$	stiffness matrix	$--$	$--$
$\bar{\mathbf{A}}$	penalty stiffness matrix	$--$	$--$
A	average seafloor age	$--$	Ma
A_{ocean}	average area of oceans	$--$	m^2
H_{wr}	heat of water release	$--$	K
$\mathbf{J}$	Jacobi matrix	$--$	$--$
K	combined finite element stiffness matrix	$--$	$--$
L	latent heat	$--$	Jkg^{-1}
$\mathbf{N}$	finite element shape function matrix	$--$	$--$
P_0	present fraction of mantle processed at ridges per year	1.0527×10^{-10}	a^{-1}
Q	planetary heat loss = radioactive heat production	$--$	$--$
R	overturn rate of the Earth's mantle	$--$	$--$
R_0	present overturn rate of the Earth's mantle	9.5	Ga
S_0	present-day average spreading rate	2.7×10^6	m^2/a
T	temperature	$--$	K
T^*	dimensionless temperature	$--$	$--$
T_m	basal asthenosphere temperature	1573	K
T_0	surface temperature	273	K
V	total volume of water in the exosphere	$--$	m^3
X	average plate length	$--$	$--$
b	temperature dependence of viscosity	15	
c	composition parameter	$--$	$--$
c_p	specific heat	1250	$Jkg^{-1}K^{-1}$
d	ocean depth	$--$	m
dp	depletion	$0 - 0.4$	$--$
$\mathbf{f}$	finite element force vector	$--$	$--$
f_{H2O}	volatile outgassing efficiency during melting	0.99	$--$
g	gravitational acceleration	9.81	$m\ s^{-1}$
h	change in sea level	$--$	m
n	time stepping index	$--$	$--$
p	pressure	$--$	Pa
t	time	$--$	s
u_0	convergence rate	6.0	cm/a
$\mathbf{u}(u,w)$	velocity vector	$--$	$m\ s^{-1}$
$\tilde{\mathbf{u}}$	nodal velocity vector	$--$	$m\ s^{-1}$
$\mathbf{x}(x,z)$	coordinate vector	$--$	m
Ψ	heat of metamorphic reaction	$--$	Ks^-1
Ω	finite element integration area	$--$	$--$
α	thermal expansion constant	3×10^{-5}	K^{-1}
β	comp. buoyancy parameter	0.5×10^{-2}	$--$
$\dot{\varepsilon}$	volumetric strain rate	$--$	$--$
κ	thermal diffusivity	10^{-6}	m^2/s
γ	penalty parameter	$10^7\mu$	
ρ	density	$--$	$kg\ m^{-3}$
ρ_0	reference mantle density	3300	$kg\ m^{-3}$
μ	viscosity	$--$	$Pa\ s$
μ_0	reference viscosity	10^{19}	$Pa\ s$
ϕ	degree of hydration	$0 - 1$	$--$
τ_{ij}	stress tensor	$--$	$--$
ξ	logical tracer coordinate vector	$--$	$--$

Table 2.1: *Complete list of symbols and parameters used in the model formulation.*

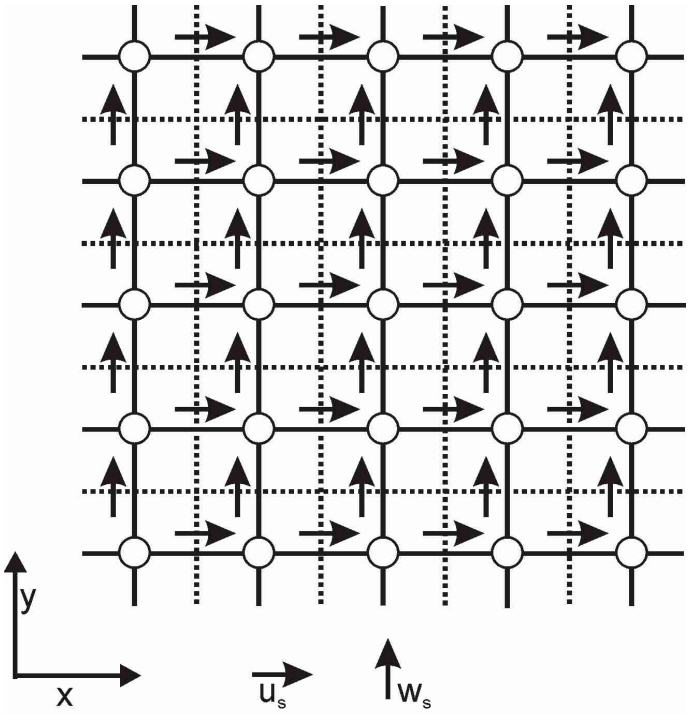

Figure 2.1: *Locations for the staggered velocities u_s and w_s. The white circles mark the location of the other model variables including the 'unstaggered' velocities u and w.*

metamorphic reactions. A full list of model variables and parameters is given in Table (2.1).

Heat transport equations like (2.1) are routinely numerically solved using both finite-difference and finite element techniques. The main problem in modeling coupled advection-diffusion problems is, however, to minimize the effects of possible 'numerical' diffusion. Numerical diffusion results from the discretization process and 'pollutes' the solution. To minimize this problem a high precision finite-difference algorithm called MPDATA is used (Smolarkiewicz 1984); it accounts for numerical diffusion problems by including a correction term into the thermal solution. MPDATA works on a staggered grid and Fig. (2.1) illustrates the employed finite-difference 'gridding' strategy.

2.2 The flow solver

The velocity field is described on the basis of a viscous flow model using the Boussinesq approximation. In this formulation, the flow solution depends upon the boundary conditions as well as viscosity and density variations within the modeling domain. It is assumed that density depends on temperature and composition:

$$\rho(T, c) = \rho_0 \left(1 - \alpha(T - T_m) - \beta c\right). \tag{2.2}$$

Here, ρ the density, c a composition parameter, and the two constants α and β are the thermal expansivity and a compositional buoyancy parameter.

Furthermore, a simple viscous rheology is assumed by using a Newtonian viscosity model that depends on temperature and pressure:

$$\mu(T, z) = \mu_0 \mu(z) \exp\left[b\left(\frac{1}{T^*} - 1\right)\right] \tag{2.3}$$

$$\mu(z) = 1 + [(250 - 1)/2][1 + \tanh(0.01(z - 450))]; \tag{2.4}$$

b is a parameter characterizing the temperature dependence of viscosity (Dumoulin et al. 1999) and $T^* = \frac{T}{T_m}$ is the dimensionless temperature.

The equations governing the flow field can now be written in form of Stoke's equation for incompressible, creeping flow:

$$\frac{\partial \tau_{ij}}{\partial x_j} - \frac{\partial p}{\partial x_i} - \rho g_i = 0 \tag{2.5}$$

$$\tau_{ij} = \mu\left(\frac{\partial u_i}{\partial x_j} + \frac{\partial u_j}{\partial x_i}\right) \tag{2.6}$$

$$\frac{\partial u_i}{\partial x_i} \equiv \dot{\varepsilon_v} = 0 \tag{2.7}$$

Equation (2.5) is the force balance, (2.6) the constituative law, and (2.7) the incompressibility constraint. The variables are the stress tensor component τ_{ij}, the pressure p, the density ρ, the gravitational attraction vector $\mathbf{g}$, the viscosity μ, the velocity vector $\mathbf{u}$, the physical coordinate vector $\mathbf{x}$, and the volumetric strain rate $\dot{\varepsilon_v}$.

To solve equations (2.5-2.7) we discretize the modeling domain into rectangular four velocity node - constant pressure finite elements (coinciding with the unstaggered grid in

Fig. (2.1)) and use a penalty, finite-element solving algorithm. In the penalty formulation pressure is expressed through a large ($\sim 10^7 \times \mu$) penalty parameter, γ,

$$-p = \gamma \nabla \mathbf{u}. \tag{2.8}$$

Inner-element velocities are expressed through the element's shape functions, $\mathbf{N}$, and the element's nodal velocities, $\tilde{\mathbf{u}}$,

$$\mathbf{u} = \mathbf{N}\tilde{\mathbf{u}}, \tag{2.9}$$

and the equations (2.5-2.7) are re-written in their weak form:

$$\int_\Omega \mathbf{A}\tilde{\mathbf{u}} d\Omega + \int_\Omega \bar{\mathbf{A}}\tilde{\mathbf{u}} d\Omega - \int_\Omega \mathbf{b}\mathbf{f} d\Omega - \int_\Gamma \mathbf{N}^\mathbf{T} \bar{t} d\Gamma = 0. \tag{2.10}$$

The terms in the left-hand side correspond in order and meaning to the terms on the left-hand side of eq. (2.5); equation (2.5) is here only written in its weak, penalized, matrix from. The last term on the left-hand side represents boundary conditions. The matrices are:

$$\mathbf{A} = \mathbf{B}^\mathbf{T}\mathbf{D}\mathbf{B} = \mathbf{B}^\mathbf{T}\mathbf{D}\mathbf{S}\mathbf{N} \tag{2.11}$$

$$\mathbf{A} = \mathbf{B}^\mathbf{T} \begin{bmatrix} 2\mu & 0 & 0 \\ 0 & 2\mu & 0 \\ 0 & 0 & 2\mu \end{bmatrix} \begin{bmatrix} \frac{\partial}{\partial x} & 0 \\ 0 & \frac{\partial}{\partial z} \\ \frac{\partial}{\partial z} & \frac{\partial}{\partial x} \end{bmatrix} \begin{bmatrix} N_1 & 0 & N_2 & 0 & N_3 & 0 & N_4 & 0 \\ 0 & N_1 & 0 & N_2 & 0 & N_3 & 0 & N_4 \end{bmatrix} \tag{2.12}$$

$$\mathbf{A} = \begin{bmatrix} \frac{\partial N_1}{\partial x} 2\mu \frac{\partial N_1}{\partial x} + \frac{\partial N_1}{\partial z} \mu \frac{\partial N_1}{\partial z} & & \frac{\partial N_1}{\partial z} \mu \frac{\partial N_1}{\partial x} & . & . & . & . & . & \frac{\partial N_1}{\partial z} \mu \frac{\partial N_4}{\partial x} \\ \frac{\partial N_1}{\partial x} \mu \frac{\partial N_1}{\partial z} & & \frac{\partial N_1}{\partial z} 2\mu \frac{\partial N_1}{\partial z} + \frac{\partial N_1}{\partial x} \mu \frac{\partial N_1}{\partial x} & . & . & . & . & . & \frac{\partial N_1}{\partial z} 2\mu \frac{\partial N_4}{\partial z} + \frac{\partial N_1}{\partial x} \mu \frac{\partial N_4}{\partial x} \\ . & & . & . & . & . & . & . & . \\ . & & . & . & . & . & . & . & . \\ . & & . & . & . & . & . & . & . \\ . & & . & . & . & . & . & . & . \\ . & & . & . & . & . & . & . & . \\ \frac{\partial N_4}{\partial x} \mu \frac{\partial N_1}{\partial z} & & \frac{\partial N_4}{\partial z} 2\mu \frac{\partial N_1}{\partial z} + \frac{\partial N_4}{\partial x} \mu \frac{\partial N_1}{\partial x} & . & . & . & . & . & \frac{\partial N_4}{\partial z} 2\mu \frac{\partial N_4}{\partial z} + \frac{\partial N_4}{\partial x} \mu \frac{\partial N_4}{\partial x} \end{bmatrix} \tag{2.13}$$

Note that the matrix $\mathbf{A}$ is symmetric. Matrix $\bar{\mathbf{A}}$, the penalty (pressure) term, can be written as:

$$\bar{\mathbf{A}} = \mathbf{B}^\mathbf{T}\mathbf{m}\gamma\mathbf{m}^\mathbf{T}\mathbf{B} = \mathbf{B}^\mathbf{T}\mathbf{m}\gamma \begin{bmatrix} 1 & 0 & 0 \end{bmatrix} \mathbf{B} \tag{2.14}$$

$$\bar{\mathbf{A}} = \begin{bmatrix} \frac{\partial N_1}{\partial x}\gamma\frac{\partial N_1}{\partial x} & \frac{\partial N_1}{\partial x}\gamma\frac{\partial N_1}{\partial z} & \frac{\partial N_1}{\partial x}\gamma\frac{\partial N_2}{\partial x} & . & . & . & . & \frac{\partial N_1}{\partial x}\gamma\frac{\partial N_4}{\partial z} \\ \frac{\partial N_1}{\partial z}\gamma\frac{\partial N_1}{\partial x} & \frac{\partial N_1}{\partial z}\gamma\frac{\partial N_1}{\partial z} & \frac{\partial N_1}{\partial z}\gamma\frac{\partial N_2}{\partial x} & . & . & . & . & \frac{\partial N_1}{\partial z}\gamma\frac{\partial N_4}{\partial z} \\ \frac{\partial N_2}{\partial x}\gamma\frac{\partial N_1}{\partial x} & \frac{\partial N_2}{\partial x}\gamma\frac{\partial N_1}{\partial z} & \frac{\partial N_2}{\partial x}\gamma\frac{\partial N_2}{\partial x} & . & . & . & . & \frac{\partial N_2}{\partial x}\gamma\frac{\partial N_4}{\partial z} \\ . & . & . & . & . & . & . & . \\ . & . & . & . & . & . & . & . \\ . & . & . & . & . & . & . & . \\ . & . & . & . & . & . & . & . \\ \frac{\partial N_4}{\partial z}\gamma\frac{\partial N_1}{\partial x} & \frac{\partial N_4}{\partial z}\gamma\frac{\partial N_1}{\partial z} & \frac{\partial N_4}{\partial z}\gamma\frac{\partial N_2}{\partial x} & . & . & . & . & \frac{\partial N_4}{\partial z}\gamma\frac{\partial N_4}{\partial z} \end{bmatrix} \tag{2.15}$$

Again the matrix $\bar{\mathbf{A}}$ is symmetric. The body force term representing gravitational attraction can be written as:

$$\mathbf{bf} = \mathbf{N^T}\rho\mathbf{N}\mathbf{g} \begin{bmatrix} 0 \\ N_1N_1g_1 + N_1N_2g_2 + N_1N_3g_3 + N_1N_4g_4 \\ 0 \\ . \\ . \\ . \\ . \\ N_4N_1g_1 + N_4N_2g_2 + N_4N_3g_3 + N_4N_4g_4 \end{bmatrix} \tag{2.16}$$

Now, we have assembled all equations, so that we can write the final, weak, finite-element equations in simplified from:

$$\mathbf{K}\tilde{\mathbf{u}} = \mathbf{f} \tag{2.17}$$

$$\mathbf{K} = \int_\Omega \mathbf{A} + \bar{\mathbf{A}} d\Omega \tag{2.18}$$

$$\mathbf{f} = \int_\Omega \mathbf{bf} d\Omega + \int_\Gamma \mathbf{N^T}\bar{t} d\Gamma \tag{2.19}$$

The matrix $\mathbf{K}$ is the stiffness matrix, $\tilde{\mathbf{u}}$ are the discrete, nodal velocities, and $\mathbf{f}$ are the body forces and boundary terms. Equation (2.17) is the governing equation for viscous flow in the model formulation. To solve it we use a direct (Gaussian elimination) solver.

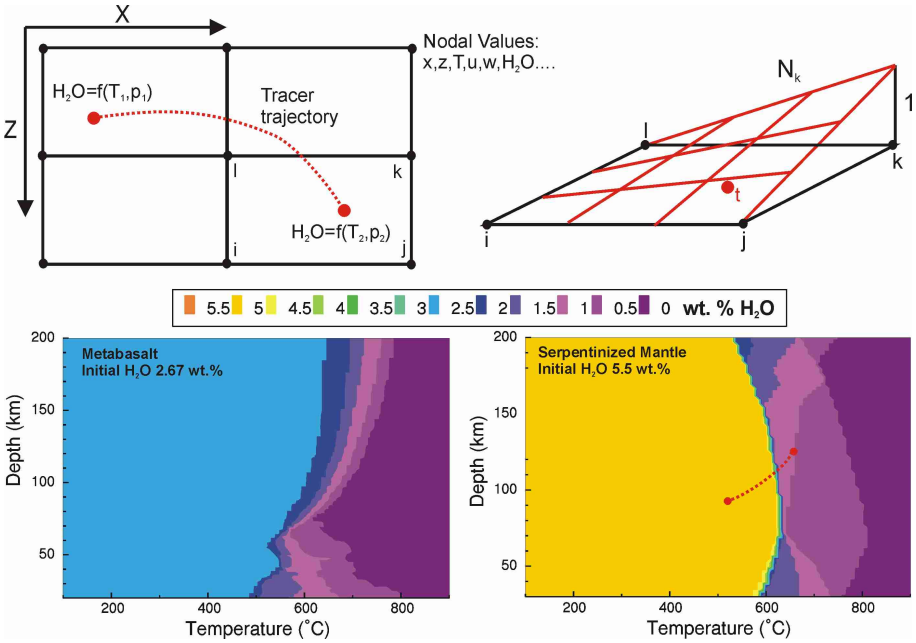

Figure 2.2: *Implemation of slab dehydration using tracer particles. Particle properties (water content) are mapped onto the grid points using the finite element shape functions; changes in particle properties are determined from pre-calculated look-up tables.*

2.3 Slab metamorphism

Central to this study is the modeling water release during metamorphic reactions. The general strategy I adopt to model these metamorphic processes is to use tracer particles (representing hydrous material) that are advected with the subducting slab. Each tracer starts with an initial hydration; during subduction pre-calculated look-up tables are used to determine the change in a tracer's degree of hydration. The necessary look-up tables are calculated with the petrologic thermo-dynamic tool-box PERPLEX (http://www.perplex.ethz.ch). PERPLEX allows the calculation of synthetic phase diagrams, and p-T property plots (of e.g density, hydration, thermal enthalpy) for any given initial chemical composition. I will next explain the tracer advection scheme and PERPLEX in more detail.

2.3.1 Tracer particle advection

Tracer advection schemes are probably the most appropriate numerical method for calculating advection of exclusively non-diffusive material, since they do not suffer from any numerical diffusion problems. This property makes a tracer particle advection scheme well suited for calculating the advection of chemically bound water. Another virtue of tracer particles is that they are 'gridless', i.e. they can take any position within the modeling domain and are not restricted to grid nodes which may thereby increase resolution. However, to actually use tracer particles in a numerical calculation the physical property represented through them usually has to be mapped onto the grid points. In conventional advection schemes this is done by evaluating the number of tracers per cell. This approach works, however, only for one physical property per tracer and suffers from statistical fluctuations in the solution (Tackley and King 2003; Christensen and Hofmann 1994). The tracer method I use is novel in that each tracer is not only a point but also an object that contains in addition to its location other variables like density, volume, and water content. These properties are mapped and scaled onto the grid points (i.e. the cell nodes) using the finite element shape functions and each tracer's 'volume' (Fig. 2.2). Making each tracer contain several variables and a volume ensures that mass is always conserved within the modeling domain and provides a multi-variable non–diffusive advection scheme that does not suffer from many of the restrictions of conventional 'binary' tracer particle methods.

Standard tracer advection algorithms consist of four parts: the advection equation (2.20), an integration scheme, a localization process, and the Jacobi matrix determinations (Brock et al. 1998). A tracer's position is determined by its cell number and location, and can be expressed in physical, $\mathbf{x}$, or logical coordinates, $\boldsymbol{\xi}$ ($0 < \xi_i < 1$, with i=x,z). The logical and physical coordinates are interconnected by the Jacobi matrix, $\mathbf{J}$, so that $\boldsymbol{\xi} = \mathbf{J^{-1}x}$. Logical coordinates have the advantage that whenever a logical coordinate is unbound after integration (i.e. $\xi_i < 0$ or $\xi_i > 1$) a tracer particle has changed cells and a localization process is necessary.

The tracer advection scheme can be written as:

$$\frac{\partial \bar{\xi}}{\partial t} = \left[\frac{\partial \mathbf{x}(\xi)}{\partial \xi}\right]^{-1} \cdot \mathbf{u_x}(\mathbf{x}(\xi, \mathbf{t})) = \mathbf{u}_\xi(\mathbf{x}(\xi, \mathbf{t})) \tag{2.20}$$

$$\bar{\xi}^{n+\frac{1}{2}} = \bar{\xi}^n + \mathbf{u^n} \cdot \frac{\Delta t}{2} \tag{2.21}$$

$$\bar{\xi}^{n+1} = \bar{\xi}^n + \mathbf{u}^{n+\frac{1}{2}} \cdot \Delta t \tag{2.22}$$

where $\mathbf{u_x}$ is the physical coordinate velocity vector and $\mathbf{u}_\xi$ the logical coordinate velocity vector; n is the time stepping index and t the time. The integration scheme always contains a trade-off between speed and accuracy. A simple Euler integration requires only one evaluation of the RHS of (2.20), but often critically reduces accuracy. We use a predictor-corrector advection scheme (2.21,2.22) that requires two evaluations of the RHS of the advection equation per time step but provides the required accuracy. The localization method is easy since a structured orthogonal grid is used.

2.3.2 Modeling fluid release with PERPLEX

It is well known in metamorphic petrology that a surface-rock may change its mineral composition when its ambient pressure and temperature changes. The mineral phase changes can be conveniently summarized in phase diagrams showing the stability fields of the different mineral phases. The phase transition from one mineral assemblage to another is, however, a complicated process. In the simplest case, the equilibrium case, the phase transition occurs as soon as pressure and temperature exceed the stability field limits, so that a new mineral phase assemblage forms. However, phase transitions generally do not occur under equilibrium conditions but a certain 'over-stepping' of the critical p-T conditions is required for a phase transitions to happen. This 'over-stepping' behavior of metamorphic reactions is known as the kinetics of the reaction. Kinetically driven reactions may, however, not only depend on p-T 'over-stepping' but also on other external variables like deformation rate and the availability of a reacting fluid. Given the complexity of kinetically driven metamorphic reactions, realistic implementation of

kinetics into a dynamic subduction zone model is beyond the scope of this study and I will only address the equilibrium case.

The main goal of this study is to explore metamorphic slab water release during subduction. Under surface conditions rocks may be able to incorporate a certain amount of water into their crystal structure. The amount of water that is chemically bound in this rock depends upon its mineral composition (and of course the availability of water). When this hydrous rock subducts, its ambient pressure and temperature increases eventually exceeding the stability field of the initial mineral assemblage, so that a new mineral assemblage forms. This new assemblage may not be able to incorporate the same amount of water into their crystal structure, so that a fraction of the initial water is released.

The thermodynamic reason for the phase transition is that for the new p-T conditions the new mineral composition is energetically more favorable. This tendency of a mineral assemblage to minimize its Gibb's free energy provides the basis for computer models like PERPLEX to calculate synthetic phase diagrams. I use PERPLEX to calculate phase diagrams for different lithospheric hydrous rocks (sediments, crust, and mantle) and from these phase diagrams p-T water content grids. Since the kinetics of metamorphic reactions are neglected, these p-T water content grids only depend on pressure and temperature and can be pre-calculated to be used in the tracer particle advection scheme.

Another aspect of metamorphic reactions that has to be accounted for is latent heat of reactions. Metamorphic reactions may either be endo- or exothermic, i.e. they consume or release latent heat. This latent heat effect is accounted for in the temperature solution by using PERPLEX to calculate from the change in thermal enthalpy during a reaction an associated latent heat that is included in the thermal solution. To obtain a self-consistent solution an iterative solving scheme is necessary, since metamorphic reactions themselves depend upon the thermal solution.

2.4 Boundary and initial conditions

In the model setup described above the flow field is determined by the density and viscosity distribution within the modeling domain and by the boundary conditions. A 'good' choice of boundary conditions is therefore critical for the quality of the modeling results. There is, however, no unique set of generally accepted boundary conditions. Moreover, the choice of boundary conditions depends upon the geologic problem that should be solved for.

Velocity boundary conditions are usually a combination of two end-member cases: (1) to study the pure dynamics of subduction BCs should be chosen in way that no external kinetic energy is fed into the system - i.e. velocity and geometry should not be prescribed. (2) For more specific studies (e.g. of a certain subduction zone) usually more 'rigorous' boundary conditions have to be applied by prescribing speed and sometimes also the angle of subduction. In this study different boundary conditions are used for different problems and the exact choice of boundary conditions are explained in the individual chapters.

One common problem in modeling subduction zones is the numerical implementation of a lithospheric fault between the overriding and subducting plate. Different approaches have been proposed for modeling pre-existing faults: the simplest way is to make the fault zone weak, i.e. prescribe a low viscosity zone along the fault. This implementation of a fault reduces the coupling of the two plates significantly - the degree of decoupling is, however, somewhat arbitrary depending only on the prescribed viscosity. Numerically more sophisticated fault implementations prescribe the plate coupling (i.e. set it to zero) directly within the flow solver's stiffness matrix. This approach allows better control of the degree of coupling between the two plates. However, since the actual amount and depth extend of coupling between the two plates is largely unknown, none of these two implementation ways is intrinsically 'better' than the other and we use the simple weak zone formulation.

The major challenge in increasing the quality of modeling fault zones is that faults should ideally form naturally from the physics of the problem. For this to happen, however, the

still not completely understood subduction initiation problem would have to be simultaneously solved with subduction along the newly formed fault. Creating such complex models will be a question of further research.

2.5 Parameterized convection

In chapter 3 and 5 of this study I use a parameterized mantle convection model to solve for the geochemical water cycle of the mantle, i.e. how water outgassing at mid-ocean ridges and hotspots and water recycling at subduction zones may have changed with time. This parameterized mantle convection model solves for average mantle overturn rate as a function of time since accretion of the Earth and is based on the one presented by Phipps Morgan (1998). Here I will briefly review the model formulation.

The principal idea of the model is that the Earth's preferred way of losing its heat is mantle convection and that its mantle temperature has remained almost constant over geologic time. This implies that the amount of radioactive heat production has always been equal to the amount of heat lost by convection. The argument that mantle temperatures have remained fairly constant is based on komatiite data. Komatiites represent some of the oldest ultramafic magmatic rocks on Earth and provide a record of the thermal and chemical characteristics of the upper mantle through time. It is inferred from Archean komatiites that they were produced by melting a mantle that was 200-300$^{\circ}C$ hotter than present-day mid-ocean ridges. Furthermore, a decline in their abundance from the from the Archean to the Phanerozoic has been observed. The simplest explanation for these observations is secular cooling on the order of 200$^{\circ}C$ through time. However, even if secular cooling on the order 200$^{\circ}C$ occurred during Earth history, the released heat would only add up to $\sim \frac{1}{4} - \frac{1}{3}$ of the heat released by radioactive decay, so that it is only of secondary importance. It is therefore a valid simplification to assume that radioactive heat production has always been equal to convective cooling; under this assumption it can be shown that the mid-ocean ridge differentiation rate (or average plate speed R) is

proportional to the square of planetary heat loss, Q (which in this scenario is equal to radioactive heat production).

Heat loss by convective cooling at the Earth surface can be written as:

$$\begin{aligned} Q &= R\sqrt{\frac{X}{R}}c\Delta T \\ Q &= R\frac{1}{\sqrt{R}}\sqrt{X}c\Delta T \\ Q &= \sqrt{R}\sqrt{X}c\Delta T \\ Q^2 &\sim R \end{aligned} \tag{2.23}$$

Here it is assumed that ΔT is the temperature difference of the cold thermal boundary layer at a trench, X is the given plate length, R the plate speed, and $c\sqrt{age} = c\frac{X}{R}$ the thickness of the boundary layer with $c = 10km/\sqrt{Ma}$. These consideration show that the average plate speed or mantle overturn rate is proportional to the square of radioactive heat production.

Based on the same arguments an average seafloor age, A, can be inferred.

$$\begin{aligned} Q = R\sqrt{\frac{X}{R}}c\Delta T = R\sqrt{A}c\Delta T \\ Q &= \frac{X}{A}\sqrt{A}c\Delta T \\ Q &= \frac{1}{\sqrt{A}}Xc\Delta T \\ Q^2 &\sim \frac{1}{A} \end{aligned} \tag{2.24}$$

This parameterized mantle convection model allows the formulation of equations for water outgassing at ridges and hotspots and water recycling at subduction zones as functions of average mantle overturn rate.

The water outgassing rate at hotspots and ridges is:

$$H_2Oout(t) = \frac{R(t)}{R_0}P_0 f_{H2O} H_2O_{mantle}(t) \tag{2.25}$$

Here it is assumed that 99% of the water/volatiles passing through the mid-ocean ridge and hotspot melting region are outgassed, so that $f_{H2O} = 0.99$; $R(t)$ is the average plate

speed at time t and R_0 the present-day value; P_0 describes the fraction of mantle that is currently processes at ridges and hotspots per time, and $H_2O_{mantle}(t)$ is the changing water content of the mantle.

The water recycling at subduction zones can be written as:

$$H_2Oin(t) = \frac{R(t)}{R_0} S_0 H_2 0ret(t) \tag{2.26}$$

Water recycling at subduction zones is expressed by the normalized plate speed $\frac{R(t)}{R_0}$ times the present day spreading rate, S_0, times the amount of water retention in subducting slabs, $H_2 0ret(t)$. This function, water retention as a function of time, is determined from the 2D subduction zone model described in the foregoing sections.

These equations are simultaneously solved for water content of the mantle and exosphere and water outgassing and recycling rates at ridges/hotspots.

Serpentine and the Subduction Zone Water Cycle

Lars H. Rüpke, Jason Phipps Morgan

IFM-GEOMAR, Geodynamics Group, Wischhofstr. 1-3, D-24148 Kiel, Germany

Matthias Hort

Universität Hamburg, Institut für Geophysik, Bundesstr. 55, D-20146 Hamburg, Germany

James A. D. Connolly

ETH-Zentrum, Institut für Mineralogie und Petrologie, Sonneggstr. 5, CH-8082, Zürich, Switzerland

Earth and Planetary Science Letters

in review

Chapter 3

Serpentine and the subduction zone water cycle

This study explores a chemo-thermo-dynamic subduction zone model that solves for slab dehydration during subduction. We investigate how changes in the incoming plate's hydration and thermal structure may effect the efficiency of sub-arc water release from sediments, crust, and serpentinized mantle. We find that serpentinized lithospheric mantle may not only be an important fluid source to trigger arc melting but is also an efficient 'transport-lithology' to recycle chemically bound water into the deeper mantle. In fact, an old slab may remain sufficiently cold during subduction to retain up to 40% of its initial 'mantle' water at 8GPa (∼240km depth) after serpentine transforms to higher pressure hydrous phase A.

Furthermore, deep water recycling at subduction zones is parameterized in terms of slab age and speed. Coupling this parameterization to a parameterized mantle convection evolution model allows us to calculate the mantle-surface geologic water cycle throughout the Earth's history. We find that the present-day Earth mantle may be highly outgassed containing only a small fraction of the Earth's water, which would mostly be recycled water from the exosphere.

3.1 Introduction

The subduction zone water cycle, i.e. the hydration and dehydration of subducting oceanic lithosphere, is a key process in understanding arc magmatism and volatile recycling processes. Hydration of oceanic crust begins at mid-ocean ridges through high-T and low-T hydrothermal alteration and, continuing more slowly as the seafloor ages. During the plate's residence at the seafloor, sediments are continuously deposited onto it adding material containing both pore and chemically bound water. Finally, there is increasing speculation that as the plate bends during subduction its cold lithospheric mantle may become significantly hydrated (e.g. Peacock 2001; Ruepke et al. 2002; Ranero et al. 2003b; Kerrick 2002).

Dehydration occurs deeper within the subduction zone by fluid releasing metamorphic reactions. These rising fluids flux the mantle wedge where they are commonly believed to trigger arc melting (Fig. 3.1). It is now commonly accepted that arc lava chemistry shows a subduction component originating from the preferential transport of fluid mobile elements from the slab into the arc melting region (e.g. Elliot et al. 1997). Likewise, most recent studies agree that subduction related recycling of altered, i.e. hydrated, oceanic lithosphere is necessary to explain some aspects of the mantle's chemical evolution (e.g. Hofmann 1997). Element recycling within the subduction factory is therefore intimately linked to the subduction zone water cycle.

But the subduction zone water cycle is also related to the formation and evolution of the oceans. Although the initial Earth probably accreted a large amount of exospheric water it is likely that the moon forming impact led to the desiccation of the exosphere. After this impact, strong volcanic activity on the young Earth led to the outgassing of water from the mantle which ultimately formed the oceans. It remains, however, a matter of vigorous debate how much water remained within the mantle, how much outgassed into the oceans, and how much water is potentially recycled back into the mantle at subduction zones. A better understanding of the subduction zone water cycle therefore helps to better understand the chemical evolution of the Earth's mantle and exosphere.

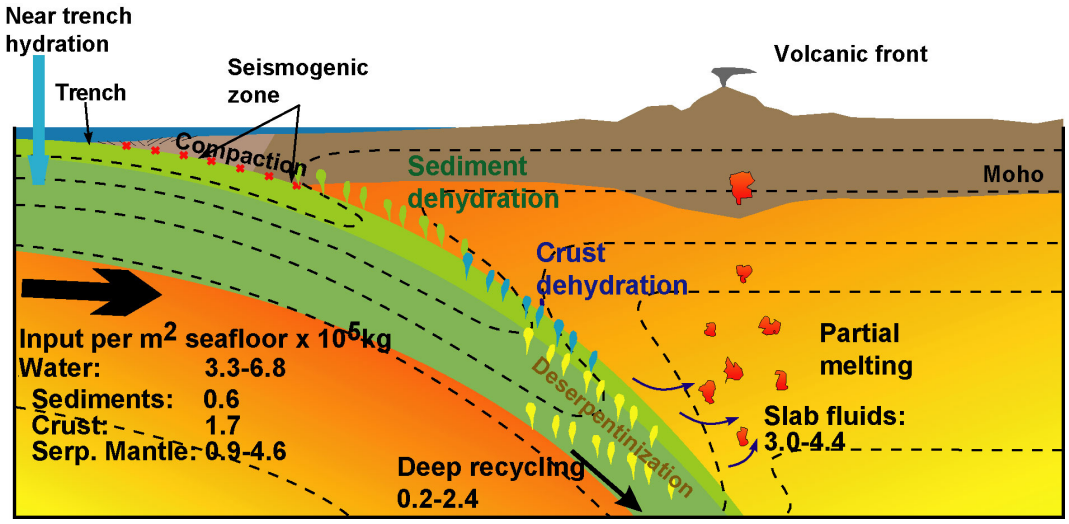

Figure 3.1: *Schematic drawing of the subduction zone water cycle. Water is chemically bound within the incoming plate's sedimentary, crustal, and mantle portions. During subduction, first the subducting sediments dewater and at sub arc depths fluids fluxing from the crust and the serpentinized mantle trigger arc melting; some fraction of the incoming plate's water content is recycled to greater mantle depths. Contour lines illustrate schematically temperatures at a subduction zone.*

To further constrain this water cycle, the water input into a subduction zone and the amount of sub-arc water release both have to be known. Unfortunately, determining the water input into a subduction zone is not easy. While fairly good (and converging) estimates exist for the sediment and crustal portions of the incoming plate (Plank and Langmuir 1998; Staudigel et al. 1996; Kerrick and Connolly 2001b; Wallmann 2001), much less is known about the lithospheric mantle's degree of hydration (Kerrick 2002; Ranero et al. 2003b; Schmidt and Poli 1998).

In order for surface fluids to hydrate mantle rocks, the fluids must be able to pass through the sediments and crust to reach the mantle. Normal faults occurring during plate bending between the outer rise and the trench axis provide possible fluid pathways for deep water transport. High resolution, deep imaging, seismic reflection profiles show normal faults that cut across the crust at least (>15km) deep into the lithospheric mantle (Ranero et al. 2003b). These 'bend-faults' may act as conduits for sea water to reach and react with lithospheric mantle rocks to make serpentine. In this scenario the incoming lithospheric

mantle would be highly serpentinized around these faults while the unfaulted parts would be practically dry. The average degree of serpentinization/hydration would then depend on the 'spacing' of bend-faults between the trench axis and the outer rise.

'Lithospheric' serpentine is commonly seen in Alpine peridotites, and based upon this evidence serpentinites have previously been proposed to be a significant source of water during sub-arc slab dewatering (Ulmer and Trommsdorf 1995; Schmidt and Poli 1998). Slab-mantle dehydration has also been related to double zone earthquakes (Seno and Yamanaka 1996; Peacock 2001; Dobson et al. 2002; Kirby et al. 1996), arc magmatism (Ruepke et al. 2002), and a water-flux-forced transition from gabbro to eclogite in the subducting slab (John and Schenk 2003). However, none of these studies can provide good estimates of the extent of downgoing lithosphere serpentinization. Serpentinites are known to have lower seismic P-wave velocities than peridotites, but as yet no good subcrustal velocity models exist save for two recent studies off Nicaragua and Chile which seem to show reduced Moho P-wave velocities between the trench axis and the outer rise (Berhorst et al. 2003; Sallares and Ranero 2003) consistent with up to $\sim$20% near Moho serpentinization.

Unfortunately, the dehydration part of the subduction zone water cycle, i.e. the efficiency of slab dewatering through metamorphic reactions, is also quite poorly constrained. Seismic tomography, as well as geochemical studies, can provide some insights into the amount of slab derived water in the mantle wedge, but so far thermal models seem to be the most promising 'tool' for study of sub-arc water release. Here, we use a numerical model to determine a self-consistent water budget for subduction zones to help to further constrain recycling processes at convergent margins.

3.2 Modeling

Several previous studies have used different approaches to model the thermal and petrologic structure of subduction zones. First, Davies and Stevenson (1992) and later Peacock

(1996) and Peacock and Wang (1999) presented 'kinematic' models in which the (steady state) flow field is completely prescribed by the boundary conditions. This type of model is mainly used to map the thermal structure of specific subduction zones. To understand the dynamics of subduction, models need to include buoyancy forces, so that the flow field is time dependent - see e.g. (Kincaid and Sacks 1997; van Hunen et al. 2000; Funiciello et al. 2003; Ruepke et al. 2002). Furthermore, there are 'hybrid' models that contain ingredients of both model-types which are mainly used to study specific aspects of subduction that do not necessarily need a fully dynamic solution. Examples of this are studies of mantle wedge dynamics in the framework of a kinematically driven slab e.g.(van Keken et al. 2002; Gerya and Yuen 2003).

Studies of the petrologic structure of subduction zones have so far mainly focussed on plotting calculated geotherms onto phase diagrams (Hacker et al. 2003a; Hacker et al. 2003b; van Keken et al. 2002; Peacock 1996). This approach is useful to generally explore which metamorphic reactions may take place during subduction but does not include any feedback mechanisms like metamorphic cooling due to latent heat consumption.

Here we present a self-consistent model for temperature, mantle flow, and water release at subduction zones. The model includes buoyancy forces but assumes a kinematically driven slab. Metamorphic reactions are self-consistently implemented using tracer particle and synthetic phase diagrams calculated with the thermodynamic tool-box PERPLEX.

3.2.1 Governing Equations

The flow field is modeled assuming a viscous (Stoke's) flow model and the Boussinesq approximation:

$$\frac{\partial \tau_{ij}}{\partial x_j} - \frac{\partial p}{\partial x_i} - \rho g_i = 0 \tag{3.1}$$

$$\tau_{ij} = \mu \left(\frac{\partial u_i}{\partial x_j} + \frac{\partial u_j}{\partial x_i} \right) \tag{3.2}$$

$$\frac{\partial u_i}{\partial x_i} \equiv \dot{\varepsilon_v} = 0 \tag{3.3}$$

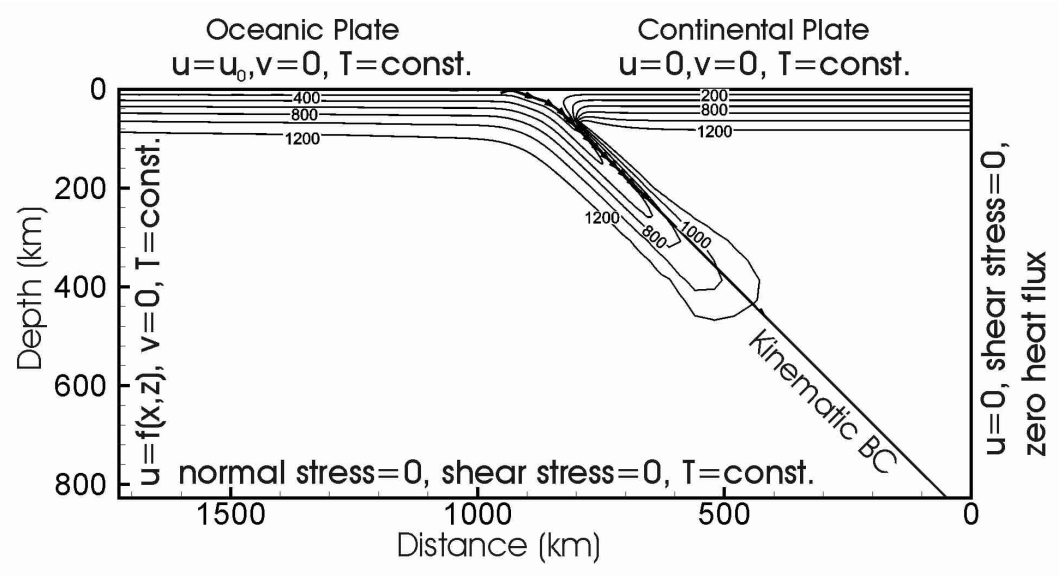

Figure 3.2: *The modeling domain. We use a asymmetric mesh with a maximum resolution of 2km in the regions of slab dewatering.*

Equation (3.1) is the force balance, (3.2) the constituative law, and (3.3) the incompressibility constraint. The variables are the stress tensor τ_{ij}, the pressure p, the density ρ, the gravitational attraction vector $\mathbf{g}$, the viscosity μ, the velocity vector $\mathbf{u}$, the physical coordinate vector $\mathbf{x}$, and the volumetric strain rate $\dot{\varepsilon_v}$ (see Table (3.1) for a complete list of variables). Density variations only affect the buoyancy term in (2.5), so that:

$$\rho(T, dp) = \rho_0 \left(1 - \alpha(T - T_m) - \beta dp\right). \tag{3.4}$$

Here, T is the temperature, ρ the density and the two constants α and β are the thermal expansivity and the depletion buoyancy parameter. The depletion, dp, represents the total amount of melt extraction experienced by a parcel of mantle. Although we do not solve for melting in our model we use this parameter to account for compositional density differences within the slab and among the incoming and overriding plate.

As a cautious note we want to emphasize that although we account for buoyancy in the model formulation, the intra-slab flow field is almost entirely prescribed by the boundary conditions since we assume a kinematically driven slab (see section on boundary conditions). Although this is a simplification that prevents us from correctly treating the

dynamics of subduction, we chose to prescribe the slab in order to be able to explore for a wide parameter range the effects of different incoming plate ages and speeds on the thermal solution without having to carefully adjust for every model run the viscous and buoyancy forces to match a certain subduction rate.

Furthermore, we use a simple temperature dependent Newtonian viscosity law and augment it with a pressure dependence that crudely simulates an increase in 'deeper mantle' viscosity beneath 450km:

$$\mu(T,z) = \mu_0 \mu(z) exp\left[b\left(\frac{1}{T^*} - 1\right)\right] \tag{3.5}$$

$$\mu(z) = 1 + [(250-1)/2][1 + tanh(0.01(z-450))]; \tag{3.6}$$

b is a parameter characterizing the temperature dependence of viscosity Dumoulin et al.1999 and $T^* = \frac{T}{T_m}$ is the dimensionless viscosity. Note that we do not explicitly account for phase changes at the 410km and 660km discontinuity.

Once the flow field is known the advection diffusion equation for temperature can be solved. Here, we use a formulation of the heat transport equation that includes the latent heat effect of metamorphic reactions, i.e. the cooling of the subducting slab due to its devolatilization:

$$\frac{\partial T}{\partial t} + \left(u\frac{\partial T}{\partial x} + w\frac{\partial T}{\partial z}\right) - \kappa\left(\frac{\partial^2 T}{\partial x^2} + \frac{\partial^2 T}{\partial z^2}\right) + H_{wr}\frac{\partial \phi}{\partial t} = 0 \tag{3.7}$$

Here, u, w, x, and z are the horizontal and vertical velocity and distance components. H_{wr} is a latent heat term ($H_{wr} = \frac{L}{c_p}$) and ϕ is the weight fraction of chemically bound water. In our model calculation we do not include hydration processes, but rather prescribe an initial hydration of the incoming plate. As the subducting plate dewaters we assume that the liberated water 'leaves' the system, so that no new hydrous phases are formed during subduction. This implies that the term $\frac{\partial \phi}{\partial t}$ is always less or equal to zero.

3.2.2 Solving the equations

We use a combined finite element - finite difference technique to solve for mantle flow and temperature. For the mantle flow part we discretize the modeling domain into rectangu-

lar four velocity node - constant pressure finite elements, and use the penalty method to solve the flow equations. To solve the advection–diffusion equation we use the high precision finite differences algorithm MPDATA which has relatively small numerical diffusion problems (Smolarkiewicz 1984). Since the heat transport equation includes a source term that accounts for metamorphic cooling, we iterate to obtain a self-consistent temperature solution.

3.2.3 A tracer based model for slab petrology

We use a tracer particle advection scheme to track the subducting slab's chemical evolution. Tracer advection schemes have the advantage that they do not suffer from numerical diffusion, so that they are well suited for advecting non-diffusive properties like chemically bound water. First, we present the tracer method. Second, we will apply it to the specific problem of tracking chemically bound water during the subduction water cycle.
Standard tracer advection algorithms consist of four parts: the advection equation (2.20), an integration scheme, a localization process, and the Jacobi matrix determinations (Brock et al. 1998). A tracer's position is determined by its cell number and location, and can be expressed in physical, $\mathbf{x}$, or logical coordinates, $\boldsymbol{\xi}(0 < \xi_i < 1$, with i=x,z). The logical and physical coordinates are interconnected by the Jacobi matrix, $\mathbf{J}$, so that $\boldsymbol{\xi}= \mathbf{J^{-1}x}$. Logical coordinates have the advantage that whenever a logical coordinate is unbound after integration (i.e. $\xi_i < 0$ or $\xi_i > 1$) a tracer particle has changed cells and a localization process is necessary.
The tracer advection scheme can be written as:

$$\frac{\partial \bar{\xi}}{\partial t} = \left[\frac{\partial \mathbf{x}(\xi)}{\partial \xi}\right]^{-1} \cdot \mathbf{u_x}(\mathbf{x}(\xi, \mathbf{t})) = \mathbf{u}_\xi(\mathbf{x}(\xi, \mathbf{t})) \tag{3.8}$$

$$\bar{\xi}^{n+\frac{1}{2}} = \bar{\xi}^n + \mathbf{u^n} \cdot \frac{\Delta t}{2} \tag{3.9}$$

$$\bar{\xi}^{n+1} = \bar{\xi}^n + \mathbf{u}^{n+\frac{1}{2}} \cdot \Delta t \tag{3.10}$$

Symbol	Meaning	Value	Dimension
A	average sea floor age	$--$	Ma
A_{ocean}	average area of oceans	$--$	m^2
H_{wr}	heat of water release	$--$	K
$\mathbf{J}$	Jacobi matrix	$--$	$--$
L	latent heat	$--$	Jkg^{-1}
P_0	present fraction of mantle processed at ridges per year	1.0527×10^{-10}	a^{-1}
R	overturn rate of the Earth's mantle	$--$	$--$
R_0	present overturn rate of the Earth's mantle	9.5	Ga
S_0	present-day average spreading rate	2.7×10^6	m^2/a
T	temperature	$--$	K
T^*	dimensionless temperature	$--$	$--$
T_m	basal asthenosphere temperature	1573	K
T_0	surface temperature	273	K
V	total volume of water in the exosphere	$--$	m^3
b	temperature dependence of viscosity	15	
c_p	specific heat	1250	$Jkg^{-1}K^{-1}$
d	ocean depth	$--$	m
dp	depletion	$0 - 0.4$	$--$
f_{H2O}	volatile outgassing efficiency during melting	0.99	$--$
g	gravitational acceleration	9.81	$m\ s^{-1}$
h	change in sea level	$--$	m
n	time stepping index	$--$	$--$
p	pressure	$--$	Pa
t	time	$--$	s
u_0	convergence rate	6.0	cm/a
$\mathbf{u}(u, w)$	velocity vector	$--$	$m\ s^{-1}$
$\mathbf{x}(x, z)$	coordinate vector	$--$	m
α	thermal expansion constant	3×10^{-5}	K^{-1}
β	comp. buoyancy parameter	0.5×10^{-2}	$--$
$\dot{\varepsilon}$	volumetric strain rate	$--$	$--$
κ	thermal diffusivity	10^{-6}	m^2/s
ρ	density	$--$	$kg\ m^{-3}$
ρ_0	reference mantle density	3300	$kg\ m^{-3}$
μ	viscosity	$--$	$Pa\ s$
μ_0	reference viscosity	10^{19}	$Pa\ s$
ϕ	degree of hydration	$0 - 1$	$--$
τ_{ij}	stress tensor	$--$	$--$
ξ	logical tracer coordinate vector	$--$	$--$

Table 3.1: *Complete list of symbols and parameters used in the model formulation.*

where $\mathbf{u_x}$ is the physical coordinate velocity vector and $\mathbf{u}_\xi$ the logical coordinate velocity vector; n is the time stepping index and t the time. The integration scheme always contains a trade-off between speed and accuracy. A simple Eulerian integration scheme requires only one evaluation of the RHS of (3.8), but often critically reduces accuracy. We use a predictor-corrector advection scheme (3.9,3.10) that requires two evaluations of the RHS of the advection equation per time step but provides the required level of accuracy. Higher order integration schemes appeared to unnecessarily increase the computational costs without a noticeable change in particle tracking in the downgoing slab. The localization method is straight-forward since we use a structured orthogonal grid.

To model metamorphic reactions we treat each tracer as an object that contains in addition to its location and cell number also density, volume, water content, and thermal enthalpy. These properties are mapped and scaled onto the grid points (i.e. the cell nodes) using the finite element shape functions and each tracer's volume. The change in tracer properties during subduction is determined with look-up tables pre-calculated with the thermodynamic tool-box PERPLEX (Connolly and Petrini 2002). PERPLEX allows the calculation of p-T property plots for any constrained bulk composition.

3.2.4 Initial and boundary conditions

We solve the equation within a (1600km × 800km) sized rectangular box (Fig. 3.2). To enhance the resolution within the region of interest we use an asymmetric mesh (∼21000 nodes) with a maximum grid resolution of 2km in the subduction 'hinge-region'. For boundary conditions we assume: on the left-hand side of the box the horizontal velocity decreases linearly from the convergence rate at the top to zero at the bottom of the box – temperature is held constant at its initial value; the bottom of the region is assumed to be stress free and the temperature is constant; the right-hand side of the region is a symmetry plane with zero heat flux across it; the top surface has zero vertical velocity with the horizontal velocity of the overriding plate set to zero; the horizontal velocity of the incoming plate equals the convergence rate, u_0, and the temperature is constant. We

initialize the temperature field using a simple half-space model for oceanic lithosphere for the incoming plate and a continental geotherm for the overriding plate that corresponds to 70mW/m^2 surface heat flux (Roehm et al. 2000). We set the depletion by assuming that the degree of depletion rises linearly from 0% at a depth of 70km to 20% at the top of the incoming plate (this would be depletion due to MOR melt extraction) and from 0% at a depth of 70km to 30% at the top of the overriding, continental plate. To decouple the motion of the overriding plate from the subducting plate we prescribe "weak nodes" along the trench according to the initial slab dip (Kincaid and Sacks 1997). To isolate the effects of plate age and speed on slab dehydration (and exclude the potential impact of differing dip angles) we set the velocities at the slab surface to a prescribed value. This modification results in a more kinematically driven slab that subducts with constant dip (45°) and speed.

3.3 Water cycling beneath an arc

Water cycling beneath an arc depends on: (1) the incoming plate's initial hydration, (2) the amount of water release from the slab, and (3) the degree of water recycling into the deeper mantle. Water release and water retention depend upon the metamorphic reactions that occur during subduction and slab metamorphism is controlled by the thermal regime of subduction. We shall therefore first discuss the thermal solution of our model.

3.3.1 Sensitivity of the thermal solution to subduction parameters

In this study we explore how changes in subduction parameters (plate age and speed) may effect the thermal structure and thereby water release beneath an arc. Figure (3.3a-c) shows calculated p-T paths for different incoming plate ages and subduction rates. All solid lines refer to the slab surface and the dashed lines to p-T conditions 8km beneath

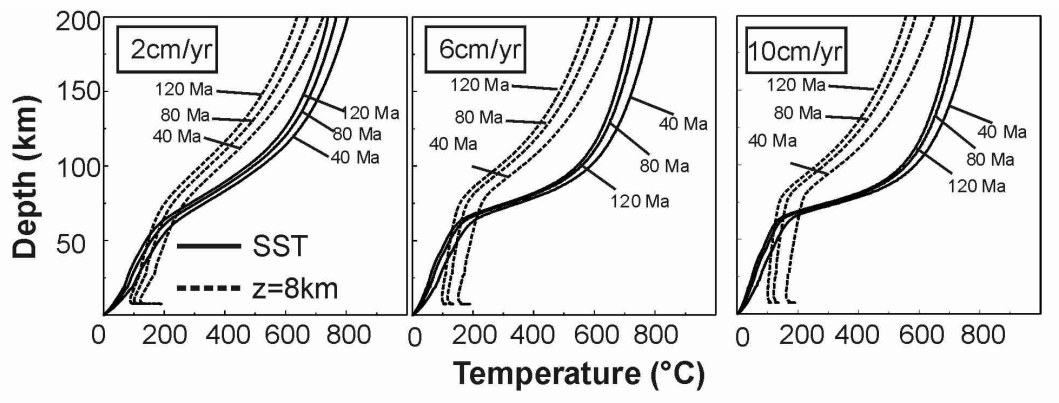

Figure 3.3: *Sensitivity of geotherms on subduction parameters. Solid lines show slab surface temperatures and dashed lines temperatures within the lithospheric mantle 8km below the slab surface.*

the slab surface within the uppermost lithospheric mantle. It is clear that for all convergence rates, temperatures within the slab are generally higher when young/hot seafloor is subducted. Differences in subduction rate do, however, influence the thermal solution in that slower subduction rates lead to hotter geotherms because the slab has more time to heat up by conduction.

Slab surface temperatures show in all cases a typical S-shaped form when plotted against depth: at depths <70km the geothermal gradient is low and the heating of the slab is dominated by heat conduction from the upper plate. At depths >70km, the slab surface is exposed to the hot convecting mantle wedge. Wedge convection leads to a steady flow of hot mantle material towards the slab which rapidly heats the slab surface and gives rise to a steeper geothermal gradient. Once the slab surface has heated up closer to mantle wedge temperatures, the geothermal gradient flattens again. However, the higher the subduction rate, the more pronounced the S-shape form of a geotherm. This results from the vigor of convection in the mantle wedge: the higher the subduction rate, the more vigorous is wedge convection with resultant stronger heating of the slab surface.

Temperatures within the subducted lithospheric mantle are not so affected by mantle wedge convection, since conduction is too sluggish to rapidly transport heat from the slab surface to the lower crust and upper mantle. Upper slab mantle geotherms therefore show

a less pronounced S-shaped form. The slab surface therefore heats up much more rapidly due to heating from the mantle wedge while the deeper parts of the slab may remain significantly colder during subduction leading to an inverted temperature profile.

These results are qualitatively and quantitatively close to the results of similar previous models: van Keken et al. (2002) found the same effects of wedge convection on slab surface temperature and when compared to Peacock and Wang (1999) estimates for 'hot' and 'cold' subduction, our geotherms represent intermediate to cold subduction temperatures. None of our geotherms comes close to 'hot' subduction because we neglect shear heating. We believe that high shear stresses are unlikely to occur within the fault zone; the feedback between shear heating and frictional strength will lead to a reduced strength of the décollement before significant heating can occur. Since the amount of shear heating is largely unconstrained, we have neglected its effects in these calculations. However, the good fit with previous models lets us believe that our thermal solution is stable and realistic.

Another geodynamic parameter we neglect but which may affect the thermal solution is the dip angle. The justification of this simplification is that the main application of this model is to calculate water recycling at paleo-subduction zones. While we get information on slab age and speed from a parameterized convection model (see section 5), no information is available for dip angle. For this reason we do not discuss how different dip angles affect the temperature field and use a constant dip angle in all model runs. Note, steeper dip angles usually result in slightly colder geotherms, since conduction has less time to heat up the slab.

3.3.2 The incoming plate composition and hydration

Plank and Langmuir (1998) defined an average composition of marine sediments (GLOSS). GLOSS contains 7.29 wt. % water and in our model runs we assume a sediment thickness of 350m. These values result in a water content of 0.6×10^5kg/m^2 in a column of sediment. Average ocean crust has a thickness of 6km and is only partially hydrated (see

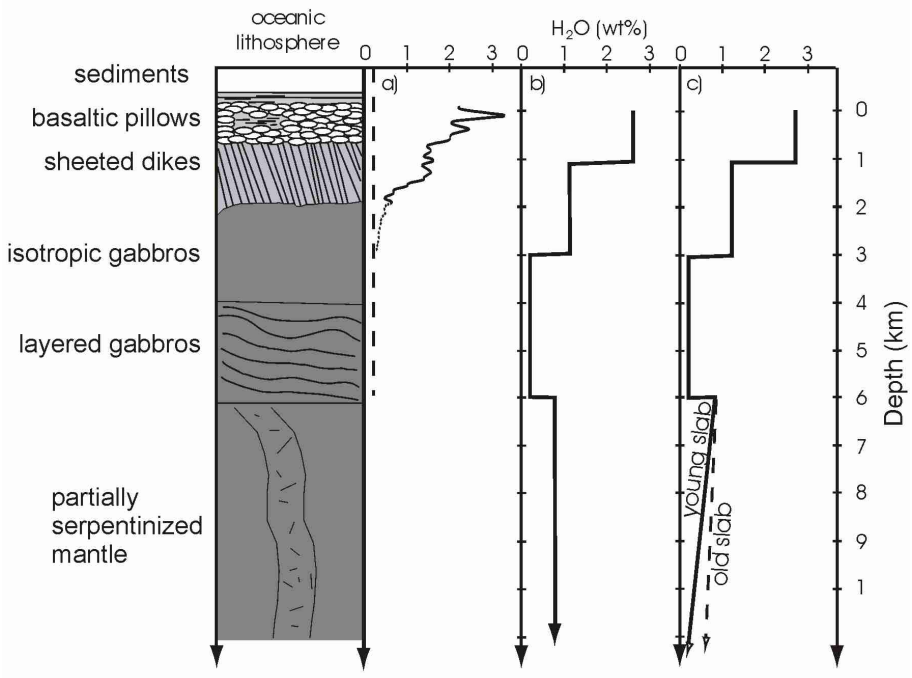

Figure 3.4: *Three different possible models illustrating the degree of hydration of typical oceanic lithosphere. The curve in (a) is based on literature values on the degree of hydration of oceanic crust. In (b) the incoming oceanic lithosphere includes a 10km thick partially serpentinized mantle layer. Our preferred model is shown in (c): we assume that the degree of lithospheric mantle serpentinization decreases linearly from 5% at the Moho to zero at the depth and temperature where serpentine becomes unstable (∼600°C). This model implies that old slabs contain more water bound in serpentine than young slabs.*

Fig. 3.4a). We make a conservative estimate of the average hydration of oceanic crust by assuming that top first kilometer is highly altered and contains 2.7 wt. % water. This highly altered layer is underlain by a less hydrated (1wt.% water) two km thick layer. The gabbroic lower portions are assumed to be anhydrous. This composition corresponds to a water content of 1.7×10^5kg/m^2 in a crustal column. In this study, we center on the role of serpentinized mantle for water cycling at convergent margins. Unfortunately, the oceanic lithospheric mantle's hydration is not well constrained. In our initial model runs we will assume that the incoming lithosphere contains a 10km thick weakly (5%) serpentinized mantle layer (2.0×10^5kg/m^2). Figure 3.4b illustrates this initial plate composition.

We use the PERPLEX tool-box to calculate the necessary phase diagrams and p-T property plots for hydrated sediments, crust, and mantle (Fig. 3.5). In a,b the phase diagram and p-T water content for GLOSS is shown (for a more detailed discussion of the phase relations see (Kerrick and Connolly 2001b)). For altered oceanic crust we use Staudigel's (1996) composition for metabasalt and c,d show the calculated phase relations and p-T water content - see (Kerrick and Connolly 2001a) for a more detailed discussion of the phase relations. As an initial composition of hydrated mantle, we use the one for harzburgite given in (Schmidt and Poli 1998) and the computed phase relations are shown in Fig. (3.5d,e).

3.3.3 Sub arc water release

We have made two example model runs assuming a young (40Ma) slab and an old (120Ma) slab to explore where fluids are released from a subducting plate. For these two cases, Fig. 3.6a,b shows the temperature field together with the regions of water release: green contour lines mark sediment dewatering, cyan contour lines water release from the crust, and yellow contour lines mantle deserpentinization, and c,d show the relative amount of water retention with depth.

The modeled pattern of water release from an 40Ma old slab, shown in Fig 3.6a, resembles the schematic scenario in Fig. 3.1. Water is continuously released from the subducting

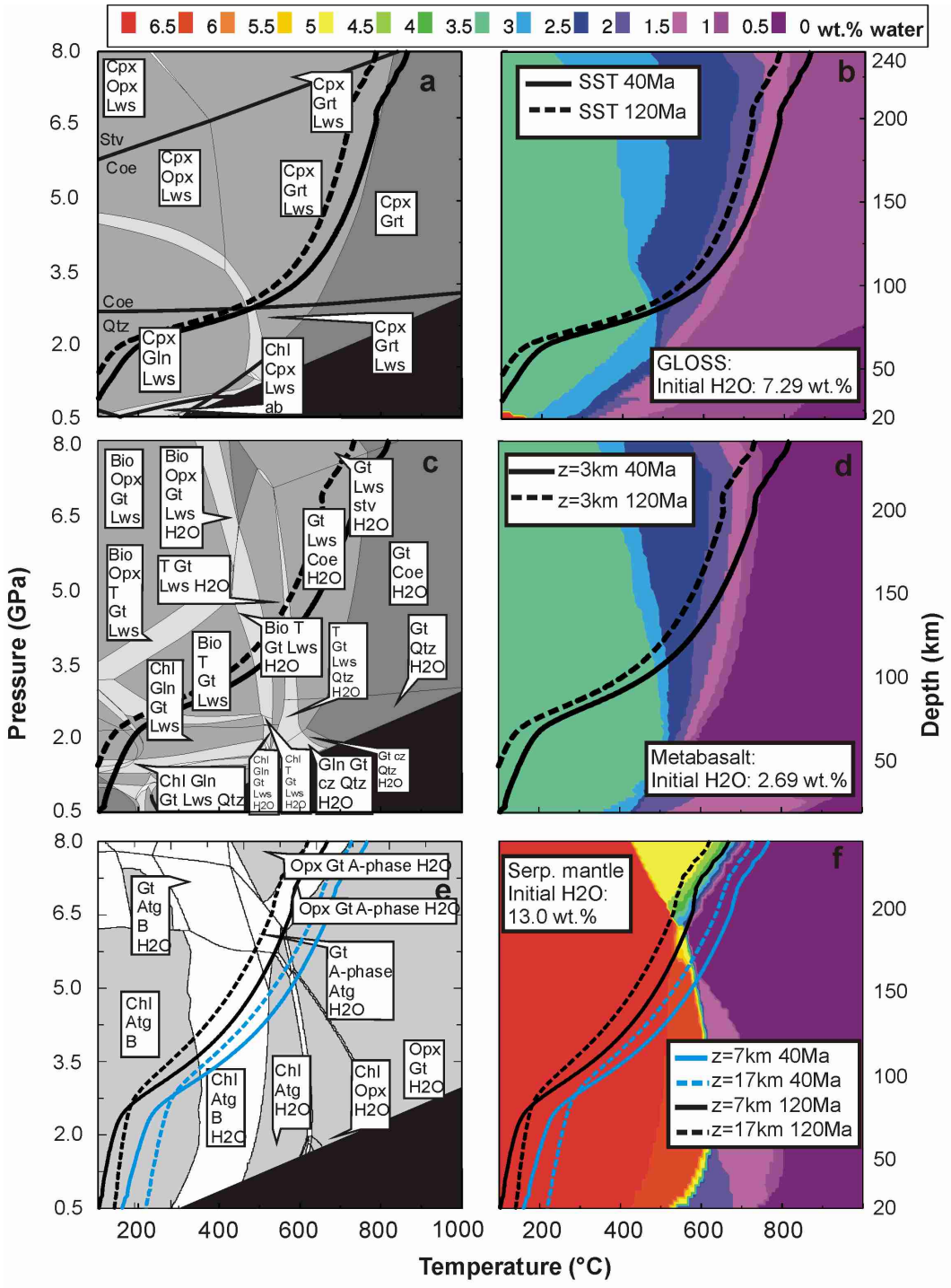

Figure 3.5: *Computed phase equilibria and p-T water content plots for the three different slab fluid sources GLOSS sediments, metabasalt, and serpentinized mantle. Mineral abbreviations are: A-phase; 'phase A'; Anth, anthophyllite; Atg, antigorite; B, brucite; Bio, biotite; Chl, chlorite; coe, coesite; Cpx, clinopyroxene; cz, clinozoisite; Gln, glaucophane; Grt, garnet; Lws, lawsonite; Opx, orthopyroxene; q, quartz; T, talc; stv, stishovite. Some mineral phases that are present in all fields have been omitted in the labelling: for GLOSS these are phengite, quartz/coesite, and fluid; for metabasalt clinopyroxene and phengite; and for hydrous peridotite olivine and clinopyroxene. Additionally, geotherms at different positions within 40Ma and 120Ma old subducting lithosphere are shown.*

slab with the host reservoir changing with depth. Sediments start to dehydrate at shallow depths, at ∼50km depth the sediments have already dewatered to over 50%, and by ∼100km they contain only ∼25% of their initial water chemically bound in residual lawsonite. The reason for the shallow dehydration is twofold: (1) the slab surface is the hottest part of the slab and (2) GLOSS contains initially a lot of water that that can only be chemically stored at low pressures and temperatures. Oceanic crust efficiently (∼92%) dewaters between ∼100km and ∼200km depth. The relatively deep dewatering of oceanic crust may partially result from the low initial water content: at low pressures and temperatures metamorphic reactions (e.g. chlorite and glaucophane breakdown) appear to be water conserving, so that dewatering does not start until the crust has heated up to approximatly $550°C$. Deep water recycling is controlled by the stability of lawsonite which is the main water carrier at higher pressures. Dehydration of serpentinized mantle occurs between 120km and 200km depth. When looking at the p-T paths plotted onto the phase diagram of hydrous peridotite in Fig. (3.5e,f) it is clear that temperatures within the entire hydrated mantle layer exceed the stability field of serpentine before 'phase A' can form, so that all water is released.

Comparing these results to the modeled pattern of water release from an older (120 Ma) slab (Fig. 3.6b,d) shows that the general pattern persists, so that first sediments, then crust and finally mantle dehydrates. The exact depths of water release do, however, change with the incoming plate's age; subduction of an older plate leads to colder geotherms (Fig. 3.3), so that fluid release from an older slab is less efficient and occurs at greater depths. Within a 120Ma old slab, oceanic crust may retain ∼23% of its initial water, and serpentinized mantle may retain even more water (∼35%). This efficient potential water retention in hydrous peridotites results from the altered thermal structure of the hydrated mantle layer: parts of this layer may remain cold enough ($<600°C$) for serpentine to transform to higher pressure 'phase A' thereby retaining some water to be recycled into the deeper mantle (Fig. 3.5e,f). It is clear that the total dehydration efficiency decreases with increasing incoming plate age: ∼95% for a 40Ma old slab and ∼71% for a 120Ma old slab. The model observation that parts of the slab's hydrated

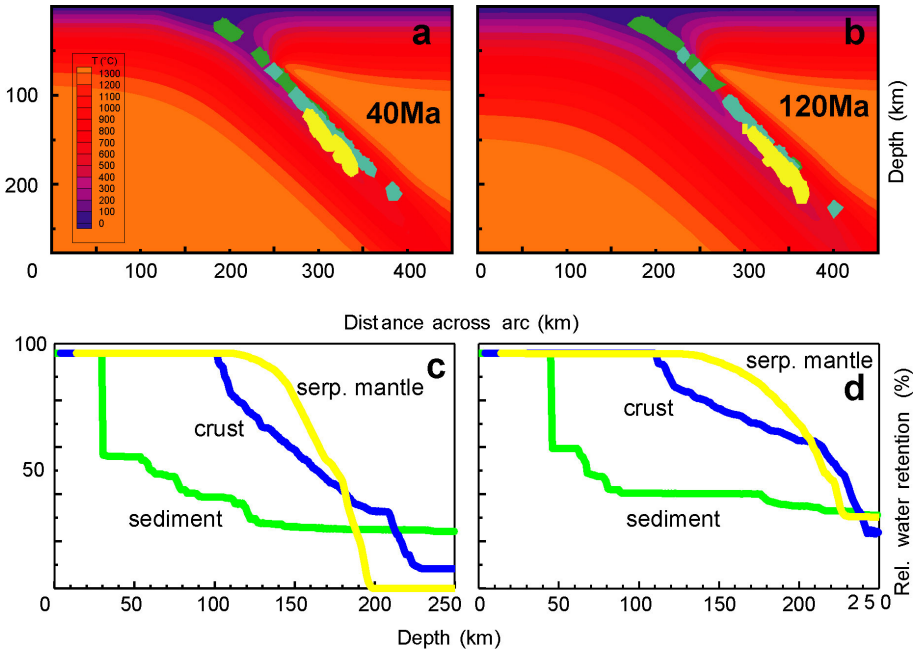

Figure 3.6: *Modeled water release at a subduction zone. In (a) and (b) the modeled regions of water release from subducting sediments (green), oceanic crust (cyan), and serpentinized mantle (yellow) is shown for a 40Ma and 120Ma old slab, respectively. (b) and (c) show th relative degrees of water retention at 8GPa for the three different lithologies.*

mantle may remain cold enough for serpentine to transform to higher pressure 'phase A' is consistent with the findings of a recent related study by Hacker et al. (2003a) and Hacker et al. (2003b)

These findings depend strongly, of course, on the validity of the computed phase relations. Especially deep water recycling in sediments and crust is strongly dependent on the accuracy of the calculated phase relations for lawsonite. To minimize potential errors, we have carefully checked the calculated stability field of lawsonite with experimental data (Schmidt and Poli 1998) and find very good agreement. Deep water recycling in hydrated peridotites depends mainly on the reaction curve serpentine->phase A. Ambiguous experimental data exist for this reaction and we will discuss the synthetic phase relations we used in the next section.

3.4 Deep water recycling

We have shown that some fraction of a slab's initial water content may still be chemically bound at 8GPa (∼240km). While a small fraction of this water is likely to be bound in subducting sediments and oceanic crust, we will show that deep water recycling may easily be dominated by subducting hydrated lithospheric mantle, so that we here focus on the role of serpentine. But what happens to chemical water that 'survives' the primary stages of sub-arc dewatering? It is a vigorous topic of current research if and how slabs can recycle water into the transition zone or the deeper mantle (Angel et al. 2001; Poli and Schmidt 2002; Bose and Navrotsky 1998) - see (Thompson 1992) for a review of water in the Earth's upper mantle. For water to be transported into the deeper mantle an uninterrupted chain of hydrous minerals has to be stable towards higher pressures and temperatures. Up to pressures of ∼6GPa and temperatures of $\sim 600^{\circ}C$, serpentine is the dominant water carrier in hydrated mantle rocks. Above this 'choke point' the most likely water carrier minerals are the dense hydrous magnesium silicates (DHMS) (e.g. (Angel et al. 2001)). Of the DHMS, phase A is probably the only mineral stable at sufficiently low pressures and temperatures to form by the consumption of water liberated from the breakdown of serpentine. Mapping the stability field of phase A is, however, experimentally difficult and this stability field varies from study to study (Luth 1995; Pawley and Wood 1996). The situation is further complicated by the fact that most experimental studies use the simplified MgO-SiO_2-H_2O (MSH) system. In this aluminum and iron free reference system the stability field of phase A is maximum. For more complicated/realistic compositions little data is available. To address this problem we have modeled iron-solution in brucite, antigorite, and phase A by making the assumption that the enthalpic effect of octahedral iron substitution in these minerals is identical to that in chlorite as evaluated from the data of Holland and Powell (1998). This results in a reduced stability field of phase-A and the computed phase relations are shown in Fig. 3.5d. In our model runs we explore deep water recycling by studying how much water is still chemically bound at 240km depth. This value is the maximum amount of water that

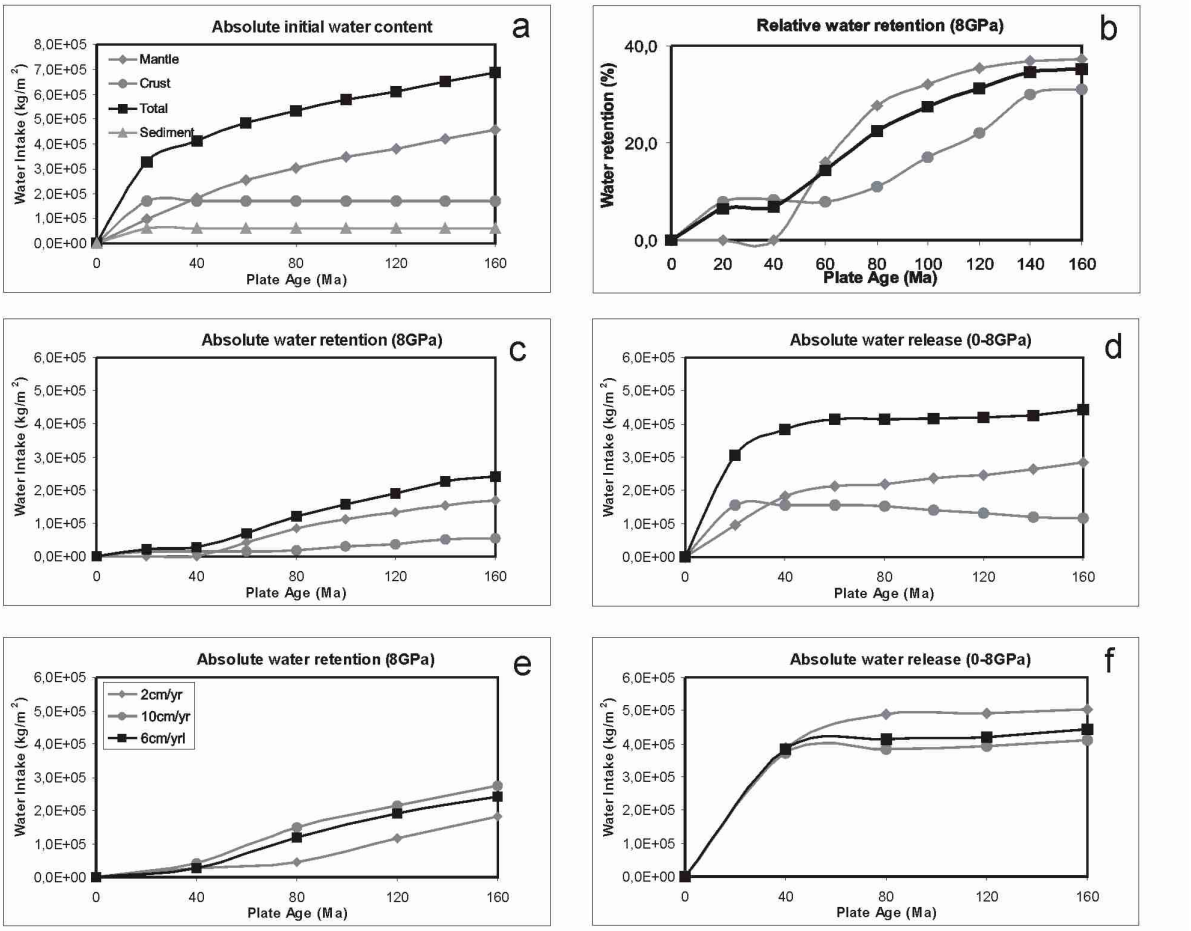

Figure 3.7: *Water intake, release, and retention of a subducting slab for varying plate ages. In (a) the amount of subducting chemically bound water is shown, (b) shows the relative water retention at 8GPa (∼240km depth), (c) the absolute amount of water retention, and (d) the amount of water release into the arc melting region. In (e) and (f) the total amount of sub arc water release and water retention at 8GPa is shown for different convergence rates.*

may be transported into the deeper mantle.

3.4.1 The role of plate age and speed

The results presented in section 3 have shown that the incoming plate's age affects the efficiency of fluid release during subduction. These calculations assumed a constant, i.e. age independent, initial plate composition. However, the thermal structure of the incoming plate may also affect its initial hydration. In our initial model runs we assumed a serpentinized mantle layer of constant thickness (10km). This thickness, however, is not consistent with the offset (up to 50km) between the upper and lower plane earthquakes in slabs that have double plane earthquakes. It has been previously speculated that the lower plane earthquakes may be triggered by serpentine dehydration (Seno and Yamanaka 1996; Peacock 2001; Dobson et al. 2002). This would, however, suggest that sea water circulation and therefore serpentinization may occur at depths of up to 50km within the bending plate. This might imply that maybe it is not the maximum penetration depth of sea water that is the depth limiting factor for slab serpentinization, but rather the fact that at a certain depth the slab simply becomes too hot ($>600°C$) to make serpentine. If the $\sim 600°C$ isotherm marks the maximum depth to which lithospheric mantle rocks may become hydrated, this implies that old plates may contain more water than young plates because the depth of this isotherm is plate age-dependent. We therefore speculate that a more likely incoming plate composition could include a hydrated mantle that is 5% serpentinized at the crust mantle boundary but the degree of serpentinization decreases linearly from an average of 5% at the Moho to 0% where serpentine becomes unstable ($\sim 600°C$) (Fig. 3.4c). Remember that these average values represent the 'spacing' of fully hydrated faults. Our incoming plate composition therefore implies that the number of hydrated faults reaching a given depth decreases linearly from the Moho with depth. In this scenario a column of serpentinized mantle of a young (20Ma) slab contains $0.9 \times 10^5 \mathrm{kg/m^2}$ of water and an old (160Ma) slab contains $4.5 \times 10^5 \mathrm{kg/m^2}$.

Figure (3.7) shows the outcome of a series of model runs in which we systematically vary

the the incoming plate's age and hydration. In (a) the total amount of subducted water is plotted, in (b) the relative water retention at 8GPa is shown, (c) shows the absolute water retention, and (d) the absolute amount of sub-arc water release as a function of incoming plate age. A closer look at the water retention at 8GPa shows that older slabs do not only contain more water (a) they also remain sufficiently cold during subduction to retain relatively more water than younger slabs (b) and thereby recycle also more water in absolute values to greater mantle depths (c). It is clear from the relative (b) and absolute (c) water retention at 8GPa that the amount of deep water recycling can easily be dominated by water retention within the subducting plate's serpentinized mantle layer. Lithospheric serpentinites may retain up to ∼40% of their initial water content (160Ma old slab; 10cm/a) and are therefore the most stable lithology to transfer chemically bound water beneath the primary depths of sub-arc water release into the deeper mantle. Note that water retention within the basaltic crust also increases with increasing plate age, so that a 160Ma old, rapidly subducting (10cm/a) slab may retain ∼35% of its initial crustal water.

It is clear from Fig. 3.7a that oceanic sediments do not contain enough water to significantly influence the subduction zone water cycle. We have therefore for clarity not explicitly plotted the results for sediments in (b-d); the sediment contribution is, however, included in the total values plotted in (b-f). In (d) the total amount of water release into the sub-arc melting region is shown. In contrast to water retention, sub-arc water release does not correlate with the total amount of subducted water. In fact, the amount of water release remains remarkably constant for differing plate ages/hydrations.

Another geodynamic parameter that may directly influence fluid release from a subducting slab is the convergence rate or plate speed. To constrain how differing plate speeds effect fluid release we have performed the same set of model runs with varying subduction rates. Plots (e) and (f) show the total amount of water retention and sub-arc water release for plates subducting at 2 cm/a and 10cm/a, respectively. These model runs show that higher subduction rates lead to 'colder' slabs and thereby less sub-arc water release.

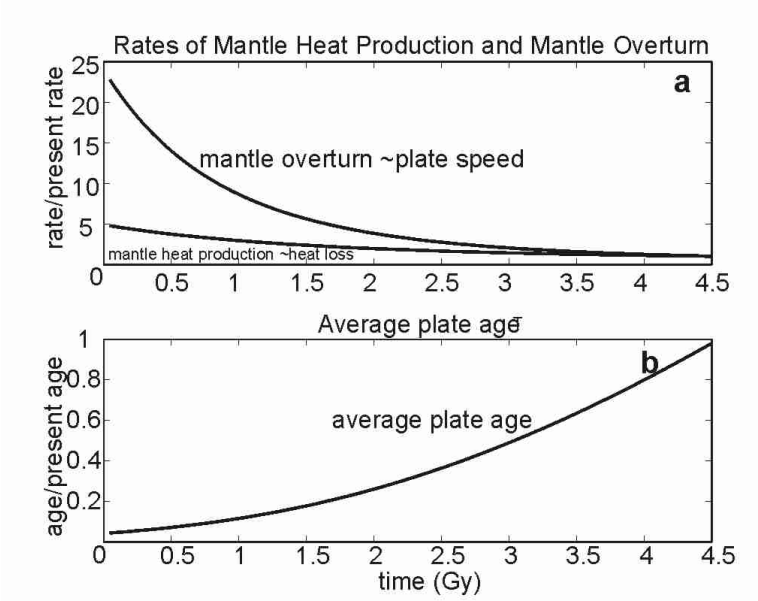

Figure 3.8: *Possible evolution of the mantle's average overturn rate (a) and ocean floor's average age (b). Estimates are based on the assumption that the overturn rate is proportional to the square of radioactive heat production.*

3.5 The geologic water cycle

So far we have discussed water cycling beneath an arc only on a local scale, i.e. we have not linked our results to the global geologic water cycle - the outgassing of water at mid-ocean ridges and hotspots and the recycling of water into the mantle at subduction zones. We will next explore water recycling at subduction zones on a global scale by linking our modeling results to the global geologic water cycle.

We have shown that the average plate age and overturn rate, i.e. the style of mantle convection, may influence the amount of water that is re-injected into the mantle at subduction zones. The style of mantle convection has probably changed over geologic time with the average overturn rate decreasing and the average seafloor (plate) age increasing with time. One way to determine the Earth's average plate age and overturn rate through time is to use a parameterized mantle convection model. Phipps Morgan (1998) proposed one possible parameterization and argued that if the Earth's mantle temperature has remained fairly constant over time then the amount of radiogenic heat production has

time since accretion (Ga)	total water retained	sediments	crust	5% serp. mantle
0.5	0.21	0.07	0.14	0.0
1.0	0.23	0.09	0.14	0.0
1.5	0.26	0.12	0.14	0.0
2.0	0.28	0.14	0.14	0.0
2.5	0.46	0.15	0.14	0.17
3.0	0.8	0.16	0.16	0.48
3.5	1.0	0.17	0.17	0.7
4.0	1.24	0.17	0.19	0.87
4.5	1.59	0.18	0.3	1.1

Table 3.2: *Water retention in a column of subducting slab as a function of the Earth's age. All values for water retention are given in $10^5 kg/m^2$.*

to be equal to the degree of convective cooling. This assumption yields the conclusion that the mantle overturn rate, R, is proportional to the square of radiogenic heating, Q, so that R$\sim$Q^2. Likewise, if subduction zones are difficult to form, the average seafloor age A will be inversely proportional to Q^2, i.e. A$\sim$1/Q^2. These considerations suggest that the average slab age and speed evolved over geologic time as shown in Fig. (3.8). In (a) it is seen that the mantle differentiation rate and thereby the average plate speed has experienced a 25 fold decrease while the average plate age has increased by a factor of $\sim$25 over time (b). Note, that these implications may be significantly different if the Earth's mantle temperature has strongly changed over geologic time; the argument that it remained constant (or cooled by less than $300°C$) is based on komatiite data and Phipps Morgan (1998) gives a more thorough explanation - see (Grove and Parman 2004) for a review of komatiites and the thermal evolution of the Earth.

We use these values to parameterize water retention in subducting plates as a function of Earth age. We do this by running a series of models assuming the different plate ages and speeds provided by the parameterized mantle convection model. To the outcome of these model runs (Table 3.2) we fit a function that thereby provides slab water retention as a function of time since accretion, H20ret(t). We can now deduce equations for water

ougassing and water recycling as a function of time:

$$H_2Oout(t) = \frac{R(t)}{R_0} P_0 f_{H2O} H_2O_{mantle}(t) \tag{3.11}$$

$$H_2Oin(t) = \frac{R(t)}{R_0} S_0 H20ret(t) \tag{3.12}$$

Here P_0 is the ridge differentiation rate that describes the fraction of mantle that is currently 'processed' at mid-ocean ridges and hotspots per time; it is deduced from the present day overturn rate of the mantle $R_0 = 9.5Ga$. The term f_{H2O} is set to 0.99 and describes the degree of volatile loss during melting and $H_2O_{mantle}(t)$ is the changing water content of the mantle, and S_0 is the average present day spreading rate $2.7km^2/a$. Note that the above equations imply that the total trench length has remained constant through time.

Solving these equations yields an evolution curve for water in the mantle and exosphere over geologic time. To make this value more comparable to geologic observations, we use a simple model to transform changes in the exosphere's water to sea level changes. This model is based on the assumption that the global area occupied by oceans (A_{oceans}) and continents, respectively, has remained constant over time. However, the average seafloor age has changed with time and we do account for changes in ocean depth (d) with seafloor age. Changes in ocean depth due to thermal subsidence can be written as:

$$d_{past} = 2500(m) + 233(\frac{m}{\sqrt{Ma}})\sqrt{\tau(Ma)} \tag{3.13}$$

$$d_{now} = 2500(m) + 233(\frac{m}{\sqrt{Ma}})\sqrt{100(Ma)}; \tag{3.14}$$

and the present-day (V_{now}) and past (V_{past}) volumes of water in the exosphere are:

$$V_{now} = (d_{now} + 0)A_{oceans} => A_{oceans} = \frac{V_{now}}{d_{now}} \tag{3.15}$$

$$V_{past} = (d_{past} + h_{past})A_{oceans}. \tag{3.16}$$

In this scenario, sea level changes, h over geologic time can be written as:

$$h_{past} = \frac{V_{past}}{V_{now}} d_{now} - d_{past} \tag{3.17}$$

In this formulation, sea level changes are only due to exosphere water volume and mean seafloor depths variations through time - other factors like glaciation are not accounted for.

We iteratively choose for each model the starting conditions, so that the present day value of water in the exosphere (cont. crust plus oceans) of 2.2×10^{21}kg (Henderson 1986) is reproduced. We further initialize all model runs by assuming that 95% of the initial water is in the mantle at time zero. Figure 3.9 shows two typical evolution scenarios: (a,b) show a model run assuming 5% sub-Moho serpentinization and (c,d) show an evolution scenario that does not include water in the slab mantle. The solid lines in the upper panel plots (a,c) show water in the exosphere and the dashed-dotted line water in the mantle. We have further plotted the exosphere's ^{36}Ar fraction (normalized to the initial mantle value) as a reference curve for mantle degassing (dotted line). We assume that degassed mantle ^{36}Ar is not recycled back into the mantle but remains entirely in the exosphere, so that the exosphere's ^{36}Ar content is a measure for the degree of 'primordial' mantle degassing.

In (b,d) the water outgassing rate, the total water recycling rate at subduction zones, and the recycling rate in serpentinized mantle is plotted. To lose its much higher early heat production, mantle differentiation rates were much higher early on in Earth history, this resulted in much higher water outgassing rates. These outgassing rates were higher then the recycling rates at subduction zones (where young seafloor was being recycled), so that the exosphere's free water content increased and the mantle's water content decreased. In the model run that includes serpentine, after ~2.0Ga subduction becomes sufficiently cold for serpentine to transform to higher pressure hydrous 'phase A' and water recycling at subduction zones starts to dominate, so that the exosphere's water fraction decreases again. These conditions persist until the present resulting in a predicted continuous drop in exosphere water over the past ~2.25Ga. Present-day conditions are characterized by 0.49 'exospheres' of water in the mantle. In the model run that neglects serpentine as a water source (b,d), water recycling at subduction zone dominates over water outgassing only for the last 1Ga. This scenario results in 0.38 'exospheres' of water in the present

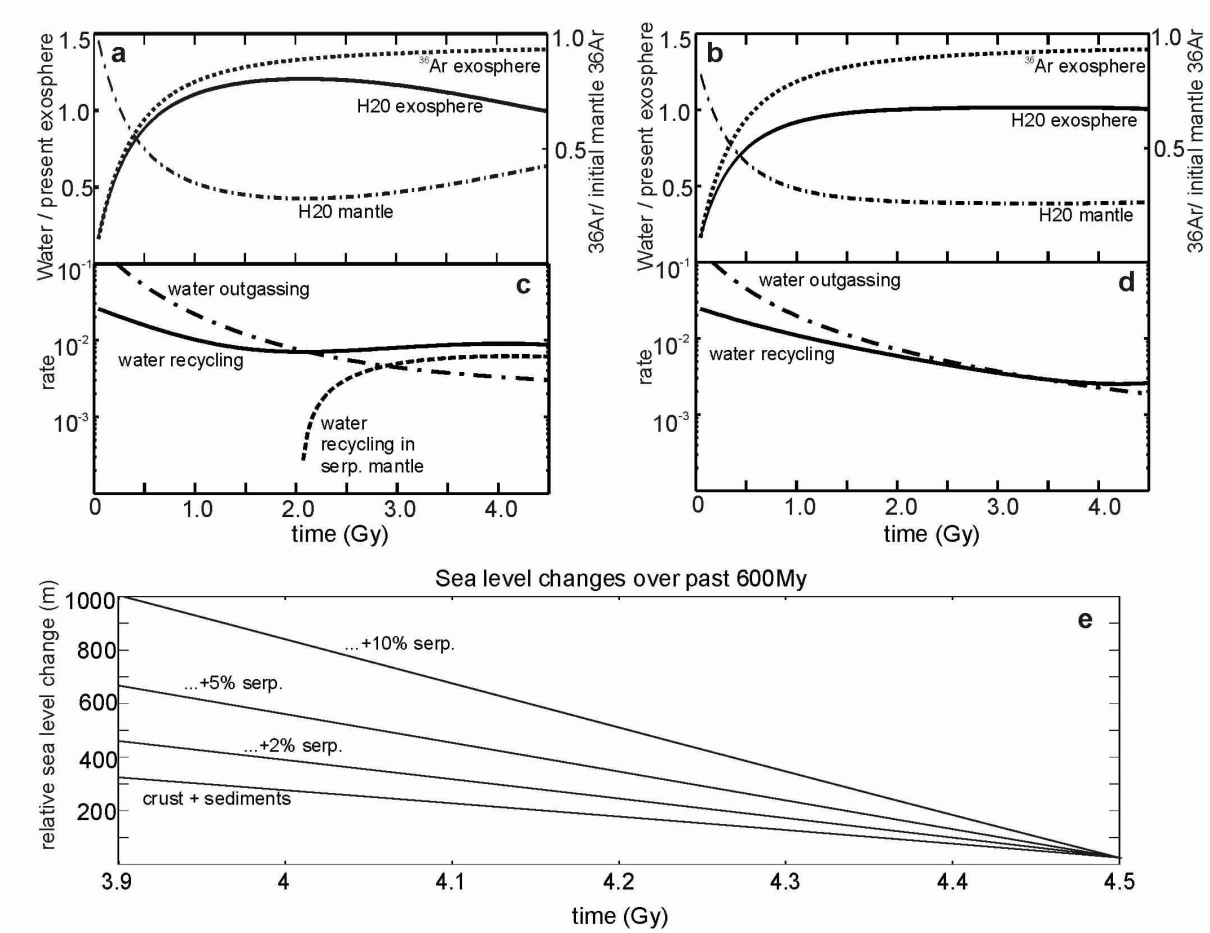

Figure 3.9: *The geologic water cycle. In (a,b) the water content of the Earth's mantle and exosphere is plotted against time along with the exosphere's ^{36}Ar content for two example model runs assuming 5% sub-Moho serpentinization (a) and no serpentinization (b); (c,d) show water recycling rates at subduction zones and the water outgassing rates at ridges and hotspots over time; (e) shows predicted sea level changes over the past 600Ma for four different model runs assuming different initial plate hydrations (degree of near Moho serpentinization). See the text for modeling details.*

mantle serp.	initial H2O	present H2O mantle	mantle H2O loss	outgassing
0%	1.4	0.39	72%	93%
2%	1.5	0.49	67%	93%
5%	1.63	0.64	61%	93%
10%	1.88	0.89	53%	93%

Table 3.3: *Model parameters used for the parameterized convection calculations. Initial water and present day water contents are in present-day 'exospheres'. In all model runs the present day water content in the exosphere is 1. See text for details.*

day mantle.

We have made a series of model runs assuming different degrees of sub-Moho serpentinization (0%-10%). The outcomes of these model runs are summarized in Table 3.3: the present day mantle has highly outgassed (93%) and contains only between 28% and 47% of its initial water content. Present day mantle water is therefore in all model runs mostly recycled water from the exosphere. Infered initial water contents of the Earth's mantle vary between 1.4 (0% serpentine) and 1.9 (10% serpentine) present-day 'exospheres' of water. In Figure 3.9e we show predicted sea level changes over the past 600Ma. We only show sea level changes for the last 600Ma because only for this age range good geologic data is available. Hallam (1992) estimated a maximum sea level drop of ∼500m over the past 600Ma. These estimates are consistent with less than ∼5% sub-Moho mantle serpentinization. Higher degrees of serpentinization seem to lead to too strong water recycling into the mantle to be consistent with global sea level changes since the Cambrian. In fact, even small degrees of serpentinization may have a big effect on sea level: 2% sub-Moho serpentinization causes a sea level change of ∼150m over the past 600Ma. However, when serpentine is neglected as a fluid host, subduction associated recycling of water in sediments and crust nonetheless influences the exosphere's water content. We find a 320m sea level drop over the past 600Ma for the 'no-serpentine' model run.

The above calculated water cycles have significant implications for the geodynamic evolution of the Earth. Depending on the degree of serpentinization, peak sea level conditions were reached between ∼2.5Ga (10% serp.) and ∼900Ma (0% serp.) ago. Also the relative

change in exosphere water volume between peak sea level and present-day conditions is strongly dependent on the amount of recycled water (i.e. the degree sub-Moho serpentinization): we find that for the four model runs (0%, 2%, 5%, 10% serpentinization) the relative change in exosphere water volume between peak sea level conditions and today are 1%, 8%, 18%, and 31%, respectively. This implies that the more water is re-injected into the mantle at subduction zones, the earlier in Earth history peak sea level conditions were reached, and the higher was the change in free water volume between peak sea level and present-day conditions.

Furthermore, the predicted geologic water cycle suggest strong water loss from the mantle into the exosphere, so that the present-day mantle contains only 'little' water that is mostly recycled water. This contradicts somewhat the results of some earlier studies that pointed out the potential existence of several 'oceans' of primordial water in the Earth's lower mantle and transition zone (e.g. Murakami et al. 2002). Part of this contradiction can be explained by the implicit pattern of mantle flow assumed in this studies. Here, we assume whole mantle flow, so that eventually the 93% of the mantle participates in near-surface upwelling, melting, and differentiation processes. The details of this mantle flow model are described in (Phipps Morgan and Morgan 1999). If a strictly layered Earth is assumed to have always existed, it is possible that this reservoir of incommunicative 'primitive' mantle water would still not yet have 'participated' in the surface geologic water cycle. However, for the reasons summarized in (Phipps Morgan and Morgan 1999), we still believe that strongly layered mantle convection is improbable. Furthermore, in this scenario water in the 'communicative' regions of the mantle will be dominated by recycled water.

3.6 Conclusions

We have formulated a two dimensional thermo-dynamical model that solves for the temperature and mantle flow within a subduction zone. Additionally, we have presented a

tracer based model to solve for slab fluid release. Using this model we have explored how slabs dewater during subduction and how water cycling at convergent margins may be related to the geologic water cycle. Several conclusions can be drawn from these calculations:

(1) Slabs seem to dewater continuously during subduction. However, the 'host' lithology of the released fluids changes with depth: first sediments dewater at shallow levels, second the altered ocean crust releases its water, and finally the hydrated lithospheric mantle deserpentinizes. This change in fluid source with depth may have strong implications for element recycling beneath arcs.

(2) Serpentinized mantle seems to be the best, i.e. most stable, lithology to transfer chemically bound water through the sub-arc dewatering region to greater mantle depths. Depending on the thermal structure of the subducting slab up to 40% of the water stored in serpentinized mantle may be transfered into the deeper mantle.

(3) The Earth mantle is likely to have lost most of its initial water (53%-78%) to exhale the oceans. Present day mantle water is mostly recycled water from the exosphere. Since ∼2-2.5Ga, when subduction became sufficiently cold, this water recycling may be dominated by serpentinized mantle even if small degrees of serpentinization are assumed.

Are the regional variations in Central American arc lava chemistry due to differing basaltic versus peridotitic slab sources of fluids?

Lars H. Rüpke, Jason Phipps Morgan

GEOMAR, Geodynamics Group, Wischhofstr. 1-3, D-24148 Kiel, Germany

Matthias Hort

Universität Hamburg, Institut für Geophysik, Bundesstr. 55, D-20146 Hamburg, Germany

James A. D. Connolly

ETH-Zentrum, Institut für Mineralogie und Petrologie, Sonneggstr. 5, CH-8082, Zürich, Switzerland

Geology

v. 40 n.11

November Issue

2002

Chapter 4

Are the regional variations in Central American arc lavas due to differing basaltic versus peridotitic slab sources of fluids?

Central American arc volcanism shows strong regional trends in lava chemistry that result from differing slab contributions to arc melting. However, the mechanism(s) that transfers slab-derived trace elements into the mantle wedge remains largely unknown. By using a dynamical model for mantle flow and fluid release, we model the fate of three different slab fluid sources: sediment, ocean crust, and serpentinized mantle. In the open sub-arc system, sediments lose almost all their highly fluid mobile elements by ∼50 km depth, so that other fluid sources are necessary to explain the 'slab signal' in arc-lava compositions. The well-documented transition from lavas with a strong geochemical slab signature (i.e., high Ba/La ratios) found in Nicaragua to lavas with a weaker slab signature (i.e., low Ba/La ratios) erupted in Costa Rica seems easiest to produce by a higher fraction of serpentine-hosted fluids released from the deeply faulted, highly serpentinized lithosphere

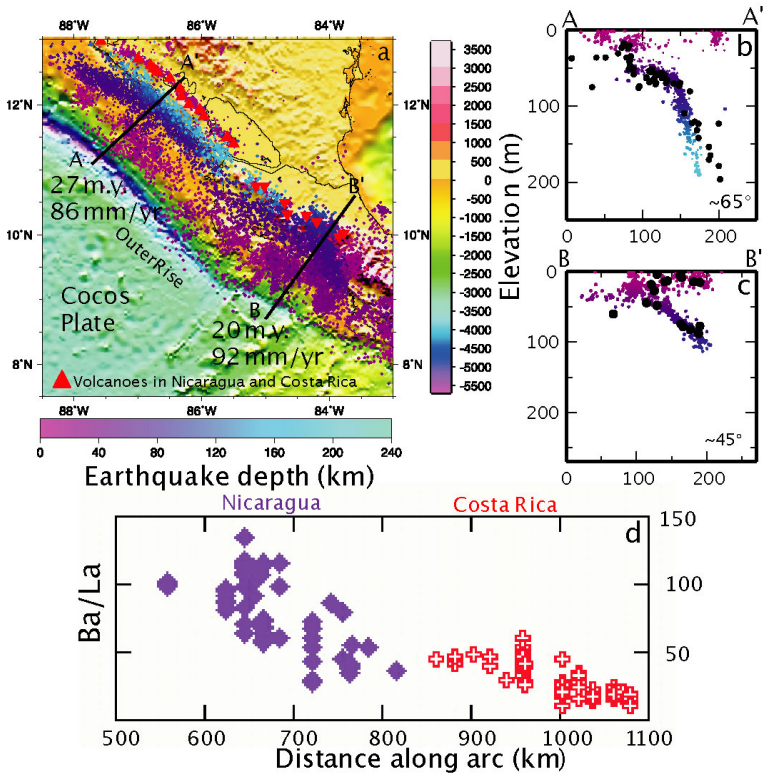

Figure 4.1: *Surface relief and earthquake distribution where Cocos plate subducts beneath Caribbean plate. Transect A-A' shows subduction beneath Nicaragua where outer rise (seaward from trench) develops numerous flexural faults (Huene et al. 2000) and dip angle is steep. Beneath Costa Rica, along transect B-B', dip angle is shallower. Changes in dip angle correlate with geochemical along-arc trends in lava chemistry as shown in D. Ba/La is chosen to exemplify the 'slab-fluid' signal in arc melting. Black dots mark newly relocated earthquakes (A. Villasenor, 2002, personal commun.).*

subducting beneath Nicaragua than from the less deeply faulted, thicker, amphibolitic oceanic-crust and oceanic-plateau lithosphere subducting beneath Costa Rica.

4.1 Introduction

Many subduction zones have well-described but poorly understood along-arc trends in the geochemistry of their arc lavas. Arc melting is generally thought to take place in the mantle wedge above the slab, where it is triggered by fluxing of hydrous fluids that are released by metamorphic dewatering reactions inside the downgoing slab. Chemically

bound water in the sedimentary, crustal, and mantle parts of the subducting plate is released at different pressure-temperature conditions that vary with the incoming slab's age, subduction rate, dip angle, and composition. At the Central American volcanic front major geochemical and tectonic variations occur within several hundred kilometers along strike for a plate of nearly constant age and subduction rate. Figure 1 summarizes the tectonic setting for subduction beneath Central America. The subduction angle changes from steep ($\sim 65^{\circ} C$) beneath Nicaragua to shallow ($\sim 40^{\circ} C$) beneath Costa Rica (Barckhausen et al. 2001; Protti et al. 1995). Nicaraguan arc lavas typically have high B/La, Ba/La, and $^{10}Be/^{9}Be$ ratios and low La/Yb ratios, characteristics that smoothly change along the arc toward Costa Rica, where arc lavas show low B/La, Ba/La, and $^{10}Be/^{9}Be$ ratios and high La/Yb ratios (Carr et al. 1990; Herrstrom et al. 1995; Patino et al. 2000). Carr et al. (1990) found that most of these variations can be effectively represented in terms of two parameters: (1) the La/Yb ratio, which represents the mantle source's enrichment in incompatible elements, and (2) the Ba/La ratio, which monitors the slab-derived fluid's contribution to arc chemistry. Nicaraguan arc-lava composition can therefore be explained by having a larger fluid contribution from the slab. The concentration of trace elements added to the produced melts by the slab-derived fluids reaches a minimum beneath Costa Rica (Carr et al. 1990; Leeman et al. 1994; Patino et al. 2000). Details of trace element transport from the slab into the mantle wedge remain unclear. In this study we further explore the mechanisms of trace element recycling at subduction zones by studying fluid fluxing from the slab with a dynamical model that solves for fluid release. We find that the depth interval and intensity of fluid release from hydrated sediments, amphibolized basalts, and serpentinized peridotites can potentially vary as a function of the incoming plate's composition and the degree of lithospheric bend-faulting at the outer rise. Along-strike chemical and tectonic changes in the incoming plate can lead to differing ratios of sediment- and serpentinite- to amphibolite-derived hydrous fluid release, which we suggest is a plausible mechanism to explain the observed changes in lava chemistry.

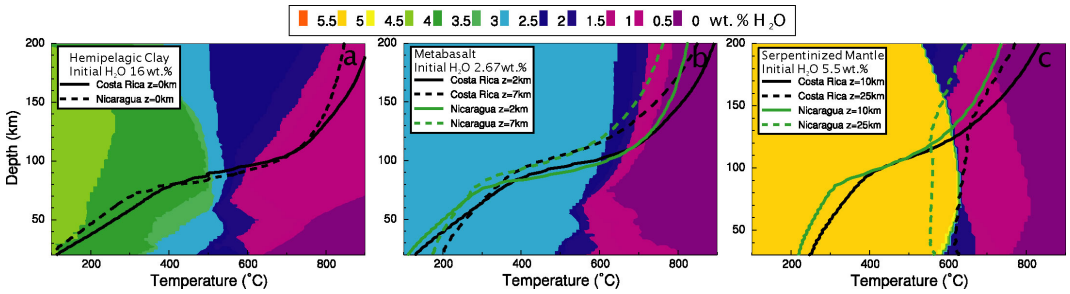

Figure 4.2: *Water content as a function of temperature and pressure for the three slab fluid sources used in the model calculations. Water contents are calculated using the PERPLEX program and the following initial compositions: (A) hemipelagic clay at DSDP Site 495 (Plank and Langmuir 1998), (B) Staudigel et al. (1996) 'Super Composite' metabasalt, and (C) serpentinized mantle (Kerrick and Connolly 1998). Also shown are geotherms for the three different lithologies for subduction beneath Costa Rica and Nicaragua. For details on PERPLEX see (Connolly 1990) and http://www.perplex.ethz.ch/.*

4.2 Modeling

Several different numerical models have been developed to analyze the tectonic, petrologic, and thermal structure of subduction zones (Davies and Stevenson 1992; Kincaid and Sacks 1997; van Hunen et al. 2000). To self-consistently model chemical dehydration reactions inside the downgoing slab, we have formulated a two-dimensional, dynamical model that continuously updates the flow, temperature, and compositional fields (see the electronic supplement for details). The flow-field solution is based on the Stokes equation for creeping flow solved by the penalty finite-element method (Zienkiewicz and Taylor 2000). The thermal evolution of the system is calculated from the heat-transport equation using finite differences (Smolarkiewicz 1984). To model fluid release we divide the downgoing lithospheric plate into hydrated sediment, amphibolite-basalt crust, and serpentinized-mantle layers. We model these layers using tracer-particles that are advected with the flow field. Each tracer-particle starts with an initial volume and hydration. As the P-T conditions of a tracer particle change, so may its water content. The model determines the changes in water content of the three different slab fluid sources using look-up tables (see Figure 2) created with the PERPLEX program (Connolly 1990). Fluid-releasing metamorphic reactions are endothermic (they consume latent heat); for proper internal consistency, we

include the associated enthalpy consumption of the metamorphic reactions in the temperature solution. The incoming plate's crustal thickness and the amount of chemically bound water in its oceanic lithosphere can vary along and between different subduction zones; e.g., seamounts and oceanic plateaus may significantly change the local incoming crustal thickness. Initial hydration of basaltic oceanic crust takes place at mid-ocean ridges. However, to hydrate mantle rocks, water has to be transported into relatively cool ($<600°C$) mantle. Lithospheric bend-faulting at the outer rise is a potentially viable mechanism to create and maintain the conduits for sea water to reach and react with cold lithospheric mantle. Such lithospheric serpentinites can store significant amounts of water that can be subsequently released during subduction (e.g., Ulmer and Trommsdorf 1995).

4.3 Fluid release beneath Nicaragua and Costa Rica

To apply this model to Central America we have to constrain the incoming plate's composition. The sediment input is reasonably well defined by DSDP (Deep Sea Drilling Project) Site 495. The sediment contribution can be divided into two layers: An ∼200-m-thick layer of hemipelagic clay overlies an ∼250-m-thick layer of carbonate oozes (Plank and Langmuir 1998). Here, we only explicitly model the upper hemipelagic layer of the sediments. We use this simplification because (1) most of the chemically bound water resides within the hemipelagic clay (16wt.% H_2O) compared to the carbonate oozes (1wt.% H_2O) and (2) most trace elements relevant to this study (i.e. B and ^{10}Be) are mainly enriched within the hemipelagic part of the sediment column. Beneath Nicaragua (transect A-A') we assume that the sediments, a 2km thick layer (Walther et al. 2000) of altered basalts (2.67wt.% H_2O), a 3km thick (Walther et al. 2000) gabbroic layer (1wt.% H_2O), and a 10km thick serpentinized mantle layer (5.5 wt.% H_2O) subduct (note that recent seismic surveys show lithospheric faults extending at least 10 km below the Moho in this region (Ranero et al. 2003a). As already explained, we believe that seawater

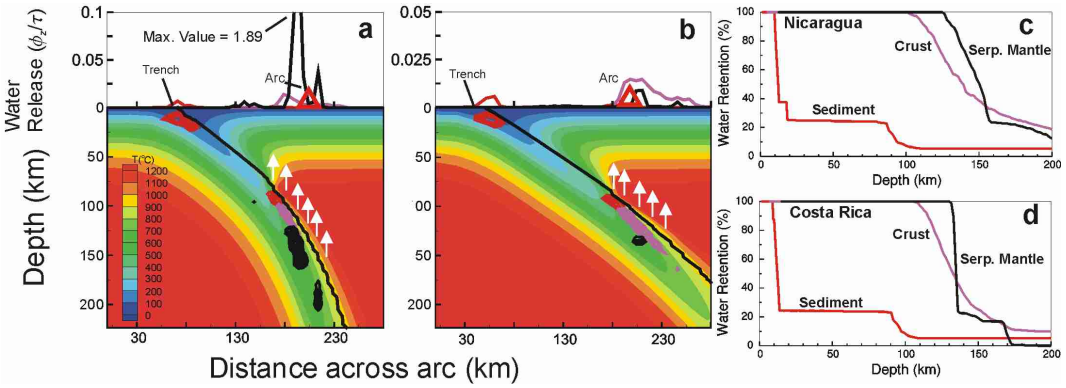

Figure 4.3: *Slab dehydration beneath (A) Nicaragua and (B) Costa Rica. Red contour lines show chemical water release from sediment; purple and black contour lines represent release from crust and serpentinized mantle, respectively. For Costa Rica the incoming columns of sediments, crust, and mantle contain* $1.1 \times 10^5 kg/m^2$, $7.9 \times 10^5 kg/m^2$, *and* $1.3 \times 10^5 kg/m^2$ *of water respectively, for Nicaragua the respective incoming columns contain* $1.1 \times 10^5 kg/m^2$, $3.6 \times 10^5 kg/m^2$, *and* $17.9 \times 10^5 kg/m^2$ *of chemically bound water. In each plot, upper panel shows depth-integrated rates of dewatering. This value* $(\Phi_z)/t$ *is proportional to the total amount of water release, where* f = *fraction of chemically bound water and* t *is dimensionless time,* $t = t/31.5$ *(where* t *is in millions of years). In (C) and (D) percentages of water retention are plotted. Sediments lose all their chemically bound water; crust and serpentinized mantle are more stable and do not completely dehydrate. The total amount of stored water is however highest in the serpentinized mantle, so that serpentinized mantle seems to be the most efficient lithology to recycle chemically bound water into the deep mantle. Note temperature contour interval is* $100^\circ C$ *; the basal astenosphere temperature is* $1300^\circ C$.

is transported through these faults into the cold lithospheric mantle to serpentinize it. Unfortunately little is yet known regarding the average degree of serpentinization in this environment. Serpentinites are known to have lower seismic velocities than peridotites, but as yet no good seismic velocity models exist for the sub-crustal part of the incoming plate in Nicaragua. We choose the composition of serpentinized peridotites and their initial water content in accordance with experimental and modeling data (Kerrick and Connolly 1998; Schmidt and Poli 1998). However, the pattern of slab dehydration reactions only weakly depends upon the initial degree of hydration, so that Figure 3A is likely to be fairly representative of the spatial dehydration pattern within transect A-A'. Figure 3A shows that the hemipelagic clay component loses ∼75% of its initial chemically bound water content during shallow (<50 km) dewatering (red contour lines). The basaltic crust dewaters mainly between 100 km and 140 km depth (purple contour lines) and the serpentinized mantle loses 80% of its initial water content between 130km and 160 km depth (black contour lines). The upper panel line plot shows the depth-integrated rates of dewatering that correlate with the total amounts of water release. Here serpentinized-mantle rocks are the dominant source of slab-derived fluids that flux the hotter regions of the overlying mantle wedge. The situation for the transect B-B' (Figure 1) across Costa Rica is quite different. Here the outer rise is much smaller, and flexural normal faulting is much less developed than it is to the north (Ranero et al. 2003a). We therefore assume a thinner (5 km) and less hydrated (2 wt% H_2O) mantle layer. The crust is slightly thicker (6-8 km) (Huene et al. 2000) - only reaching its maximum >20 km thickness (Cocos Rise) 100 km to the south of this transect. Here the incoming crust's layer 2 is thicker (∼4km), so that we assume that a 4km thick hydrated (2.67 wt. % H_2O) basaltic layer overlies a 4 km thick gabbroic layer (1 wt. % H_2O). Figure 3B shows the modeled situation along this transect: The sediments lose ∼75% of their chemically bound water during shallow dewatering; the crust mainly dewaters between 100 km and 140 km depth, whereas the serpentinites lose most of their stored water between 130 km and 150 km depth. The upper-panel plot in Figure 3B shows that amphibolites are the main source of the slab-derived fluid flux into this melting region.

4.4 Implications for trends in arc lava chemistry

4.4.1 Nicaragua Arc

Nicaragua arc lavas show high B/La and Ba/La ratios that both correlate with $^{10}Be/^{9}Be$. Because Ba/La and B/La are ratios of fluid-loving to rock-loving elements, the high values in these ratios in the arc lavas are usually thought to result from hydrous fluid fluxing out of subducting sediments and crust (Leeman et al. 1994; Patino et al. 2000). Figure 3 shows that water release from the basaltic crust, serpentinized mantle, and the deepest 'tail' of the sediments can occur near the proposed depths of arc melting, so that three different scenarios for trace element transport from the slab into the mantle wedge may be possible. One scenario is that either an aqueous fluid or melt released from the sediment layer produces the arc lava's enrichment in trace elements like B and ^{10}Be. Observed correlations between B/La and $^{10}Be/^{9}Be$ appear to support this (Morris et al. 1990). However, for highly fluid mobile elements, such as boron, this will only work if the bulk sediment reaches the melting region mostly unaltered, i.e., still containing its boron. In an open sub-arc system this is problematic. Most of the hemipelagic sediment's pore water and chemically bound water is lost at depths of <50 km, and You et al. (1996) showed in a series of experiments that boron is easily mobilized by a hydrous fluid at low temperatures. Thus it seems that shallow sediment dewatering will remove most of the sediment's fluid mobile trace elements and volatiles. For example, we can treat the water loss as open-system Rayleigh-fractionation for which $C_{solid}/C_{initial} = (1-f)(1-D)/D$, where D is boron's the partition coefficient, and $C_{initial}$ and C_{solid} are the initial and residual boron concentration of the rock after loss of a fluid fraction f. We will choose D = 0.1 as an upper bound and D = 0.01 as a lower bound to the likely value (W. E. Seyfried and R. H. James, 2002, personal commun.). If the sediments lose ∼12 wt% H_2O (as they do by ∼50 km depth), for D = 0.1 and D = 0.01, they will also lose ∼68% and ∼99% , respectively, of their initial boron content. This result implies that subducted sediments will retain relatively little of their initial boron by the time they reach the main

depths of arc melting in which case sediments cannot be the enriched source needed to produce the high B/La ratio in some arc lavas. The second scenario uses two fluid phases, one from the sediments and one from the crust. Figure 3 shows that fluids are released from both potential fluid sources at the supposed depth of arc melting. However, very small amounts of water are released from the sediments at this depth, so that a transfer of the relatively immobile ^{10}Be is unlikely; transfer by sediment melts would be possible only for unrealistically high temperatures. Crustal fluids could, however, be enriched in boron which is also enriched in the altered ocean crust. This model is consistent with the ideas of Ishikawa and Nakamura (1994) who argue on the basis of δ^{11}B systematics that the generally positive δ^{11}B values of arc lavas requires a boron source of the same isotopic signature (i.e. δ^{11}B>0). Sediments generally have negative δ^{11}B values, while the altered ocean crust has δ^{11}B>0. The biggest problem for this scenario is that transfer of B and ^{10}Be in two separate fluid phases is not easily reconciled with the observed correlations between these two elements. Furthermore it is not clear how small amounts of sub-arc fluid release from sediments can transport the observed radiogenic Be anomaly. Thus, it seems that Nicaragua arc-lava composition cannot be easily explained without yet another fluid source. Much larger amounts of high-temperature hydrous fluids can be released during slab 'deserpentinization' as shown in Figure 3. Such fluids must pass through overlying crust and sediments on their way to the mantle wedge. During this process, the fluids can potentially interact with and dissolve enough of the sediment's still trapped Be to produce the observed high ^{10}Be/^{9}Be ratios (Be only becomes relatively fluid mobile in high-T, reducing fluid environments). Tatsumi and Isoyama (1988) have shown that Be is potentially mobile in high-temperature fluids released from a serpentinite. In addition, studies of serpentinites from the Atlantic show that sea-water induced serpentinization enriches the host-peridotites in boron and leads to positive δ^{11}B values (Spivack and Edmond 1987). Fluids released during slab 'deserpentinization' are therefore enriched in boron, carry the right (i.e. positive) isotopic signature (δ^{11}B), and have the ability to dissolve enough of the sediment's ^{10}Be to explain the high ^{10}Be/^{9}Be and B/La ratios observed in Nicaraguan arc lavas.

4.4.2 Costa Rica Arc

Beneath Costa Rica, subduction is hotter, the dip angle is shallower, and the downgoing slab is younger. Here the erupted lavas do not show a strong 'slab-fluid' signal. Figure 3B shows that, primarily due to the shallower slab dip, dehydration of the slab occurs over a wider horizontal extent consistent with the idea that a shallower dip leads to less fluid input per unit mantle volume into the melting region (Carr et al. 1990.) This provides a possible explanation for the diluted slab signature and the low degree of melting typical for volcanism in Costa Rica (Carr et al. 1990). This interpretation does not, however, explain why the Costa Rican lavas lack a ^{10}Be anomaly although the slab is hotter and sediment melting would be more likely in this part of the arc. Patino et al. (2000) argued that the missing slab signature may be partly due to a mechanical loss of the uppermost part of the sediment column during accretionary processes. However a striking modeled difference between fluid release beneath Nicaragua and Costa Rica is the lack of a strong fluid release from serpentinized mantle beneath Costa Rica. Perhaps this is responsible for the lack of a Costa Rican ^{10}Be signal-without high-T serpentine-breakdown-derived fluids fluxing through the slab's sediment layer, more of the sediment's ^{10}Be would simply subduct instead of being leached mobilized into the sub-arc melting region.

4.5 Conclusions

Regional trends in Central American arc lavas can be explained by an outer-rise faulting related change from a serpentinized slab mantle deep fluid source beneath Nicaragua to a basalt-amphibolites source beneath Costa Rica; the difference caused by a transition from deeply faulted, serpentinized, lithosphere steeply subducting beneath Nicaragua to less deeply faulted lithosphere subducting less steeply beneath Costa Rica. We further show that lithospheric mantle - serpentinized as a byproduct of flexural faulting at the outer rise - has the potential to release significant amounts of hydrous fluids into the melting

region. Fluxing of these hot, hydrous, serpentine-breakdown-derived fluids through overlying sediments can potentially scavenge and transfer ^{10}Be from the sedimentary layer into the mantle wedge. We infer that this process is maybe more ubiquitous than sediment melting, since it does not require an extremely high slab surface temperature. Serpentinites are also the best slab lithology for transferring chemically bound water through the arc-dewatering region to greater mantle depths. Flexural faulting-induced lithospheric mantle serpentinization beneath the outer rise may therefore play an important role in the global water cycle and in recycling processes at subduction zones in general.

Implications of Subduction Rehydration for Earth's Deep Water Cycle

Lars H. Rüpke, Jason Phipps Morgan

IFM-GEOMAR, Geodynamics Group, Wischhofstr. 1-3, D-24148 Kiel, Germany

Jacqueline E. Dixon

RSMAS/MGG, University of Miami, 4600 Rickenbacker Causeway, Miami, Florida, 33149, USA

Nature

in review

Chapter 5

Implications of subduction rehydration for Earth's deep water cycle

The Earths mantle contains several isotopically distinct components of which some are thought to form by the mixing with recycled sediments and oceanic crust (EM1, EM2, HIMU). Recently Dixon et al. (2002) estimated water concentrations for some of these components and concluded that the most primitive (FOZO) are significantly wetter than the recycling associated EM or HIMU mantle components and the even drier depleted mantle source that melts to form MORB. These findings are in striking agreement with the results of chemo-thermo-dynamic modelling of the global water cycle. We find that the Dixon et al. (2002) results are consistent with a global water cycle model in which the oceans have formed by efficient ($\sim$93%) outgassing of the mantle. Present day depleted mantle will contain a small volume fraction ($\sim$7%) of primitive wet mantle in addition to drier recycling related enriched components. This scenario is consistent with the observation that hotspots with a FOZO-component in their source will make wetter basalts than hotspots whose mantle sources contain a larger fraction of EM and HIMU components.

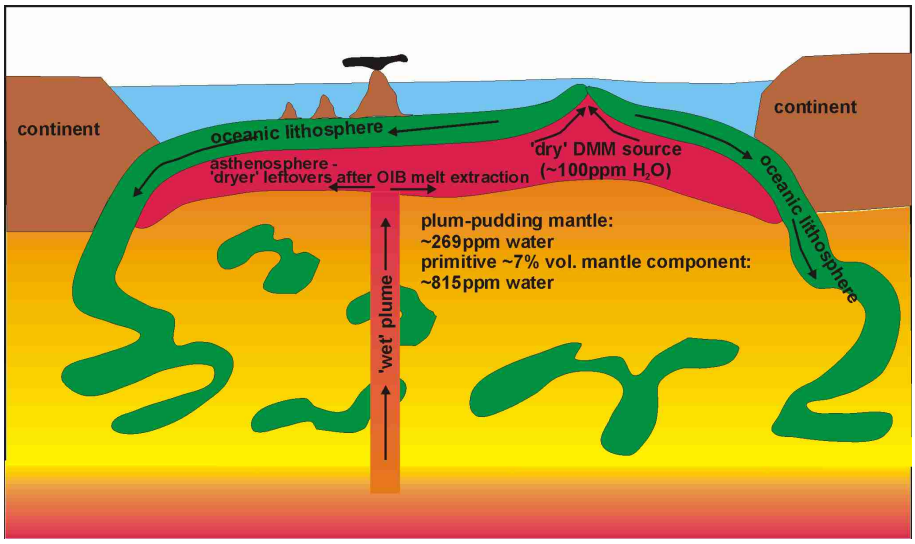

Figure 5.1: *A plum-pludding type whole mantle convection scenario. Subducting slabs are much dryer than primitive mantle but remain sufficiently 'wet' to feed surface water back into the mantle, so that the average mantle's water content includes about 80% of recycled water from the exosphere. Plumes sampling the most primitive 'FOZO' mantle component will make much wetter basalts than plumes sampling one of the recycling associated mantle components (EM&HIMU), and the even drier mid-ocean ridge basalts.*

5.1 Introduction

The 'standard model' for the genesis of Earths oceans is that they are exhalations from Earths deep interior, continually rinsed through surface rocks by the global hydrologic cycle. Here we suggest that this paradigm should be slightly modified to recognize that Earths surface and deep mantle water may still be in close contact through the competing processes of mantle dehydration during plume and mid-ocean ridge melting, and mantle rehydration by plate subduction. Recently, independent geochemical (Dixon et al. 2002) and geophysical (Ruepke et al. 2002; Ruepke et al. 2003) arguments have been used to infer that, during plate subduction a large fraction of the water contained in the crustal and sediment portions of the downgoing slab is efficiently dehydrated before these materials are recycled into the mantle where they will contribute to the distinct slab-flavours in the sources of global hotspot volcanism (Hofman 1997). Here we will briefly review these arguments to show that detailed thermo-chemical models of slab dehydration during

plate subduction are completely consistent with the water abundances and H2O/LREE ratios measured in the mantle source components of both hotspot and mid-ocean ridge volcanism. Both are also consistent with a mantle that has dehydrated by ∼67% to exhale the near-surface water now concentrated in the oceans and continental rocks. The consequence is that since ∼2-2.5Ga Earths mantle has had a near-balance between water loss through hotspot and ridge melting and water gain by slab recycling, and that the present-day Earths mantle may even be slowly rehydrating, so inducing a long-term secular drop in sea level. In this interpretation, most of Earths present-day mantle water is recycled in origin, but the mantles most primitive and volatile-rich component, FOZO (sometimes called C), although currently only a small net volume fraction of the convecting mantle, formerly was the source of the water now concentrated at Earths surface.

The sources of both mid-ocean ridge basalts (MORB) and ocean island basalts (OIB) contain several isotopically distinct source components (Hofman 1997) which leave their fingerprints on observed basalts to which their melts contribute, with arrays of basalts produced at a given hotspot typically occupying a tubelike subregion in the isotope-space spanned by terrestrial basaltic volcanism (Hart et al. 1992; Phipps Morgan 1999). It is now generally agreed that at least several of the isotopically most extreme components contain material that was originally formed by melting and alteration processes near Earths surface and then recycled by plate subduction back into the mantle to rise and melt beneath present-day hotspots and mid-ocean ridges (Chase 1979; Hofman and White 1982; Hofman 1997). Two Enriched mantle source components EM1 and EM2 and the HIMU source component are believed to have formed in this way through the recycling of sediments and OIB for the EM components, and the recycling of the lower MORB crust for the HIMU component. Another mantle component called FOZO appears to be linked to the melting of the most primitive, undifferentiated, and undegassed component of the mantle mélange. In particular, the partial melting of this component correlates with the most ^{3}He-rich basalts erupted at ocean islands and mid-ocean ridges. Other, more incompatible trace element-poor and isotopically depleted components have also been inferred, in particular the prevalent depleted DMM component evident in many MORB

5.2 Water content of MORB and OIB

Recently Dixon and coworkers have measured the water contents of the DMM, FOZO, EM1, and LOMU mantle components and inferred the value for HIMU (Dixon et al. 2002). During mantle melting beneath hotspots and ridges, water partitions from a source component into its melt with roughly the same affinity for the melt phase as the light rare-earth element Ce, i.e. it behaves as a moderately incompatible element during pressure-release melting. Even though both the EM and HIMU mantle components are much richer in incompatible elements than the mantle average, Dixon et al. (2002) found that the recycled EM and HIMU components have lower ratios of water to cerium (H2O/Ce$\sim$100) than either typical MORB source (H2O/Ce $\sim$200 -250) or FOZO-influenced OIB (e.g. H2O/Ce $\sim$210 (Pacific South Atlantic), $\sim$250 North Atlantic, and up to $\sim$400-550 for some Hawaiian basalts). Dixon et al. (2002) also estimated the absolute water abundances of these source components, with the FOZO component determined to have an average of 750$\pm$210ppm water, the average source for mid-ocean ridge basalts to have a water abundance of $\sim$100ppm, and the source of the more depleted MORB a water abundance of $\sim$60ppm. Dixon et al. (2002) concluded that the high H2O/Ce in the FOZO source component cannot be derived from recycled oceanic crust, and that instead a significant amount of the water in the FOZO component must be juvenile, left over from planetary accretion. They also concluded that the EM and HIMU components lost most of their chemically-bound water, but not their incompatible rare-earth elements by subduction-induced slab-dehydration.

Dixon et al. (2002) conclusions on preferential slab-dehydration of recycled sediments and ocean crust are in striking agreement with recent conclusions from numerical chemo-thermo-mechanical modelling of slab dehydration beneath modern and paleo-subduction zones (Ruepke et al. 2002; Ruepke et al. 2003) when coupled to a parameterised mantle convection model.

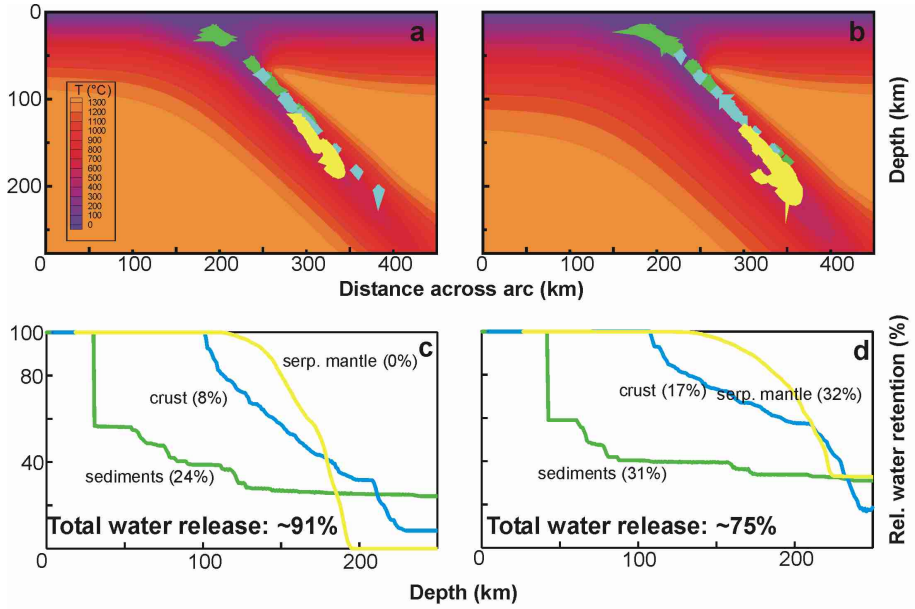

Figure 5.2: *The outcomes of two different model runs. In (a,c), 40My old oceanic lithosphere and in (b,d), 100My old oceanic subducts at an angle of ∼45°C and a convergence rate of 60mm/yr. We assume an incoming plate petrologic profile that includes a 350m thick layer of GLOSS sediments containing 7.3wt.% H2O, a 1km thick highly altered/hydrated crustal layer (2.3wt.% H2O) overlying a 2km thick less hydrated layer (1wt.% H2O), and a 3km thick dry gabbroic layer. Beneath the crust we assume that the lithospheric mantle is 2% serpentinized at the Moho and that the degree of serpentinization decreases linearly to the p-T conditions (∼600°C) where serpentine becomes unstable. These estimates result in an absolute water content of* $0.6 \times 10^5 kg/m^2$ *in a sediment column,* $1.7 \times 10^5 kg/m^2$ *of water in a crustal column, and* $0.7 \times 10^5 kg/m^2$ *of water in a mantle column of a 40Ma old slab, and* $1.4 \times 10^5 kg/m^2$ *of water in a mantle column of a 100Ma old slab. In (a) and (b) the modelled regions of water release from subducting sediments (green), oceanic crust (cyan), and serpentinized mantle (yellow) are shown. In (c) and (d) the slabs changing relative water content. In the case of a 40Ma year old slab sediments lose ∼76% of their water (∼16% of total water release), crust ∼92% (∼58% of total), and serpentinized mantle 100% (26% of total). In the case of the 100Ma old slab sediments lose ∼69% of their water (∼15% of total water release), crust ∼83% (∼51% of total), and serpentinized mantle ∼68% (∼34% of total). In these calculations sediments seem to be a surprisingly stable lithology to recycle water into the deeper mantle. Note, however, that GLOSS sediments are a non-existing, imaginary, average of oceanic sediments; real-world sediments may be much more unstable (Kerrick and Connolly 2001b; Ruepke et al. 2002).*

5.3 A model for the geochemical evolution of the mantle

The Ruepke et al. (2003) model for the geologic water cycle, i.e. the water outgassing at mid-ocean ridges and hotspots and the recycling of water at subduction zones, uses a 2-D subduction model to solve for water release and deep water recycling at subduction zones. Figure 2 shows the outcome of two example model runs assuming a young (40Ma) slab (a,c) and an old (100Ma) slab (b,d). In (a) and (b) the pattern of water release are shown: water release from sediments is marked in green, crustal dewatering is shown in blue, and mantle deserpentinization in yellow. To determine the efficiency of water release in (c) and (d) the relative amounts of water retention per column of sediment (green), crust (blue), and serpentinized mantle (yellow) are plotted. We find that a 40Ma old slab loses ∼91% of its total initial water while the older colder 100Ma old slab releases only ∼75%. Old and cold slabs may, therefore, retain and recycle significant amounts of water to greater mantle depths.

To determine the effects of water recycling at subduction zones on the water cycle of the Earth, the Ruepke et al. (2003) model parameterises slab water recycling as a function of Earth age and incorporates this into a parameterised convection model of whole mantle flow that includes the effects of mantle dehydration by pressure-release melting at hotspots and mid-ocean ridges (see Fig 3 and (Ruepke et al. 2003) for further details).

Figure 3 shows a characteristic evolution model for the Earth. Early on, outgassing at ridges and hotspots dominates over water recycling at subduction zones. Starting ∼2.5Ga ago water recycling matches the now much slower rate of hotspot/ridge outgassing so that the exospheres water content stabilizes and even can begin to decrease slowly. The present day Earth is characterized by a mantle that has been largely, but not completely outgassed of its original volatiles (∼93%). Due to slab recycling, it contains about ∼49% of the exospheres water content and ∼33% of its initial water content, of which ∼80% has been recycled back from the exosphere. Note, that these numbers imply whole mantle flow, so

that eventually the 93% of the mantle participates in near-surface upwelling, melting, and differentiation processes. If a strictly layered Earth is assumed to have always existed, it is possible that a reservoir of incommunicative primitive mantle water exists that would still not yet have participated in the surface + communicative mantle geologic water cycle.
To compare these numbers to the results of Dixon et al. (2002) we translate the above results into average water concentrations of the different mantle components. The model is initialised to reproduce the present day water in the exosphere (oceans and continental crust), i.e. $\sim 2.2 \times 10^{21}$kg of water (Henderson 1986). The starting conditions that reproduce the present-day conditions are that the Earth contained about 1.5 present exospheres of water stored in the initial mantle. This implies that $1.5 \times 2.2 \times 10^{21}$kg of water were stored in 4.0×10^{24}kg mantle, so that the water concentration in primitive mantle is 815-ppm. At present-day conditions the average mantle contains 33% of its initial water and 49% of the present-day exospheres water which correspond to an average water concentration of ∼269ppm. Without replenishment by subduction the present day depleted mantle would contain an average of only 7% of its initial water, i.e. ∼57ppm H2O. Of the average 269ppm H2O abundance in the current mantle ∼212-ppm are, therefore, due to recycled water from the exosphere and 57ppm are due to a surviving juvenile water component with ∼815-ppm water that makes up a 7% volume-fraction of the mantle. The estimated primitive mantle water abundance from this Deep Earth evolution scenario, 815 ppm, is strikingly similar to the 750±210ppm estimate of Dixon et al. (2002). Furthermore, the average recycled slab is inferred to be much dryer than primitive mantle, although we find that crust dehydration of plates older than 40Ma may be less efficient than inferred by Dixon et al. (∼97% in recycled crust (Dixon et al. 2002) vs. ∼92% our 40Ma old crust and ∼83% our 100Ma crust). One explanation for this is that the Dixon et al. estimates refer to the water content of ancient ocean crust that led to the formation of the average HIMU mantle component which is ∼2Ga old. At this time in Earth history the average subducting seafloor age was close to 40Ma in the Ruepke et al. (2003). model, so that its estimates of paleo-plate dehydration fit well with Dixon et al.s observations.

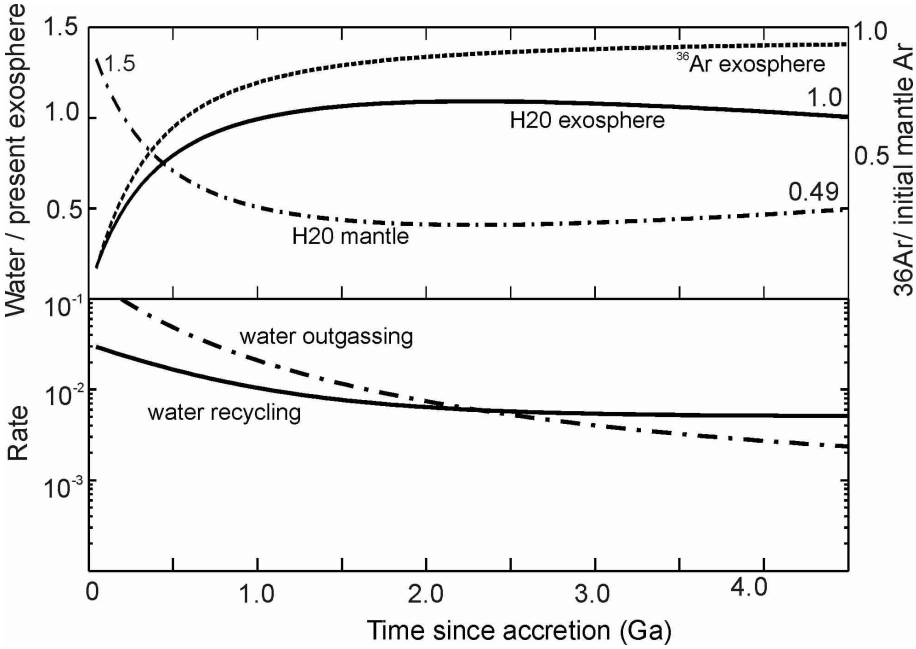

Figure 5.3: *Modelled geologic water cycle, i.e. the outgassing of water at ridges and hotspots and the recycling of water at subduction zones, over time. The model uses a parameterised mantle convection model that is based on the one by Phipps Morgan (1998). Phipps Morgan (1998) argued that the mantle overturn rate, R, is proportional to the square of radiogenic heating, Q, so that $R \sim Q^2$. Likewise, the average seafloor age A will be inversely proportional to Q^2, i.e. $A \sim 1/Q^2$. From these estimates the outgassing of water at ridges and hotspots and the recycling of water can be modelled. For water outgassing we assume that the mantle loses its volatiles at a depth of 100km and loses 99% of the volatiles that rise shallower than this depth. Recycling of water at subduction zones is determined from a look-up table of slab dehydration as a function of the subducting plates age and speed, all based upon a suite of numerical experiments done by Ruepke et al. (2003). In (a) the water content of the Earth's mantle and exosphere is plotted against time along with the exosphere's ^{36}Ar content which is a convenient measure of the cumulate extent of mantle outgassing; (b) shows water recycling rates at subduction zones and the water outgassing rates at ridges and hotspots over time.*

5.4 Conclucions

We conclude that this model of the deep Earths water cycle predicts realistic water concentrations for the different mantle components; concentrations consistent with the independent estimates by Dixon et al. (2002). This implies that if mantle melting preferentially occurs first in its most volatile-rich or incompatible element-rich components (plausible since both volatiles and incompatible elements tend to reduce the solidus (Phipps Morgan and Morgan 1999)), then it would be completely consistent that hotspots with a FOZO-component in their source will make wetter basalts than hotspots whose mantle sources contain a larger fraction of EM and HIMU components, and also consistent that progressive upwelling and pressure-release melting beneath a mid-ocean ridge should eventually be able to melt the average mantle to the point where ∼100-ppm depleted, slab influenced mantle components are the only remaining water source to contribute to the more depleted MORB. Thus these results (summarized in Fig. 1) are consistent with a plum-pudding whole mantle convection evolution scenario in which plate subduction plays an important role in partially filtering the water content of the recycled sediments and crust that form the sources of the more enriched mantle plums.

References

Angel, R.J., D.J. Frost, N.L. Ross, and R. Hemley, 2001. STabilities and equation of state of dense hydrous magnesium silicates. Phys. Earth Planet. Int., 127: 181-196.

Barckhausen, U., C.R. Ranero, R. von Huene, S.C. Cande, and H.A. Roeser, 2001. Revised Tectonic Boundaries in the Cocos Plate off Costa Rica: Implications for the Segmentation of the Convergent Margin and for Plate Tectonic Models. J. Geophys. Res., 106: 19,207-19220.

Berhorst, A., E.R. Flueh, K.D. McIntosh, C.R. Ranero, I. Ahmed, E.A. Silver, and U. Barckhausen, 2003. The crustal structure of the convergent Nicaraguan margin from a combined reflection and refraction study. Geophysical Research Abstracts, 5: 09692.

Billen, M.I., and M. Gurnis, 2001. A low viscosity wedge in subduction zones. Earth Planet. Sci. Lett., 193: 227-236.

Bose, K., and A. Navrotsky, 1998. Thermochemistry and phase equilibria of hydrous phases in the system MgO-SiO2-H2O: Implications for volatile transport to the mantle. J. Geophys. Res., 103: 9713-9719.

Brock, J.S., J.W. Painter, and D.B. Kothe, 1998. Tracer-particle advection: algorithm components and implementation methods. Los Alamos National Laboratory Reports,

Carr, M.J., M.D. Feigenson, and E.A. Bennett, 1990. Incompatible element and isotopic evidence for the tectonic control of source mixing and melt extraction along the Central American arc. Contrib. Mineral. Petrol., 105: 369-380.

Chase, C.G., 1979. Subduction, the geoid, and lower mantle convection. Nature, 282: 464-468.

Christensen, U.R., and A.W. Hofmann, 1994. Segregation of subducted oceanic crust in the convecting mantle. J. Geophys. Res., 99: 19867-19884.

Connolly, J.A.D., 1990. Multivariable Phase Diagrams: An Algorithm Based on Generalized Thermodynamics. Am. J. Sci., 290: 666-718.

Connolly, J.A.D., and K. Petrini, 2002. An automated strategy for calculation of phase diagram sections and retrieval of rock properties as a function of physical conditions. Journal of Metamorphic Geology, 20: 697-708.

Davies, J.H., and D.J. Stevenson, 1992. Physical Model of Source Region of Subduction Zone Volcanics. J. Geophys. Res., 97: 2037-2070.

Dixon, J.E., L. Leist, C. Langmuir, and J.-G. Schilling, 2002. Recycled dehydrated lithosphere observed in plume-influenced mid-ocean-ridge basalt. Nature, 420: 385-389

Dobson, D., P., P. Meredith, G., and S.A. Boon, 2002. Simulation of Subduction Zone Seismicity by Dehydration of Serpentine. Science, 298: 1407-1410.

Duggen, S., K. Hoernle, P. van den Bogaard, L.H. Ruepke, and J. Phipps Morgan, 2003. Deep roots of the Messinian salinity crisis. Nature, 422: 602-606.

Dumoulin, C., M.-P. Doin, and L. Fleitout, 1999. Heat transport in stagnant lid convection with temperature- and pressure-dependent Newtonian or non-Newtonian rheology. J. Geophys. Res., 104: 12759-12777.

Elliot, T., T. Plank, A. Zindler, W. White, and B. Bourdon, 1997. Element transport from slab to volcanic front at the Mariana arc. J. Geophys. Res., 102: 14,991-15,019.

Funiciello, F., G. Morra, K. Regenauer-Lieb, and D. Giardini, 2003. Dynamics of retreating slabs: 1. Insights from two-dimensional numerical experiments. J. Geophys. Res., 108: 10.1029/2001JB000898.

Gerya, T., and D. Yuen, 2003. Rayleigh-Taylor instabilities from hydration and melting propel cold plumes at subduction zones. Earth Planet. Sci. Lett., 212: 47-62.

Gerya, T.V., B. Stockhert, and A.L. Perchuk, 2002. Exhumation of high-pressure metamorphic rocks in a subduction channel: A numerical simulation. Tectonics, 21: 10.1029/2002TC001406.

Grove, T.L., and S.W. Parman, 2004. Thermal evolution of the Earth as recorded by komatiites. Earth Planet. Sci. Lett., 219: 173-187.

Hacker, B.R., G.A. Aber, and S.M. Peacock, 2003a. Subduction factory: 1. Theorectical mineralogy, densities, seismic wave speeds, and H20 contents. J. Geophys. Res., 108: 2029 doi:10.1029/2001JB001127.

Hacker, B.R., S.M. Peacock, G.A. Aber, and D. Holloway, 2003b. Subduction factory 2. Are intermediate-depth earthquakes in subducting slabs linked to metamorphic dehydration reactions? J. Geophys. Res., 108: dio:10.1029/2001JB001129.

Hallam, A., 1992. Phanerozoic Sea-Level Changes. Columbia University Press,

Hart, S.R., L.A. Hauri, L.A. Oschman, and J.A. Whitehead, 1992. Mantle plumes and entrainment: isotopic evidence. Science, 256: 517-520.

Henderson, P., 1986. Inorganic Geochemistry. Pergamon Press,

Hensen, C., K. Wallmann, M. Schmidt, C.R. Ranero, and E. Suess, 2004. Fluid expulsion related to mud extrusion off Costa Rica - A window to the subducting slab. Geology, 32: 201-204.

Herrstrom, E.A., M.K. Reagan, and J.D. Morris, 1995. Variations in lava compostion associated with flow of asthenosphere beneath southern Central America. Geology, 23: 617-620.

Hilst, R.D.v.d., S. Widiyantoro, and E.R. Engdahl, 1997. Evidence for deep mantle circulation from global tomography. Nature, 386: 578-584.

Hofman, A.W., 1997. Mantle geochemistry: the message from oceanic volcanism. Nature, 385: 219-229.

Hofman, A.W., and W.M. White, 1982. Mantle plumes from ancient oceanic crust. Earth Planet. Sci. Lett., 57: 421-436.

Holland, T.J.B.H., and R. Powell, 1998. An internally consistent thermodynamic data set for phases of petrologic interest. Journal of Metamorphic Geology, 16: 309-343.

Huene, v.R., C.R. Ranero, and W. Weinrebe, 2000. Quaternary convergent margin tectonics of Costa Rica , segmentation of the Cocos Plate, and Central American voncanism. TECTONICS, 19: 314-334.

Ishikawa, T., and E. Nakamura, 1994. Origin of the slab component in arc lavas from across-arc variations of B and Pb isotopes. Nature, 370: 205-208.

John, T., and V. Schenk, 2003. Partial eclogitisation of gabbroic rocks in a late Precambrian subduction zone (Zambia): prograde metamorphism triggered by fluid infiltration. Contrib. Mineral. Petrol., in press.

Kerrick, D.M., 2002. Serpentinite Seduction. Science, 298: 1344-1345.

Kerrick, D.M., and J.A.D. Connolly, 1998. Subduction of ophicarbonates and recycling of CO2 and H2O. Geology, 26: 375-378.

Kerrick, D.M., and J.A.D. Connolly, 2001a. Metamorphic devolatilization of subducted oceanic metabasalts: implications for seismicity, arc magmatism and volatile recycling. Earth Planet. Sci. Lett., 189: 19-29.

Kerrick, D.M., and J.A.D. Connolly, 2001b. Metamorphic devolotilization of subducted marine sediments and the transport of volatiles into the Earth's mantle. Nature, 411: 293-296.

Kincaid, C., and I.S. Sacks, 1997. Thermal and dynamical evolution of the upper mantle in subduction zones. J. Geophys. Res., 102: 12,295-12,315.

Kirby, S., E.R. Engdahl, and R. Denlinger, 1996. Intermediate-Depth Intraslab Earthquakes and Arc Volcanism as Physical Expresstions of Crustal and Uppermost Mantle Metamorphism in Subducting Slabs. In: G.E. Bebout, D.W. Scholl, S.H. Kirby, and J.P. Platt (Ed.), Subduction: Top to Bottom. American Geophysical Union,

Leeman, W.P., M.J. Carr, and J.D. Morris, 1994. Boron geochemistry of the Central American Volcanic Arc: Constraints on the genesis of subduction-related magmas. Geochim. Cosmochim. Acta, 58: 149-168.

Luth, R.W., 1995. Is phase A relevant to the Earth's mantle? Geochim. Cosmochim. Acta, 59: 679-682.

Montelli, R., G. Nolet, A. Dahlen, G. Masters, E.R. Engdahl, and S.-H. Hung, 2004. Finite-Frequency Tomography Reveals a Variety of Plumes in the Mantle. Science, 303: 338-343.

Morris, J.D., W.P. Leeman, and F. Tera, 1990. The subducted component in island arc lavas: constraints from Be isotopes and B-Be systematics. Nature, 344: 31-36.

Murakami, M., K. Hirose, H. Yurimoto, S. Nakashima, and N. Takafuji, 2002. Water in Earth's Lower Mantle. Science, 295: 1885-1887.

Patino, L.C., M.J. Carr, and M.D. Feigenson, 2000. Local and regional variations in Central American arc lavas controlled by variations in subducted sediment input. Contrib. Mineral. Petrol., 138: 265-283.

Pawley, A.R., and B.J. Wood, 1996. The low-pressure stability of phase A; Mg7Si2O8(OH)6. Contrib. Mineral. Petrol., 124: 90-97.

Peacock, S.M., 1996. Thermal and Petrological Structure of Subduction Zones. In: G.E. Bebout, D.W. Scholl, S.H. Kirby, and J.P. Platt (Ed.), Subduction: Top to Bottom. American Geophysical Union,

Peacock, S.M., 2001. Are the lower planes of double seismic zones caused by serpentine dehydration in subducting oceanic mantle? Geology, 29: 299-302.

Peacock, S.M., and K. Wang, 1999. Seismic Consequences of Warm Versus Cool Subduction Metamorphism: Examples from Southwest and Northeast Japan. Science, 286: 937-939.

Phipps Morgan, J., 1998. Thermal and rare gas evolution of the mantle. Chem. Geol., 145: 431-445.

Phipps Morgan, J., 1999. The Isotope Topology of Individual Hotspot Basalt Arrays:

Mixing Curves or Melt Extraction Trajectories? Geochemistry Geophysics Geosystems, 1: 1999GC000004.

Phipps Morgan, J., and J. Morgan, 1999. Two-stage melting and the geochemical evolution of the mantle: a recipe for mantle plum-pudding. Earth Planet. Sci. Lett., 170: 215-239.

Plank, T., and H. Langmuir, 1998. The chemical composition of subducting sediment and its conssequences for the crust and mantle. Chem. Geol., 145: 325-394.

Poli, S., and M.W. Schmidt, 2002. Petrology of Subducted Slabs. Ann. Rev. Earth Planet. Sci., 30: 207-235.

Protti, M., F. Gendel, and K. McNally, 1995. Correlation between the age of the subducting Cocos Plate and the geometry of the Wadati-Benioff zone under Nicaragua and Costa Rica. Geol. Soc. Am. Bull., 295: 309-326.

Ranero, C., A. Villasenor, and J. Phipps Morgan, 2003a. Relationship between bend-faulting at trenches and intra-slab seismicity. J. Geophys. Res., submitted:

Ranero, C.R., J. Phipps Morgan, K.D. McIntosh, and C. Reichert, 2003b. Bending, faulting, and mantle serpentinization at the Middle America trench. Nature, 425: 367 - 373.

Regenauer-Lieb, K., and T. Kohl, 2003. Water solubility and diffusivity in olivine: its role in planetary tectonics. Min. Mag., 67: 697-715.

Regenauer-Lieb, K., D. Yuen, and J. Branlund, 2001. The initiation of Subduction: Criticality by Addition of Water? Science, 294: 587-580.

Roehm, A.H.E., R. Snieder, S. Goes, and J. Trampert, 2000. Thermal structure of continental upper mantle inferred from S-wave velocity and surface heat flow. Earth Planet. Sci. Lett., 181: 395-407.

Ruepke, L.H., J. Phipps Morgan, M. Hort, and J.A.D. Connolly, 2002. Are the regional

variations in Central American arc lavas due to differing basaltic versus peridotitic slab sources of fluids? Geology, 30: 1035-1038.

Ruepke, L.H., J. Phipps Morgan, M. Hort, and J.A.D. Connolly, 2003. Serpentine and the subduction zone wate cycle. Earth Planet. Sci. Lett., in review:

Sallares, V., and C.R. Ranero, 2003. Structure of the incoming ocean plate and the erosional convergent margin off Antofagasta, northern Chile. Geophysical Research Abstracts, 5: 02839.

Schmidt, M.W., and S. Poli, 1998. Experimentally based water budgets for dehydrating slabs and consequences for arc magma generation. Earth Planet. Sci. Lett., 163: 361-379.

Seno, T., and Y. Yamanaka, 1996. Double Seismic Zones, Compressional Deep Trench-Outer Rise Events, and Superplumes. In: G.E. Bebout, D.W. Scholl, S.H. Kirby, and J.P. Platt (Ed.), Subduction: Top to Bottom.

Sleep, N.H., 2000. Evolution of the mode of convection within terrestrial planets. Journal of Geophysical Research-Planets, 105: 17563-17578.

Smolarkiewicz, P.K., 1984. A Fully Multidimensional Positive Definite Advection Transport Algorithm with Small Implicit Diffusion. J. Comp. Phys., 54: 325-362.

Spivack, A.J., and J.M. Edmond, 1987. Boron isotopic exchange between seawater and the oceanic crust. Geochim. Cosmochim. Acta, 51: 1033-1043.

Staudigel, H., T. Plank, B. White, and H.-U. Schmincke, 1996. Geochemical Fluxes During Seafloor Alteratrion of the Basaltic Upper Ocean Crust: DSDP Sites 417 and 418. In: G.E. Bebout, D.W. Scholl, S.H. Kirby, and J.P. Platt (Ed.), Subduction Top to Bottom. 19-38. American Geophysical Union,

Tackley, P.J., and S.D. King, 2003. Testing the tracer ratio method for modeling active compositional fields in mantle convection simulations. Geochemistry Geophysics Geosystems, in press:

Tatsumi, Y., and H. Isoyama, 1988. Transportation of Beryllium with H20 at High Temperatures: Implications for Magma Genesis in Subduction Zones. Geophys. Res. Lett., 15: 180-183.

Thompson, A.B., 1992. Water in the Earth's upper mantle. Nature, 358: 295-302.

Ulmer, P., and V. Trommsdorf, 1995. Serpentine Stability to Mantle Depths and Subduction-Related Magmatism. Science, 268: 858-861.

van Hunen, J., A.P. van den Berg, and N.J. Vlaar, 2000. A thermo-mechanical model of horizontal subduction below an overriding plate. Earth Planet. Sci. Lett., 182: 157-169.

van Keken, P.E., B. Kiefer, and S.M. Peacock, 2002. High-resolution models of subduction zones: Implications for mineral dehydration reactions and the transport of water into the deep mantle. Geochemistry Geophysics Geosystems, 1: 10.1029/2000GC000045.

Wallmann, K., 2001. The geological water cycle and the volution of marine d18O values. Geochim. Cosmochim. Acta, 65: 2469-2485.

Walther, C.H.E., E.R. Flueh, C.R. Ranero, and R. von Huene, 2000. Crustal structure across the Pacific margin of Nicaragua: evidence of ophiolitic basement and a shallow mantle sliver. Geophys. J. Int., 141: 759-777.

Zienkiewicz, O.C., and L.R. Taylor, 2000. The Finite Element Method Vol 3: Fluid Dynamics. Butterworth-Heinemann, Oxford.

Danksagung

Viele haben mich bei der Anfertigung dieser Arbeit unterstützt. Diesen Freunden und Kollegen möchte ich ganz herzlich danken.

Extra erwähnen möchte ich

Meine beiden Betreuer Jason Phipps Morgan und Matthias Hort. Sie sind in erster Linie dafür "verantwortlich", dass ich diese Arbeit überhaupt begonnen...und beendet habe. Ganz herzlich möchte ich mich bei ihnen auch für die persönliche Unterstützung und Beratung bedanken und dafür, dass sie mir diese erstaunliche Freiheit in wissenschaftlicher Ausrichtung und "Arbeitsweise" gelassen haben. Danke!

James Connolly. He contributed a lot to the success of this thesis. Thanks Jamie!

Klaus Regenauer-Lieb und Gabriele Morra. Sie haben mir an der ETH-Zürich gezeigt, was in der Geomodellierung eigentlich möglich ist - durch sie verstehe ich langsam auch, was eine elasto-visco-plastische Rheologie ist.

Timm John, Klaus Wallmann, Erwin Suess und den gesamten SFB 574. Vielen Dank für die vielen interessanten wissenschaftlichen Diskussionen.

Den 1. Zwölf-Kampf Club zu Kiel e.V.

Nicht zuletzt möchte ich meiner Familie und meinen Freunden von ganzem Herzen danken. Ohne eure Unterstützung hätte ich entweder gar nicht, oder frühestens in 2007 promoviert. Danke, ihr seid großartig und ich weiß, was ich an euch habe!

Lebenslauf

Lars Helmuth Rüpke wurde am 9. Oktober 1975 in Hamburg geboren. 1995 schloss er seine Schulbildung mit dem Abitur am Gymnasium Buckhorn in Hamburg ab. Es folgte ein Jahr als Zivildienstleistener im Rettungsdienst. Das Studium der Geowissenschaften begann er im Jahre 1996 an der Christian-Albrechts-Universiät zu Kiel, wo er 1998 sein Vordiplom in Geophysik bestand. Es folgte ein weiteres Jahr an der Universität Kiel, bevor er in Frankreich von 1999-2000 an der UBO-Brest den Studiengang 'Géosciences Marines' studierte und diesen mit dem 'Diplôme d'Etudes Approfondies" (DEA) abschloss. Seit 2000 arbeitet Lars Helmuth Rüpke am Leibniz Institut für Meereswissenschaften und der Christian-Albrechts-Universität zu Kiel als wissenschaftlicher Angestellter; aus dieser Tätigkeit enstand diese Doktorarbeit.

Appendix

Deep Roots of the Messinian Salinity Crisis

Svend Duggen, Kaj Hoernle, Paul van den Bogaard,
Lars Rüpke & Jason Phipps Morgan
GEOMAR, Wischhofstr. 1-3, D-24148 Kiel, Germany

Nature
v. 422
April Issue
2003

laser (266 nm) as excitation source. No midgap yellow emission was observed. Band-edge emission was observed in these nanotube samples between 375 and 360 nm, with the thinner tubes emitting at shorter wavelengths (Supplementary Information). This slight blueshift of the emission[18] could be attributed to the quantum confinement effect, as some of the nanotubes have walls as thin as 5 nm, which is smaller than the exciton Bohr radius of GaN. Electron transport measurements indicate the resistances of these nanotubes are of the order of 10 MΩ at room temperature, and increase with decreasing temperature (Supplementary Information), similar to those of high-quality GaN nanowires[19,20].

The semiconductor nanotubes that we report here are mechanically robust, and electrically and optically active. They could therefore offer opportunities for further fundamental research, as well as for technological applications in nanocapillary electrophoresis, nanofluidic biochemical sensing, nanoscale electronics and optoelectronics[21]. The successful preparation of single-crystal GaN nanotubes using this 'epitaxial casting' approach suggests that it is possible to prepare single-crystal nanotubes of other inorganic solids that have non-layered crystal structures[22,23]. □

Received 14 November 2002; accepted 26 February 2003; doi:10.1038/nature01551.

1. Iijima, S. Helical microtubules of graphitic carbon. *Nature* **354,** 56–58 (1991).
2. Tenne, R. & Zettl, A. K. Nanotubes from inorganic materials. *Top. Appl. Phys.* **80,** 81–112 (2001).
3. Tenne, R. Inorganic nanoclusters with fullerene-like structure and nanotubes. *Prog. Inorg. Chem.* **50,** 269–315 (2001).
4. Patzke, G. R., Krumeich, F. & Nesper, R. Oxidic nanotubes and nanorods—Anisotropic modules for a future nanotechnology. *Angew. Chem. Int. Edn Engl.* **41,** 2446–2461 (2002).
5. Martin, C. R. Nanomaterials—a membrane-based synthetic approach. *Science* **266,** 1961–1965 (1994).
6. Ajayan, P. M. *et al.* Carbon nanotubes as removable templates for metal-oxide nanocomposites and nanostructures. *Nature* **375,** 564–566 (1996).
7. Yang, S. M. *et al.* Formation of hollow helicoids in mesoporous silica: Supramolecular origami. *Adv. Mater.* **11,** 1427–1430 (1999).
8. Kondo, Y. & Takanayagi, K. Synthesis and characterization of helical multi-shell gold nanowires. *Science* **289,** 606–608 (2000).
9. Li, Y. *et al.* Bismuth nanotubes. *J. Am. Chem. Soc.* **123,** 9904–9905 (2001).
10. Wu, Y. & Yang, P. Melting and welding semiconductor nanowires in nanotubes. *Adv. Mater.* **13,** 520–523 (2001).
11. Schmidt, O. G. & Eberl, K. Thin solid films roll up into nanotubes. *Nature* **410,** 168 (2001).
12. Huang, M. *et al.* Room-temperature ultraviolet nanowire nanolasers. *Science* **292,** 1897–1899 (2001).
13. Caruso, R. A. & Antonietti, M. Sol-gel nanocoating: an approach to the preparation of structured materials. *Chem. Mater.* **13,** 3272–3282 (2001).
14. Hamdani, F. *et al.* Effect of buffer layer and substrate surface polarity on the growth by molecular beam epitaxy of GaN on ZnO. *Appl. Phys. Lett.* **71,** 3111–3113 (1997).
15. Lee, S. M. *et al.* Stability and electronic structure of GaN nanotubes from density-functional calculations. *Phys. Rev. B* **60,** 7788–7791 (1999).
16. Li, J. Y. *et al.* Synthesis of GaN nanotubes. *J. Mater. Sci. Lett.* **20,** 1987–1988 (2001).
17. Vayssieres, L., Keis, K., Hagfeldt, A. & Lindquist, S. Three-dimensional array of highly oriented crystalline ZnO microtubes. *Chem. Mater.* **13,** 4395–4398 (2001).
18. Hamdani, F. *et al.* Microstructure and optical properties of epitaxial GaN on ZnO (0001) grown by reactive molecular beam epitaxy. *J. Appl. Phys.* **83,** 983–990 (1998).
19. Huang, Y., Duan, X., Cui, Y. & Lieber, C. M. Gallium nitride nanowire nanodevices. *Nano Lett.* **2,** 101–104 (2002).
20. Kim, J. *et al.* Electrical transport properties of individual gallium nitride nanowires synthesized by chemical vapor deposition. *Appl. Phys. Lett.* **80,** 3548–3550 (2002).
21. Schoening, M. & Poghossian, A. Recent advances in biologically sensitive field-effect transistors (BioFETs). *Analyst* **127,** 1137–1151 (2002).
22. Lauhon, L. J., Gudiksen, M. S., Wang, D. & Lieber, C. M. Epitaxial core-shell and core-multishell nanowire heterostructures. *Nature* **420,** 57–61 (2002).
23. He, R., Law, M., Fan, R., Kim, F. & Yang, P. Functional bimorph composite nanotapes. *Nano Lett.* **2,** 1109–1112 (2002).

Supplementary Information accompanies the paper on *Nature*'s website (http://www.nature.com/nature).

Acknowledgements We thank the National Center for Electron Microscopy for the use of their facilities. This work was supported by the Camille and Henry Dreyfus Foundation, the Research Corporation, the Hellman Family Faculty Foundation and the Beckman Foundation. J.G. thanks the National Science Foundation for Graduate Fellowship support. P.Y. is an Alfred P. Sloan Research Fellow. Work at the Lawrence Berkeley National Laboratory was supported by the Office of Science, Basic Energy Sciences, Division of Materials Science of the US Department of Energy.

Competing interests statement The authors declare that they have no competing financial interests.

Correspondence and requests for materials should be addressed to P.Y. (e-mail: p_yang@uclink.berkeley.edu).

Deep roots of the Messinian salinity crisis

Svend Duggen*†, Kaj Hoernle*, Paul van den Bogaard*, Lars Rüpke* & Jason Phipps Morgan*

** GEOMAR Research Center for Marine Geosciences, Wischhofstrasse 1-3, 24148 Kiel, Germany*

The Messinian salinity crisis—the desiccation of the Mediterranean Sea between 5.96 and 5.33 million years (Myr) ago[1]—was one of the most dramatic events on Earth during the Cenozoic era[2]. It resulted from the closure of marine gateways between the Atlantic Ocean and the Mediterranean Sea, the causes of which remain enigmatic. Here we use the age and composition of volcanic rocks to reconstruct the geodynamic evolution of the westernmost Mediterranean from the Middle Miocene epoch to the Pleistocene epoch (about 12.1–0.65 Myr ago). Our data show that a marked shift in the geochemistry of mantle-derived volcanic rocks, reflecting a change from subduction-related to intraplate-type volcanism, occurred between 6.3 and 4.8 Myr ago, largely synchronous with the Messinian salinity crisis. Using a thermomechanical model, we show that westward roll back of subducted Tethys oceanic lithosphere and associated asthenospheric upwelling provides a plausible mechanism for producing the shift in magma chemistry and the necessary uplift (~1 km) along the African and Iberian continental margins to close the Miocene marine gateways, thereby causing the Messinian salinity crisis.

In the Late Miocene (~8 Myr ago), marine passages in southern Spain and northern Morocco linked the Mediterranean Sea to the Atlantic Ocean (Fig. 1). The palaeodepth of the Rifean corridor in Morocco—the deepest of these gateways—was estimated at 600–800 m (refs 3, 4). Marine sediments, such as terraced reef complexes from these former channels, now outcrop several hundred metres above sea level[5,6]. Three possible mechanisms have been proposed to close these marine passages: (1) global sea level drop of ~60 m (refs 7, 8); (2) horizontal shortening associated with crustal nappe movements[9]; and (3) tectonic uplift[3,4,10].

Not only was the ~60-m drop in sea level in the Messinian insufficient to have closed all of the Late Miocene marine gateways, but also it has recently been shown that the onset of evaporite deposition at 5.96 ± 0.02 Myr does not correspond to the open-ocean benthic $\delta^{18}O$ signal, which is commonly interpreted to reflect glacio-eustatic sea-level changes. Therefore a global sea-level drop cannot have caused the Messinian salinity crisis (MSC)[1,11]. Horizontal shortening is also an unlikely mechanism, for two reasons. First, because emplacement of crustal nappes in the Early Miocene, connected with extensional collapse of the Alborán block thickened through the collision of Africa and Iberia[12], had already ceased before the Late Miocene in the Betics[13], and second, there is no evidence that nappe emplacement blocked the Rifean corridor in the Late Miocene (Fig. 1)[3]. It has, however, been shown that sediments in the former marine gateways were uplifted in the Late Miocene and Pliocene to their present elevations[3,5,10]. Palaeodepth reconstructions indicate a rapid shallowing in the Late Miocene with rates as high as 5 mm yr^{-1} at 7.2 Myr ago in the southern Rifean corridor, which was emergent by ~6.0 Myr (ref. 3). An increase of continental detritus in the uppermost Pliocene deposits of the Alborán basin indicates a continuation of this uplift into the Pliocene[14].

† Present address: Department of Geology, Royal Holloway University of London, Egham, Surrey TW20 0EX, UK.

The Betic and Rifean corridors are traversed by a north-north-east-trending volcanic belt, ~500 km long by ~200 km wide, extending from southeastern Spain through the eastern Alborán Sea into northwestern Africa (Fig. 1b). As volcanism is the surface expression of mantle processes, we use the age and geochemistry of volcanic rocks from this belt to trace the geodynamic evolution of the Alborán mantle, in order to elucidate the origin of uplift from the Late Miocene to Pliocene. We have dated more than 70 volcanic rocks, covering the entire Alborán volcanic province, using the laser ^{40}Ar–^{39}Ar technique on amphibole, biotite and feldspar phenocrysts, microcrystalline rock matrix and glass separates. The dated samples were also analysed for major and trace elements, and Sr, Nd, Pb and O isotopic composition.

Two distinct groups of volcanic rocks occur throughout the eastern Alborán volcanic belt, as defined by their SiO_2 and alkali contents (Fig. 1b and 2a): (1) a Middle Miocene to Lower Pliocene (12.1–4.8 Myr ago) high-Si group, and (2) an Upper Miocene to Pleistocene (6.3–0.65 Myr ago) low-Si group. The older, high-Si, group can be further subdivided into two subgroups: a K-poor tholeiitic and calc-alkaline series of basalts through rhyolites with relatively low concentrations of incompatible elements, and K-rich shoshonites and lamproites with high concentrations of highly to moderately incompatible elements (Fig. 2c). The younger, low-Si volcanic rocks are alkalic, ranging from alkali basalt and basanite to hawaiite and tephrite.

Mafic members from both age groups also exhibit distinct trace-element and isotopic compositions. Whereas mafic rocks of the older high-Si group show relative enrichment in U, K and Pb and depletion in Nb and Ta (Fig. 2c), mafic rocks from the younger low-Si group show the opposite: relative depletion in U, K and Pb and enrichment in Nb and Ta (Fig. 2b). In addition, the low-Si group have lower Pb/Ce, K/La, K/Nb and $^{87}Sr/^{86}Sr$ but higher Nb/U, $^{143}Nd/^{144}Nd$, $^{206}Pb/^{204}Pb$ and $^{208}Pb/^{204}Pb$ ratios (Fig. 3).

The major-element, trace-element and Sr-Nd-Pb-O isotope geochemistry of the older high-Si mafic volcanic rocks are characteristic of volcanism occurring in subduction zones (for example, the Izu and Aeolian arcs, Fig. 2c). Trace-element modelling and combined Sr and O isotope data provide the strongest evidence for subduction beneath the Alborán in the Middle and Late Miocene. The O and Sr isotopic compositions of plagioclase and clinopyroxene phenocrysts in the most mafic K-poor, high-Si rocks fall along a convex-down mixing curve between mid-ocean-ridge basalt (MORB) mantle and sediments on a $^{87}Sr/^{86}Sr$ versus $\delta^{18}O$ diagram, as do K-rich whole-rock samples from southern Spain[15]. These isotopic compositions thus cannot be explained through crustal assimilation[16], which generates a convex-up mixing curve. The combined O and Sr isotopic data are therefore diagnostic of mantle source contamination with fluids or melts from subducted sediments[17,18]. In addition, the K-rich subgroup and low-Si group commonly contain mantle xenoliths, also ruling out significant crustal assimilation in these rocks. Therefore the dramatic change in the composition of mafic, mantle-derived volcanic rocks in the eastern Alborán realm between 6.3 Myr ago (earliest alkali basalt) and 4.8 Myr ago (latest shoshonite) indicates that a major change in mantle dynamics occurred slightly before, or at the beginning of, this time interval.

The geochemistry of the younger low-Si mafic volcanic rocks are similar to Na-rich, alkalic intraplate basaltic rocks from the North Atlantic (for example, Canary Islands, Fig. 2b) and Africa (for example, Ahaggar)[19] derived from asthenospheric sources. Intraplate-type volcanism results from the decompression melting of upwelling asthenospheric mantle. We however discount derivation of this volcanism from a mantle plume, because of the lack of an age progression in the younger low-Si volcanism, and because of

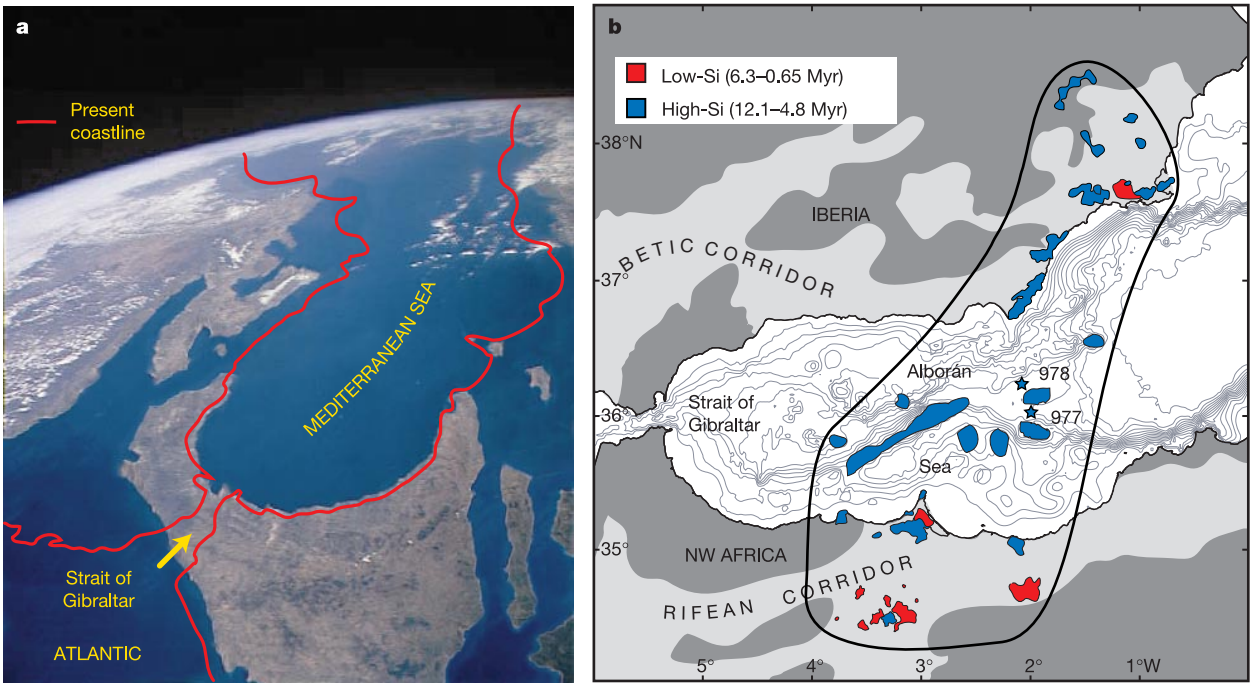

Figure 1 Maps illustrating Late Miocene Atlantic–Mediterranean marine gateways, and the distribution of Miocene–Pleistocene volcanism in the westernmost Mediterranean. **a**, NASA photograph of the westernmost Mediterranean, modified to show Atlantic–Mediterranean marine gateways in southern Spain and northwestern Africa about 8 Myr ago, based on the distribution of Upper Miocene reef complexes and marine sediments[5]. **b**, Map showing the westernmost Mediterranean and the 500 × 200 km north-northeast-trending eastern Alborán volcanic belt crossing the marine gateways in both southern Spain (Betic corridor) and in northwestern Africa (Rifean corridor). Middle Miocene to Lower Pliocene high-Si group volcanic rocks are shown in blue, and Upper Miocene to Pleistocene low-Si group volcanic rocks are shown in red. Numbers 977 and 978 refer to drill holes during Ocean Drilling Program (ODP) Leg 161 (ref. 28).

lacking evidence in seismic tomographic studies for low-velocity cylindrical structures beneath southeastern Spain, the Alborán Sea and northern Morocco[20,21].

In fact, new seismic data provide compelling evidence for active east-dipping subduction beneath Gibraltar[20]. Seismic tomography shows an ~250-km-wide, near-vertical slab extending from the surface to the boundary between the upper and lower mantle[20,21]. In a continental collisional setting, intraplate-type volcanism can also be generated by removal of a lithospheric body (oceanic lithosphere or subcontinental lithospheric mantle); for example, the Pannonian basin, eastern Europe[22], and the Andes, South America[23]. Westward roll back and steepening of the subducting slab in the Late Miocene would allow hotter, less-dense asthenosphere to ascend into the void left by the removal of the slab. Decompression melting of the upwelling asthenosphere can generate alkalic volcanism.

In order to determine if these mantle processes could produce the necessary uplift to close the Miocene marine gateways, we have done two-endmember, two-dimensional calculations to estimate the possible uplift resulting from roll back of the Tethys lithosphere (Fig. 4). With the modelling, we examine the effect of removing cold, dense material from the base of the Alborán lithosphere, replacing it with hot asthenosphere. For the current Gibraltar geometry, the 'slab-hinge effect' can lead to flexural-bending-induced uplift of ~100 m at the hinge, and uplift of ~300 m in the region where asthenosphere has infilled above the former slab (Fig. 4a). The removal of lithosperic mantle beneath the margins of

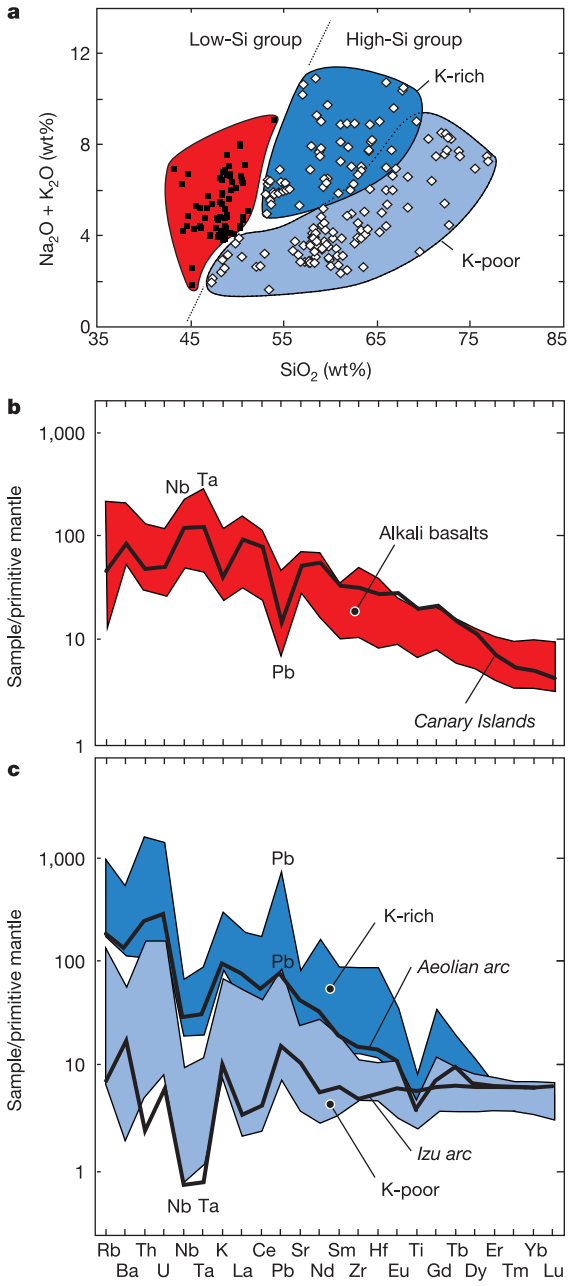

Figure 2 The major- and trace-element geochemistry of Miocene–Pleistocene volcanic rocks in the westernmost Mediterranean changes from subduction-related to intraplate-type during the Messinian. **a**–**c**, Major-element (**a**) and mantle-normalized trace-element diagrams (**b**, **c**) show the differences between the Upper Miocene to Pleistocene (6.3–0.65 Myr ago) low-Si group volcanic rocks (intraplate-type; **b**) and the most mafic Middle Miocene to Lower Pliocene (12.1–4.8 Myr ago) high-Si group volcanic rocks (subduction-related; **c**). Solid lines are representative samples from Canary Islands intraplate volcanic rocks in **b**, and Aeolian[25,26] and Izu (Ta = Nb/17) arc[27] (subduction zone) magmas in **c**. Additional Alborán Sea data from ref. 28. Primitive mantle after ref. 29.

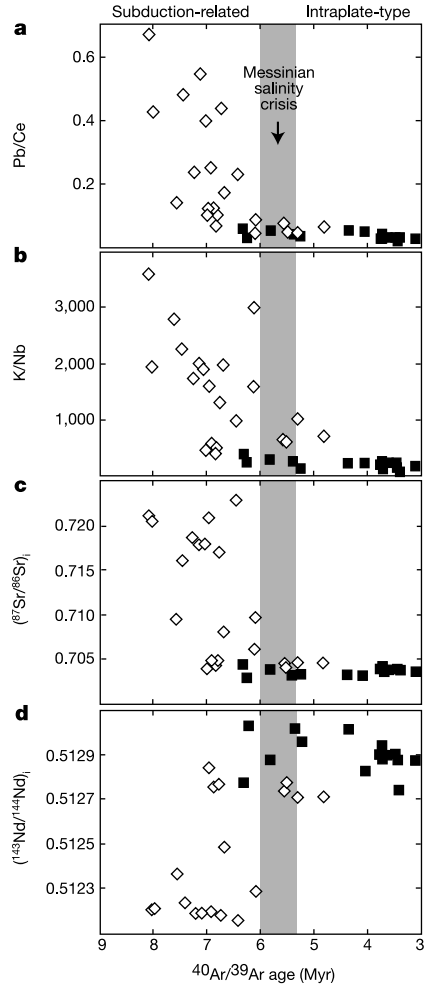

Figure 3 Trace-element and isotope ratios change during the MSC, consistent with the change from subduction-related to intraplate-type magmatism. Pb/Ce, K/Nb, initial $^{87}Sr/^{86}Sr$ and $^{143}Nd/^{144}Nd$ versus $^{40}Ar/^{39}Ar$ ages show a marked change between about 6.3 and 4.8 Myr ago, reflecting the shift from subduction-related volcanism (diamonds) to intraplate-type volcanism (squares). Intermediate compositions (<6.5 Myr) indicate interaction of intraplate-type magmas with the shallow mantle metasomatized by subduction processes, which was completed by ~4.8 Myr ago. Additional data sources, refs 16, 28, 30. Duration of MSC after ref. 1.

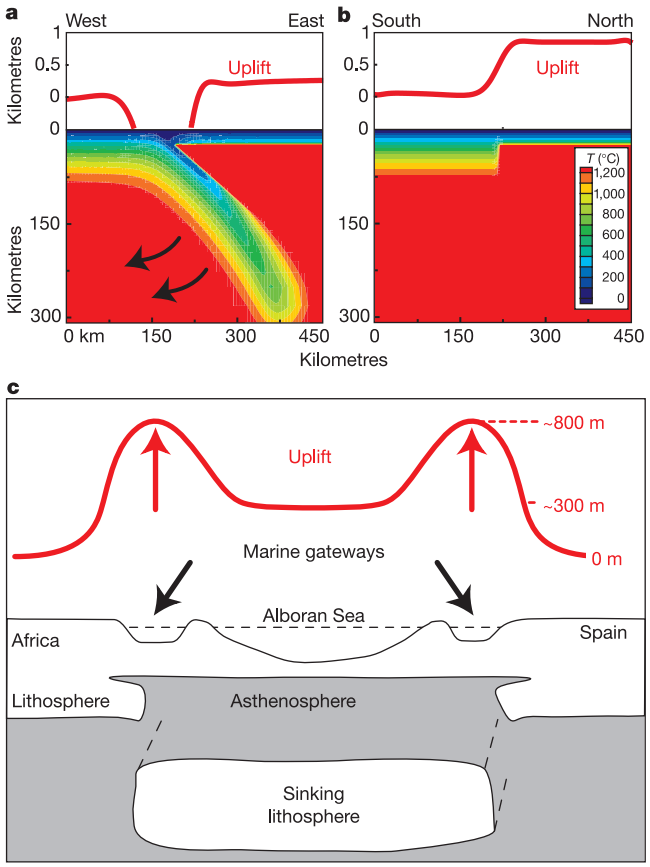

Figure 4 Thermomechanical models illustrating the uplift resulting from roll back of subducted Tethys oceanic lithosphere and associated asthenosphere upwelling as a plausible mechanism for the closure of Late Miocene Atlantic–Mediterranean marine gateways. **a**, 'Slab-hinge effect' from slab weight shown on a west–east profile; **b**, 'edge-effect' resulting from delamination of lithospheric mantle beneath the continental margins shown on a north–south profile. The edge-effect is larger in magnitude (~1 km). Relief is calculated assuming (1) a temperature-dependent viscous rheology, and (2) changes in the buoyancy resulting from replacement of cold oceanic lithosphere (blue and green) with hot 1,300 °C asthenosphere (red). The thermal model is based on the model formulation of ref. 31. To calculate the dynamic topography, we assume that the surface will deform with the uplifted 'overburden' being supported by flow-induced normal stresses[32]. **c**, A composite model for uplift in the Alborán region, combining the thermodynamical models of **a** and **b**. It illustrates that maximum uplift (~1 km) will occur on the continental margins, where the Late Miocene marine gateways linking the Mediterranean Sea to the Atlantic Ocean were located.

Morocco and southern Spain (the continental-ocean 'edge-effect') can lead to rapid uplift of the continental margins of the order of 800 m (Fig. 4b). We therefore propose that the roll back of Tethys oceanic lithosphere also peels away (delaminates) bands of lithospheric mantle from beneath the continental margins (Fig. 4c). Therefore, westward slab roll back is a plausible mechanism that can explain not only the location and composition of volcanism in the Alborán region, but also the uplift of the northern African and the southern Iberian margins, closing the Miocene gateways to the Atlantic Ocean.

The timing, location and magnitude of inferred mantle events and crustal uplift[3,5,10] correlate well. Therefore the asthenospheric and crustal response (~6.3–4.8 Myr ago) to westward roll back of oceanic lithosphere (8–7 Myr ago) provides a possible trigger and driving force for the uplift that led to the exhumation of the marine gateways between the Atlantic and Mediterranean in the Late Miocene. The isolation of the Mediterranean Sea from the world-wide network of oceans ultimately allowed for its desiccation during the MSC (5.96–5.33 Myr ago)[1]. We note that the catastrophic flooding of the Mediterranean at the end of the MSC[1,24] may also have had a mantle-related cause. Westward-migrating Late Miocene uplift may have also caused gravity-induced slumping from the western margin of the Gibraltar arc into the Atlantic abyssal plains, which—coupled with faulting—may have allowed a new marine gateway to open at the Strait of Gibraltar. □

Received 2 December 2002; accepted 27 February 2003; doi:10.1038/nature01553.

1. Krijgsman, W., Hilgen, F. J., Raffi, I., Sierro, F. J. & Wilson, D. S. Chronology, causes and progression of the Messinian salinity crisis. *Nature* **400,** 652–655 (1999).
2. Hsü, K. J., Ryan, W. B. F. & Cita, M. B. Late Miocene desiccation of the Mediterranean. *Nature* **242,** 240–244 (1973).
3. Krijgsman, W. *et al.* Late Neogene evolution of the Taza-Guercif Basin (Rifean Corridor, Morocco) and implications for the Messinian salinity crisis. *Mar. Geol.* **153,** 147–160 (1999).
4. Hodell, D. A., Benson, R. H., Kennet, J. P. & El Bied, K. R. Stable isotope stratigraphy of Latest Miocene sequences in northwest Morocco: The Bou Regreg section. *Palaeoceanography* **4,** 467–482 (1989).
5. Esteban, M., Braga, J. C., Martín, J. & de Santisteban, C. in *Models for Carbonate Stratigraphy from Miocene Reef Complexes of Mediterranean Regions* (eds Franseen, E. K., Esteban, M., Ward, W. C. & Rouchy, J.-M.) 55–72 (SEPM, Society for Sedimentary Geology, Tulsa, 1996).
6. Roger, S. *et al.* $^{40}Ar/^{39}Ar$ dating of the pre-evaporitic Messinian marine sequences of the Melilla basin (Morocco): a proposal for some biosedimentary events as isochrons around the Alboran Sea. *Earth Planet. Sci. Lett.* **179,** 101–113 (2000).
7. Adams, C. G., Benson, R. H., Kidd, R. B., Ryan, W. B. F. & Wright, R. C. The Messinian salinity crisis and evidence of late Miocene eustatic changes in the world ocean. *Nature* **269,** 383–386 (1977).
8. Hodell, D. A., Elmstrom, K. M. & Kennett, J. P. Latest Miocene benthic $\delta^{18}O$ changes, global ice volume, sea level and the 'Messinian salinity crisis'. *Nature* **320,** 411–414 (1986).
9. Weijermars, R. Neogene tectonics in the Western Mediterranean may have caused the Messinian salinity crisis and an associated glacial event. *Tectonophysics* **148,** 211–219 (1988).
10. Garcés, M., Krijgsman, W. & Agustí, J. Chronology of the late Turolian deposits of the Fortuna basin (SE Spain): implications for the Messinian evolution of the eastern Betics. *Earth Planet. Sci. Lett.* **163,** 69–81 (1998).
11. Hodell, D. A., Curtis, J. H., Sierro, F. J. & Raymo, M. E. Correlation of late Miocene to early Pliocene sequences between the Mediterranean and North Atlantic. *Palaeoceanography* **16,** 164–178 (2001).
12. Platt, J. P. & Vissers, R. L. M. Extensional collapse of thickened continental lithosphere: A working hypothesis for the Alboran Sea and Gibraltar Arc. *Geology* **17,** 540–543 (1989).
13. Comas, M. C., Platt, J. P., Soto, J. I. & Watts, A. B. The origin and tectonic history of the Alboran Basin. *Proc. ODP Sci. Res.* **161,** 555–580 (1999).
14. Martínez-Ruíz, F., Comas, M. C. & Alonso, B. Mineral associations and geochemical indicators in Upper Miocene to Pleistocene sediments in the Alboran Basin. *Proc. ODP Sci. Res.* **161,** 21–36 (1999).
15. Benito, R. *et al.* Sr and O isotope constraints on source and crustal contamination in the high-K calc-alkaline and shoshonitic neogene volcanic rocks of SE Spain. *Lithos* **46,** 733–802 (1999).
16. Turner, S. P. *et al.* Magmatism associated with orogenic collapse of the Betic-Alboran Domain, SE Spain. *J. Petrol.* **40,** 1011–1036 (1999).
17. James, D. E. The combined use of oxygen and radiogenic isotopes as indicators of crustal contamination. *Annu. Rev. Earth Planet. Sci.* **9,** 311–344 (1981).
18. Taylor, H. P. Jr & Sheppard, S. M. F. in *Stable Isotopes in High Temperature Geologic Processes* (eds Valley, J. W., Taylor, H. P. Jr & O'Neil, J. R.) 227–271 (Reviews in Mineralogy 16, Mineralogical Society of America, Washington DC, 1986).
19. Allègre, C.-J., Dupré, B., Lambret, B. & Richard, P. The subcontinental versus suboceanic debate; I, Lead-neodymium-strontium isotopes in primary alkali basalts from a shield area; the Ahaggar volcanic suite. *Earth Planet. Sci. Lett.* **52,** 85–92 (1981).
20. Gutscher, M.-A. *et al.* Evidence for active subduction beneath Gibraltar. *Geology* **30,** 1071–1074 (2002).
21. Calvert, A. *et al.* Geodynamic evolution of the lithosphere and upper mantle beneath the Alboran region of the western Mediterranean: Constraints from travel time tomography. *J. Geophys. Res.* **105,** 10871–10898 (2000).
22. Gîrbacea, R. & Frisch, W. Slab in the wrong place: Lower lithospheric mantle delamination in the last stage of the Eastern Carpathian subduction retreat. *Geology* **26,** 611–614 (1998).
23. Kay, R. W. & Mahlburg Kay, S. Delamination and delamination magmatism. *Tectonophysics* **219,** 177–189 (1993).
24. Hsü, K. J. *et al.* in *Initial Reports of the Deep Sea Drilling Project 42* (eds Hsü, K. J. *et al.*) 1053–1078 (US Government Printing Office, 1978).
25. Ellam, R. M. *et al.* The transition from calc-alkaline to potassic orogenic magmatism in the Aeolian Islands, Southern Italy. *Bull. Volcanol.* **50,** 386–398 (1988).
26. Ellam, R. M., Hawkesworth, C. J., Menzies, M. A. & Rogers, N. W. The volcanism of Southern Italy: Role of subduction and the relationship between potassic and sodic alkaline magmatism. *J. Geophys. Res.* **94,** 4589–4601 (1989).
27. Taylor, R. N. & Nesbitt, R. W. Isotopic characteristics of subduction fluids in an intra-oceanic setting, Izu-Bonin Arc, Japan. *Earth Planet. Sci. Lett.* **164,** 79–98 (1998).
28. Hoernle, K., Bogaard, P. v. d., Duggen, S., Mocek, B. & Garbe-Schönberg, D. Evidence for Miocene subduction beneath the Alboran Sea: $^{40}Ar/^{39}Ar$ dating and geochemistry of volcanic rocks from Holes 977A and 978A. *Proc. ODP Sci. Res.* **161,** 357–373 (1999).
29. Hofmann, A. W. Chemical differentiation of the Earth. The relationship between mantle, continental crust, and oceanic crust. *Earth Planet. Sci. Lett.* **90,** 297–314 (1988).
30. El Bakkali, S., Gourgaud, A., Bourdier, J.-L., Bellon, H. & Gundogdu, N. Post-collision neogene volcanism of the Eastern Rif (Morocco): magmatic evolution through time. *Lithos* **45,** 523–543 (1998).
31. Rüpke, L. H., Phipps Morgan, J., Hort, M. & Conolly, J. A. D. Are the regional variations in Central American arc lavas due to differing basaltic versus peridotitic slab sources of fluids? *Geology* **30,** 1035–1038 (2002).
32. Zong, S. & Gurnis, M. Controls on trench topography from dynamic models of subducted slabs. *J. Geophys. Res.* **99,** 15683–15695 (1994).

Acknowledgements We thank K. Reicherter, M. Hort and T. Hansteen for discussions, and M. Bouabdellah, M. Chaieb, D. Garbe-Schönberg, C. Harris, F. Hauff, M. Jadid, J. M. Fernandez Soler, M. Milhi, A. Moukadiri, D. Rau and J. Sticklus for analytical, field or logistic support. This work was supported by the Deutsche Forschungsgemeinschaft.

Competing interests statement The authors declare that they have no competing financial interests.

Correspondence and requests for materials should be addressed to S.D. (e-mail: s.duggen@gl.rhul.ac.uk).

N_2 production by the anammox reaction in the anoxic water column of Golfo Dulce, Costa Rica

Tage Dalsgaard*, Donald E. Canfield†, Jan Petersen†, Bo Thamdrup† & Jenaro Acuña-González‡

** Department of Marine Ecology, National Environmental Research Institute, Vejlsøvej 25 PO Box 314, DK-8600 Silkeborg, Denmark*
† Institute of Biology, Danish Centre for Earth System Science, University of Southern Denmark, Campusvej 55, DK-5230 Odense M, Denmark
‡ Centro de Investigación en Ciencias del Mar y Limnología, CIMAR, Universidad de Costa Rica, San José, Costa Rica

In oxygen-depleted zones of the open ocean, and in anoxic basins and fjords, denitrification (the bacterial reduction of nitrate to give N_2) is recognized as the only significant process converting fixed nitrogen to gaseous N_2. Primary production in the oceans is often limited by the availability of fixed nitrogen such as ammonium or nitrate[1], and nitrogen-removal processes consequently affect both ecosystem function and global biogeochemical cycles. It was recently discovered that the anaerobic oxidation of ammonium with nitrite—the 'anammox' reaction, performed by bacteria—was responsible for a significant fraction of N_2 production in some marine sediments[2]. Here we show that this reaction is also important in the anoxic waters of Golfo Dulce, a 200-m-deep coastal bay in Costa Rica, where it accounts for 19–35% of the total N_2 formation in the water column. The water-column chemistry in Golfo Dulce is very similar to that in oxygen-depleted zones of the oceans—in which one-half to one-third of the global nitrogen removal is believed to occur[3,4]. We therefore expect the anammox reaction to be a globally significant sink for oceanic nitrogen.

Golfo Dulce is connected to the equatorial tropical North Pacific Ocean through a 14-km-wide opening with a sill at 60 m depth. The bay is about 50 km long, with anoxic, nitrate-rich water in the bottom depths of the basin[5,6]. During the sampling reported here, the pycnocline was located at 40–55 m depth, and the water column was anoxic at depths greater than about 100 m, although sulphide did not accumulate until the bottom 10–20 m (Fig. 1a). Nitrate reduction, and not sulphate reduction, dominated water-column processes through most of the anoxic zone, similar to well-developed oxygen-minimum zones in the eastern Pacific and Indian oceans[7–9]. Curiously, ammonium (a normal product of anoxic organic matter mineralization) did not accumulate in the anoxic waters until nitrate was depleted and H_2S appeared (Fig. 1a). This observation alone indicates a significant role for anaerobic ammonium oxidation, where the ammonium liberated in the water column during denitrification is further oxidized with nitrate (through nitrite) as shown in equation (1) (refs 10, 11):

$$(CH_2O)_{106}(NH_3)_{16}H_3PO_4 + 94.4HNO_3 \rightarrow 106CO_2 + 55.2N_2 + 177.2H_2O + H_3PO_4 \quad (1)$$

This stoichiometry can be explained by the simultaneous operation of two known bacterial processes, denitrification (equation (2)), and the anammox reaction (equation (3) (refs 2, 12, 13).

$$(CH_2O)_{106}(NH_3)_{16}H_3PO_4 + 94.4NO_3^- + 94.4H^+ \rightarrow 106CO_2 + 16NH_4^+ + 16NO_2^- + 39.2N_2 + 145.2H_2O + H_3PO_4 \quad (2)$$

$$16NH_4^+ + 16NO_2^- \rightarrow 16N_2 + 32H_2O \quad (3)$$

The stoichiometric expression for denitrification (equation (2)) is somewhat modified from the 'standard' formulation[10,11], showing here the production of nitrite, a free intermediate of denitrification[14], in equal proportions to ammonium liberation. This is because anammox bacteria utilize nitrite and ammonium in a 1:1 ratio to form N_2 gas (equation (3)). It follows from equations (2) and (3) that the anammox reaction is responsible for 29% of the total N_2 production if all of the ammonium liberated during denitrification is subsequently oxidized by anammox. This possibility was recognized many years ago[10,11], although it was not then known whether organisms in nature could in fact conduct the anammox process.

We used ^{15}N-labelling techniques to explore for anammox in the water column of Golfo Dulce. Samples were retrieved from four depths in the anoxic water column at two sites (stations A and B) in the 200-m-deep central part of the basin, and amended with different combinations of ^{15}N- and ^{14}N-labelled nitrate and ammonium. At both sites and all depths, we observed anaerobic oxidation of NH_4^+ to N_2, as illustrated by the formation of $^{14}N^{15}N$ from added $^{15}NH_4^+$ (Fig. 2a). The formation of $^{14}N^{15}N$ started immediately after addition of $^{15}NH_4^+$, and the rate was constant over time. The formation of $^{15}N^{15}N$ was at the limit of detection. Therefore, the added $^{15}NH_4^+$ was combined with nitrogen from the natural $^{14}NO_3^-$ or $^{14}NO_2^-$ pools to form N_2, which is characteristic of the anammox reaction[12,13]. It has been suggested that anaerobic

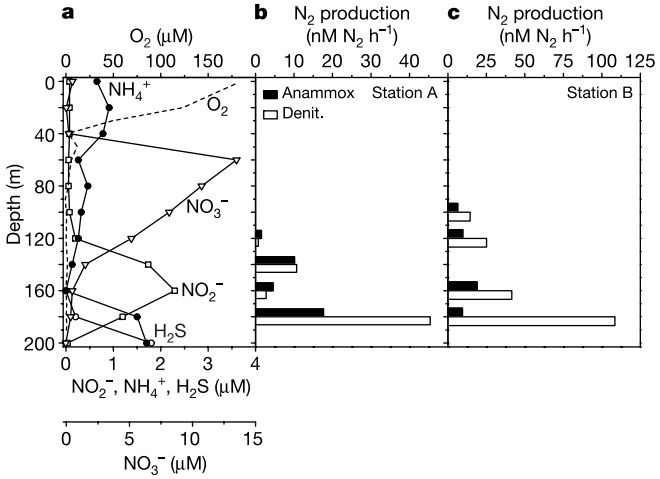

Figure 1 Water column data. **a**, Concentrations of O_2 (dashed line), NO_3^- (open triangles), NO_2^- (open squares), NH_4^+ (filled circles) and H_2S (open circles) versus depth. The data presented are from Station B, but the water chemistry at Station A was almost identical. The main differences are that at Station A the NO_2^- peak only reached 0.6 μM, and H_2S was only detected at 200 m depth. **b**, **c**, Rates of anammox (black bars) and denitrification (white bars) at Station A (**b**) and Station B (**c**). Note the different scales in **b** and **c**. Rates are determined as averages of three incubations.

